NORTHWESTERN UNIVERSITY

Kainate Receptors in the Development of Adult-born Dentate Granule Cells in the Hippocampus

A DISSERTATION

SUBMITTED TO THE GRADUATE SCHOOL

IN PARTIAL FULFILLMENT OF THE REQUIREMENTS

for the degree

DOCTOR OF PHILOSOPHY

Life Sciences

By

Yiwen Zhu

EVANSTON, ILLINOIS

March 2022

Abstract

Kainate Receptors in the Development of Adult-born Dentate Granule Cells in the Hippocampus

Yiwen Zhu

In the adult hippocampus of many mammalian species, populations of newborn dentate granule cells (DGCs) are continuously generated and undergo subsequent activity-dependent neuronal maturation and incorporation into the preexisting hippocampal circuitry. Increasing evidence has demonstrated that these young adult-born DGCs (abDGCs) participate in numerous cognitive and affective processes such as pattern separation, acquisition and retrieval of hippocampal-dependent memories, and stress responses. Therefore, the mechanisms that control the functional properties of maturing abDGCs are of relevance to multiple neurocognitive processes. Both inhibitory and excitatory neurotransmitter receptors can influence maturation and survival of adult-born neurons in the dentate gyrus; yet how these two neurotransmitter systems affect integration of new neurons into the existing circuitry is still not fully characterized. In this thesis project I demonstrate that glutamate receptors of the kainate receptor (KAR) subfamily are expressed in young abDGCs and that, through potential interaction with GABAergic signaling mechanisms, KARs regulate the functional properties of abDGCs during a critical period of their development. Both the measured intrinsic properties and synaptic connectivity of young abDGCs were altered after ablation of GluK2. Timed GluK2 loss in a cohort of young abDGCs in mice disrupted their performance in a spatial discrimination task but not in other hippocampal-dependent tasks. Together my study has revealed a novel and important role of KARs in the proper functional development of newborn neurons and further highlighted the tight cooperation between excitatory and inhibitory neurotransmitter signaling in the hippocampus.

Acknowledgements

This body of work would not have been completed without the support from many parties. I would like to express my eternal gratitude to all the people who have made important contributions to my PhD journey experience.

First and foremost, I sincerely thank my advisor, Dr. Anis Contractor, for his great mentorship and tremendous support during all these years. It has been a privilege to be his student. He provided me with abundant resources to carry out all the desired experiments, timely guidance at key stages during my research process, confidence in proceeding to each of my milestones, and the flexibility to balance work and life. I also thank him so much for always listening, understanding, and being patient with me.

Many thanks to all the professors who served on my thesis committee for their commitment to guide and aid my doctoral training: Dr. John Kessler, Dr. Geoffrey Swanson, Dr. Linda Overstreet-Wadiche, and Dr. Murali Prakriya. I truly appreciate their constructive criticisms, valuable suggestions and kind encouragement in all my past committee meetings, and as well as their efforts in reviewing an early draft of this dissertation and providing thoughtful feedbacks.

Thanks also to all my present and past colleagues with whom I closely worked, consulted, and discussed research problems in the Contractor laboratory. Thanks to Dr. John Armstrong for performing a significant part of the immunohistochemical experiments in this project. Thanks to Stephen Kraniotis, Dr. Jian Xu, Dr. Toshihiro Nomura, Dr. John Marshall, Dr. Claire Piochon, Dr. Shintaro Otsuka, and Dr. Christine Remmers for generously sharing their ideas and technical

know-how with me. I would not have been able to independently perform all the experiments I have done without their help.

In addition, a special note of thanks to Dr. Matthieu Flourakis, an incredible person who taught me the patch clamp technique and inspired me to become an electrophysiologist. I would also like to extend thanks to my amazing peer friends at Northwestern University such as Dr. Sali Liu, Dr. Xiaobao Li, Dr. Xiaojun Bao, Dr. Fangke Xu, and Dr. Yeqing Yang, just to name a few. Because of them my life in graduate school has never been dull. I treasure our friendship and all the memories we share together.

Finally, immense thanks to my family: my dearest parents, thank you for everything you gave me; and my husband, Guangyuan, for your wonderful love and companionship in the final years of my graduate study.

This work was supported by NIH/NIMH grant R01MH099114 and NIH/NINDS grant R01NS115471 to Dr. Anis Contractor and a Cancer Center Support Grant (NCI CA060553) to Northwestern University's Center for Advanced Microscopy.

List of Abbreviations

abDGC: adult-born dentate granule cell

ACSF: artificial cerebrospinal fluid

AHN: adult hippocampal neurogenesis

AMPA: α-amino-3-hydroxy-5-methyl-4-isoxazolapropionic acid

AMPAR: α-amino-3-hydroxy-5-methyl-4-isoxazolapropionic acid receptor

AP: action potential

BIC: bicuculline

BrdU: bromodeoxyuridine

CA3: cornu ammonis 3

cKO: conditional knockout

CNQX: cyanquixaline

CNS: central nervous system

CS: conditioned stimulus

D-APV: D-2-amino-5-phosphonovalerate

DCX: doublecortin

DG: dentate gyrus

DGC: dentate granule cell

DI: discrimination index

DIC: differential interference contrast

Dom: domoic acid, or domoate

dpi: days post injection

EC: entorhinal cortex

***E*$_{GABA}$**: GABA reversal potential

FBI: feedback inhibition

FFI: feedforward inhibition

GABA: γ-aminobutyric acid

GABA$_A$R: γ-aminobutyric acid type A (ionotropic) receptor

GC: granule cell

GCL: granule cell layer

GFP: green fluorescent protein

GYKI 52466: 4-(8-Methyl-9*H*-1,3-dioxolo[4,5-*h*][2,3]benzodiazepin-5-yl)-benzenamine dihydrochloride

IP: intraperitoneal

KAR: kainate receptor

KCC2: K^+-Cl^- cotransporter 2

KO: knockout

LEC: lateral entorhinal cortex

LTP: long-term potentiation

MEC: medial entorhinal cortex

mEPSC: miniature excitatory postsynaptic current

MF: mossy fiber

mIPSC: miniature inhibitory postsynaptic current

NKCC1: Na^+-K^+-Cl^- cotransporter 1

NMDA: N-methyl-D-aspartate

NMDAR: N-methyl-D-aspartate receptor

OLM: object location memory

PBS: phosphate buffered saline

PFA: paraformaldehyde

PIC: picrotoxin

RFP: red fluorescent protein

R_{in}: input resistance

RMP: resting membrane potential

R_{seal}: seal resistance

RV: retrovirus

sEPSC: spontaneous excitatory postsynaptic current

SGZ: subgranular zone

sIPSC: spontaneous inhibitory postsynaptic current

SVZ: subventricular zone

TAM: tamoxifen

TTX: tetrodotoxin

US: unconditioned stimulus

WT: wild type

wpi: weeks post injection

Table of Contents

Abstract **3**

Acknowledgements **4**

List of Abbreviations **6**

List of Figures **13**

Chapter 1 – Introduction **15**

1.1 Adult hippocampal neurogenesis and adult-born dentate granule cells: an overview **15**

Behavioral significance of abDGCs *16*

Characterization of abDGCs and their critical period of immaturity *19*

Activity-dependent maturation of abDGCs *21*

Regulation of abDGC development by neurotransmitter receptor signaling *23*

1.2 A plausible role of kainate receptors in the development of abDGCs **25**

1.3 Specific aims **27**

Chapter 2 – Materials and Methods **29**

2.1 Animals **29**

2.2 Retroviral birth-dating of abDGCs **29**

2.3 Hippocampal slice electrophysiology **31**

2.4 Immunohistochemistry **33**

Preparation of hippocampal sections *33*

Immunohistochemistry *34*

Post-hoc biocytin staining and imaging of abDGCs *35*

2.5 Behavioral studies 36

Object location memory 36

Trace fear conditioning and contextual fear memory 37

Two-choice spatial discrimination pattern separation task 38

2.6 Statistical analysis of data 41

Chapter 3 – Results: Cellular Phenotypes Due to Loss of KARs 42

3.1 Young abDGCs display KAR-mediated currents 42

3.2 Passive and active membrane properties of young abDGCs during an early critical period are disrupted by ablation of GluK2 46

Lower input resistances in 21 dpi GluK2-ablated abDGCs 46

Increased excitability in 21 dpi GluK2-ablated abDGCs 48

Morphological development is unaffected in GluK2-ablated abDGCs 52

3.3 Effect of GluK2 ablation on afferent synaptic integration of abDGCs 55

GABAergic synaptic events are elevated in 21 dpi GluK2-ablated abDGCs 56

Glutamatergic synaptic events are unaffected in 21 dpi GluK2-ablated abDGCs 59

3.4 GluK2-ablated abDGCs demonstrate a more depolarized E_{GABA} at 21 dpi 61

Chapter 4 – Results: Behavioral Phenotypes Due to Loss of KARs 64

4.1 Behavioral consequences of cell-specific ablation of GluK2 in young abDGCs 64

Spatial discrimination is impaired in 21-22 dpi Ascl1cKO mice 65

Trace fear conditioning and contextual fear memory is normal in Ascl1cKO mice 67

Two-choice spatial discrimination performance is normal in 21-26 dpi Ascl1cKO mice 69

Chapter 5 – Discussion 72

5.1 Interplay between GABA and glutamatergic signaling in the development of abDGCs 72

Cellular phenotypes in developing abDGCs due to loss of GluK2 73

A potential interaction between KCC2 and GluK2 in the development of abDGCs..... 74

How GluK2-containing KARs may normally regulate abDGC functional properties..... 75

Why depolarizing E_{GABA} induces no change in dendritic growth and glutamatergic synapses 76

5.2 Behavioral significance of GluK2 KARs in hippocampal function 79

GluK2 ablation has a selective effect on a spatial discrimination behavior..... 79

Understanding the deficit in the object location memory 80

3 wpi GluK2 cKO abDGCs may prematurely engage in behavior due to lower input specificity 81

A potential undermined coupling between 3 wpi GluK2 cKO abDGC and downstream targets 82

A cohort of 21-26 dpi GluK2 cKO abDGCs do not impact two-choice spatial pattern separation..... 84

21-24 dpi GluK2 cKO abDGCs do not disrupt trace fear conditioning and contextual fear memory 86

5.3 Limitations 88

Inadequate staining data for GluK2 and KCC2 in abDGCs..... 88

5.4 Future directions 90

The efferent synaptic connectivity and plasticity of GluK2 cKO abDGCs 90

Test the causative role of GluK2 in altering the functional properties of abDGCs..... 91

In vivo calcium imaging to study the neural substrates of altered behavior 92

5.5 Concluding remarks..... 93

References..... 94

List of Figures

Chapter 3

Figure 3.1 Young abDGCs display kainate receptor-mediated currents that are eliminated in the GluK2 KO mice 43

Figure 3.2 GluK2-containing KARs are present in young abDGCs 45

Figure 3.3 GluK4 is not required for the expression of functional KARs in young abDGCs 46

Figure 3.4 Development of intrinsic properties is altered in 21 dpi GluK2 cKO abDGCs 47

Figure 3.5 Development of input resistance in abDGCs in GluK2 KO mice compared with controls 47

Figure 3.6 Development of AP firing properties is altered in 21 dpi GluK2 cKO abDGCs 50

Figure 3.7 AP firing properties of young abDGCs in GluK2 KO mice 51

Figure 3.8 Development of resting membrane potentials and action potential thresholds in young GluK2-ablated abDGCs 52

Figure 3.9 Morphological development of GluK2 cKO abDGCs 55

Figure 3.10 Dendritic morphology of abDGCs in GluK2 KO mice 56

Figure 3.11 GABAergic synapses are elevated in 21 dpi GluK2 cKO abDGCs 59

Figure 3.12 Spontaneous IPSCs in young abDGCs in GluK2 KO mice 59

Figure 3.13 Spontaneous EPSCs in 21 dpi abDGCs from GluK2 global KO mice and after GluK2 cKO 60

Figure 3.14 E_{GABA} polarity switch is disrupted in 21 dpi GluK2 cKO abDGCs 62

Figure 3.15 E_{GABA} polarity switch in abDGCs in GluK2 KO mice 63

Chapter 4

Figure 4.1 Spatial discrimination is impaired by cKO of GluK2 in a young cohort of abDGCs . 67

Figure 4.2 Trace fear conditioning and contextual fear memory three weeks after TAM-induced cKO of GluK2 69

Figure 4.3 Two-choice spatial discrimination pattern separation performance is normal in 21-26 dpi Ascl1cKO mice 71

Chapter 5

Figure 5.1 KCC2 staining in 21 dpi Ascl1tdTom and Ascl1cKO abDGCs 90

Chapter 1 – Introduction

1.1 Adult hippocampal neurogenesis and adult-born dentate granule cells: an overview

Adult hippocampal neurogenesis (AHN) refers to the continuous generation of new dentate granule cells (DGCs) in the subgranular zone of the hippocampus and their subsequent maturation and incorporation into the preexisting hippocampal circuitry in the adult brain throughout postnatal life (Ming and Song, 2011; Toda et al., 2019; Zhao et al., 2008). A substantial number of studies detail the existence of AHN and adult-born dentate granule cells (abDGCs) in most mammalian species including rodents, monkeys, and humans (Boldrini et al., 2018; Gould et al., 1997; Lepousez et al., 2015; Spalding et al., 2013). It is widely perceived that abDGCs contribute an unparalleled form of structural plasticity to the hippocampus (Eriksson et al., 1998; Kempermann et al., 2018; Spalding et al., 2013; Toda et al., 2019). Because of the implications of these newborn neurons in many hippocampal-dependent cognitive and pathological processes, there has been a focus on how AHN can be subject to intricate regulation by numerous intrinsic and extrinsic factors, including but not limited to, aging (Klempin and Kempermann, 2007; Kuhn et al., 1996), enriched environment (Kempermann et al., 1997), physical exercise (van Praag et al., 1999; Sah et al., 2017), learning of hippocampus-dependent tasks (Gould et al., 1999), stress (Mirescu and Gould, 2006), antidepressant treatment (Malberg et al., 2000; Santarelli et al., 2003), and disease state (Jessberger and Parent, 2015; Moreno-Jiménez et al., 2019). Overall, the discovery of adult-generated neurons in the mammalian hippocampus has not only abolished the old dogma that the number of neurons no longer increases after birth, but also fueled an entire new field of research centering around the mechanisms and functions of AHN (Gage, 2019).

Behavioral significance of abDGCs

The functional relevance of abDGCs has been a subject of intensive investigation. Manipulations of AHN that either eliminate or increase the population of abDGCs have demonstrated that these new neurons play critical roles in a wide array of hippocampal-dependent learning, memories and affective behaviors (Drew et al., 2013). First of all, convergent lines of evidence support a prominent role of abDGCs in mediating pattern separation, a process that refers to the formation of distinct output representations of overlapping input patterns of neural activities, thus permitting separate encoding and fine discrimination of similar experiences in life (Johnston et al., 2016; Sahay et al., 2011a). The dentate gyrus (DG) has been viewed as a gate for information processing at the entrance of the hippocampus; DGCs receive unidirectional excitatory inputs from the entorhinal cortex (EC) then relay the information through mossy fiber outputs to the CA3 region of the hippocampus (Amaral et al., 2007; Lopez-Rojas and Kreutz, 2016; O'Reilly and McClelland, 1994). The large number of DGCs relative to their upstream EC and downstream CA3 principle cell counterparts (e.g., in rats DGCs are up to 5-10 times more abundant than their EC and CA3 synaptic partners) inherently enables an expansion of recoding of incoming EC activity patterns in the DG so that the transformed representations of similar episodes are more likely encoded by less overlapping subpopulations of DGCs (Drew et al., 2013; Johnston et al., 2016; Lopez-Rojas and Kreutz, 2016). The exceptionally low firing rate of DGCs (Jung and McNaughton, 1993; O'Reilly and McClelland, 1994) further increases the probability that small changes in EC inputs activate non-overlapping cohorts of DGCs. Moreover, the sparse connectivity between DGCs and CA3 principle cells (each mossy fiber axon contacts no more than 20 CA3 pyramids) (Amaral et al., 2007; Johnston et al., 2016; Lopez-Rojas and Kreutz, 2016) would predict that the distributed representations by the DG are conserved and relayed to the CA3. Together, these anatomical and

physiological properties of DGCs have led to the proposal that the DG circuit is essential for pattern separation. Importantly, experimental evidence has highlighted an indispensable role of abDGCs in this function. For instance, ablation of all newborn neurons via focal x-irradiation impaired spatial discrimination of mice, both in a navigable radial arm maze task and a non-navigable touch screen task, specifically when the two arms or stimuli to be discriminated were close to each other (Clelland et al., 2009). In addition, genetic depletion of abDGCs (by overexpressing the proapoptotic Bax protein in adult neural precursor cells) in mice resulted in impaired contextual discrimination in a variation of the contextual fear conditioning task (Tronel et al., 2012). Oppositely, mice with an increased level of AHN displayed improved performance of spatial and contextual pattern separation in the touch screen task (Creer et al., 2010) and contextual fear-discrimination learning task (Sahay et al., 2011b), respectively. Furthermore, using a transgenic mouse in which the output of old DGCs but not that of young abDGCs was selectively blocked by the tetanus toxin, it has been demonstrated that the sole synaptic transmission of young abDGCs (up to 3-4 weeks old) is sufficient to mediate pattern separation, whereas the rest population of more mature DGCs interestingly compromise this process and instead facilitate pattern completion (the ability to recall full memory representations upon exposure to a partial retrieval cue), a process that theoretically counteracts pattern separation (Nakashiba et al., 2012).

Besides an evident role in pattern separation, abDGCs have also been shown to contribute to multiple aspects of memory processing including acquisition/encoding, consolidation, storage, retrieval, and even forgetting of memories (Drew et al., 2013). For example, 2-week treatment with a toxin for proliferating cells to diminish the number of abDGCs in rats disrupted trace memory formation, a hippocampus-dependent task in which an animal learns to associate a

conditioned stimulus with an unconditioned stimulus separated by a time interval (Misane et al., 2005; Shors et al., 2001). Optogenetic inhibition of a cohort of 6-week-old and younger abDGCs during a fear conditioning training paradigm significantly reduced freezing when mice were reintroduced to the same environment a day later, supporting participation of these neurons in contextual information encoding (Danielson et al., 2016). There is also evidence that finely tuned activity of young abDGCs during rapid eye movement sleep is necessary for memory consolidation, as either suppressing or randomly activating a population of 4-week-old and younger abDGCs in this period impaired contextual fear memory that had been acquired (Kumar et al., 2020). Furthermore, it has been demonstrated that activity of 4-week-old abDGCs is required for retrieval (but not for acquisition) of spatial memories in a water maze test and as well as contextual fear memory (Gu et al., 2012). There is no doubt that abDGCs play critical roles in numerous memory processes, although the observed impact of altering the number or activity of abDGCs on hippocampal-dependent learning and memories may not always be consistent, presumably due to variations such as the age of abDGCs affected at the time of behavioral test and the method of manipulation (Deng et al., 2010). Importantly, in addition to their roles in temporal, spatial and contextual information processing, abDGCs have also been implicated in regulating other aspects of cognitive abilities in rodents, such as improving cognitive flexibility (Burghardt et al., 2012) and promoting decision-making towards obtaining delayed but larger rewards (Seib et al., 2021).

Finally, there has also been a strong link between adult hippocampal neurogenesis and affective behaviors including mood regulation, anxiety levels, and stress responses (Zhao et al., 2008). It has been generally acknowledged that AHN is required for antidepressant-mediated improvements in depression-like behaviors in rodent models, such as the novelty-suppressed feeding test, chronic

unpredictable stress paradigm, and tail suspension test (Drew et al., 2013; Sahay and Hen, 2007; Santarelli et al., 2003; Tunc-Ozcan et al., 2019). Existing evidence also suggests that abDGCs are crucially involved in mitigating stress responses, as mice lacking new neurons displayed increased latency to feed in the novelty-suppressed feeding test, indicative of increased anxiety/depression-like behavior, after pre-exposure to stressful events but not under normal conditions (Snyder et al., 2011). In contrast, mice with increased number of newborn neurons were protected from such stress-induced anxiety-like behaviors compared with control animals, which exhibited decreased social interaction time and as well as reduced center exploration in the open field test following a social defeat event (Anacker et al., 2018). While previous manipulation of AHN often caused an increase or decrease in the total population of abDGCs, recent studies employing chemogenetics in transgenic mice allowed selective control of the activity of abDGCs without changing their quantity. For example, chemogenetic suppression of abDGCs in the ventral DG promoted stress reactions in mice in a subthreshold social defeat paradigm (Anacker et al., 2018), whereas chemogenetic activation of abDGCs effectively resulted in antidepressant-like behaviors including decreased time spent immobile in the tail suspension test and increased open field center exploration distance, demonstrating a causal role of abDGC activity in stress resilience (Tunc-Ozcan et al., 2019).

Characterization of abDGCs and their critical period of immaturity

While it is unequivocal that adult hippocampal neurogenesis has implications in a large array of cognitive domains and offers operational advantages to hippocampal function, the mechanisms by which AHN mediates these behavioral effects remain unclear. As the essential products of AHN, abDGCs have been studied in detail and compared with mature DGCs in various aspects of their

electrophysiological and synaptic properties (Drew et al., 2013). Are abDGCs functionally separate from or similar to the mature DGC population? It has been demonstrated that abDGCs exhibit similar differentiation stages compared with embryonic neuronal development (Espósito et al., 2005), and that they integrate into the existing circuitry by receiving functional inputs as well as forming outputs to the CA3 area (Gu et al., 2012). Remarkably, it has been consistently found that young abDGCs exhibit a critical time window around 4-6 weeks following their birth during which they develop elevated intrinsic excitability, receive less inhibition and display enhanced synaptic plasticity, thus potentially representing a more excitable population of neurons that could make distinct contributions to information processing within the DG (Deng et al., 2010). For instance, it has been demonstrated that young abDGCs differ substantially from mature DGCs by high input resistance and expression of T-type Ca^{2+} channels that facilitate the generation of action potentials and contribute to a lower threshold for LTP induction (Schmidt-Hieber et al., 2004). Indeed, young abDGCs between 4-6 weeks of age exhibit heightened LTP compared with DGCs of other postmitotic ages (Ge et al., 2007). In addition, 4-week-old abDGCs respond to perforant path stimulation in the molecular layer with a greater spiking probability compared with mature DGCs due to much weaker feedback inhibition (FBI) (Dieni et al., 2013; Li et al., 2012; Marín-Burgin et al., 2012; Temprana et al., 2015). Paradoxically, when the perforant path is stimulated at its source in the EC, abDGCs between 4-5 weeks old are less likely to spike than mature DGCs due to contemporaneously much sparser excitatory innervation (Dieni et al., 2016). It is still inconclusive whether young abDGCs have lower or higher input specificity than mature DGCs under physiological conditions, however the distinct properties of young abDGCs suggest that they shall play different roles than mature DGCs regarding DG function. Once passing that critical time window, abDGCs gradually and eventually become indistinguishable from

developmentally born DGCs or other older mature abDGCs in terms of their basic structural and physiological properties (Deng et al., 2010; Laplagne et al., 2006), though some fine morphological distinctions may persist (Cole et al., 2020; Kerloch et al., 2019).

Activity-dependent maturation of abDGCs

The distinct functional properties of young abDGCs therefore endow the duration of their immaturity with specific importance, and how soon abDGCs develop out of their immature phase will likely impact how the hippocampal circuit functions and processes memory. The behavioral effect of an altered maturation rate of abDGCs has not been tested yet, however, it has been proposed that the rate of neuronal maturation in the DG could determine the temporal resolution of encoded memories (Piatti et al., 2011). Computational models based on the elevated excitability of immature neurons predict that abDGCs belonging to the same age subset will undergo critical period of immaturity together and more likely be activated repeatedly to encode events that happen close in time so that these memories can be temporally associated upon reactivation of the original subset of abDGCs (Deng et al., 2010). For two events that occur far apart in time, as abDGCs activated during the earlier event would have become mature and no longer hyperexcitable, a new subset of abDGCs will be activated to encode the later event so that these memories will not be associated by the same subset of abDGCs and thus can be temporally separated (Deng et al., 2010). As a result, temporal relationships between memories can be carried through different ‘waves’ of immature abDGCs (Becker and Wojtowicz, 2007), and how fast a cohort of abDGCs develop out of their immaturity can set the maximum duration between two episodes for them to be temporally associated together. When abDGCs develop at a slower rate and the window for increased excitability and plasticity is extended such as a natural result of aging (Trinchero et al., 2017),

events spanning a longer period will still be represented by an overlapping population of immature abDGCs, resulting in reduced temporal precision of memories. Interestingly, this might explain the common feeling that time flies faster when we grow older. On the contrary, when abDGCs develop at a faster speed and the window of the expression of immature properties is shortened, events that would originally activate the same cohort of abDGCs will instead be encoded by different cohorts of abDGCs, and only events occurred within a shorter period will be tagged by the same group of immature abDGCs that allow for future association, resulting in a more refined temporal resolution of memories.

Therefore, describing the mechanisms that regulate the functional properties of young abDGCs during their critical period of immaturity is of great relevance to defining how the hippocampus functions in the adult brain. While such mechanisms are still far from being fully characterized, it has been demonstrated that the maturation speed and synaptic integration of abDGCs in the hippocampal circuitry depend on both extrinsic network activities and intrinsic excitability. For example, in sedentary mice abDGCs mature more rapidly in the dorsal DG compared with the ventral DG, which correlates with a higher level of network activity in the dorsal DG as indicated by expression of the immediate early gene Arc (Piatti et al., 2011). Moreover, stimulating network activity by voluntary running not only promoted the proliferation of neural stem cells but also increased the maturation speed of developing abDGCs in the ventral DG (Piatti et al., 2011). On the other hand, increasing intrinsic excitability of abDGCs by retroviral expression of a voltage-gated bacterial sodium channel lead to certain changes suggestive of an accelerated maturation, including increased GABAergic inhibition and early downregulation of immature neuronal markers (Sim et al., 2013). Conversely, decreasing intrinsic excitability of abDGCs by

overexpressing the inward-rectifying potassium channel Kir2.1 lead to reduced dendritic length and altered expression of neuronal maturity markers consistent with a delayed maturation phenotype, in spite of increased hippocampal network activities in running mice (Piatti et al., 2011). Overall, the maturation of abDGCs is highly activity-dependent and hence can be subject to complex regulation by various cell-intrinsic and environmental factors that affect the activity of abDGCs during their development.

Regulation of abDGC development by neurotransmitter receptor signaling

Network activity in the hippocampal environment can be sensed by developing abDGCs via neurotransmitter signaling, and numerous studies have demonstrated that both GABA and glutamate receptors, the two major inhibitory and excitatory neurotransmitter signaling systems, not only regulate the proliferation and differentiation phases of AHN but also influence the survival, maturation, and synaptic integration of young abDGCs at different time points (Catavero et al., 2018; Zhao et al., 2008). Resembling immature neurons during embryonic development, new abDGCs during approximately the first two postmitotic weeks initially receive GABAergic inputs that can potentially depolarize and cause excitation of young neurons because of their high intracellular Cl^- concentration that renders a relatively depolarized reversal potential for GABA (E_{GABA}) (Zhao et al., 2008). Such depolarizing action of GABA promotes differentiation, morphological maturation, survival, and as well as synaptic integration of abDGCs (Alvarez et al., 2016; Jagasia et al., 2009; Song et al., 2013; Tozuka et al., 2005). Converting GABA-induced depolarizing responses to being hyperpolarizing by knockdown of NKCC1, the Na^+-K^+-Cl^- cotransporter (a Cl^- importer expressed at high levels in young neurons), leads to marked defects in dendritic growth in 2-week-old abDGCs as well as a significant decrease in formation of both

inhibitory and excitatory synapses in abDGCs reaching 4 weeks old (Ge et al., 2006). Synaptic activation of GABA receptors also produces sufficient depolarization to unsilence NMDAR-only synapses that are prevalent in young neurons, and acutely induces insertion of AMPARs and promotes AMPAR-mediated transmission in immature abDGCs (Chancey et al., 2013). Between 2-4 weeks post mitosis E_{GABA} becomes more hyperpolarized (Ge et al., 2006), likely due to the upregulation of neuron-specific K^+-Cl^- cotransporter 2 (KCC2, a Cl^- extruder), which maintains a lower intracellular Cl^- concentration in older neurons and thus switches $GABA_A$ receptor ($GABA_AR$) responses to the mature inhibitory profile (Catavero et al., 2018; Rivera et al., 1999; Wang et al., 2002). Concurrently, abDGCs start to receive functional glutamatergic synaptic inputs as GABAergic responses become hyperpolarizing: evoked glutamate-mediated postsynaptic currents can be first detected in 14- to 18-day postmitotic abDGCs (Espósito et al., 2005; Ge et al., 2006), and morphologically identifiable dendritic spines appear as early as 16 days after abDGC birth (Zhao et al., 2006). It is also within this time window that abDGCs display increased excitability and plasticity as mentioned above (Zhao et al., 2008).

The role of glutamatergic signaling in regulating the development of newborn neurons in the adult hippocampus is less extensively studied than that of GABA. Despite lacking glutamatergic synapses within the first two weeks, abDGCs of 4 days old express functional ionotropic glutamate receptors, as indicated by responsiveness to exogenous application of glutamate (Espósito et al., 2005). Early expression of NMDA receptors has also been described in adult hippocampal neural progenitor cells to promote neuronal differentiation potentially through activation by ambient glutamate (Deisseroth et al., 2004). Developing abDGCs first receive monosynaptic glutamatergic inputs from local hilar mossy cells starting around 2 weeks after birth, followed by inputs from the

EC within another 1-3 weeks (Chancey et al., 2014; Deshpande et al., 2013). During the third to fourth week post-mitosis, NMDA receptor signaling plays a cell-autonomous role in supporting abDGC survival and promoting initial spine formation (Mu et al., 2015; Tashiro et al., 2006a). However, the potential roles of the other members of the ionotropic glutamate receptor families, namely AMPA receptors and kainate receptors (KARs), in regulating maturation and circuit integration of young abDGCs have not been examined yet. KARs are of particular interest because they have multiple roles in synaptic and neuronal development in developmentally born neurons (Jack et al., 2019; Lauri et al., 2006; Orav et al., 2017; Sakha et al., 2016). It has been shown that KAR subunits are amply expressed in the dentate gyrus (Bureau et al., 1999) but as in many other neuronal types they are not localized and available at synapses under normal conditions (Epsztein et al., 2005). Still, it is not clear when KARs are first expressed by newly generated DGCs during early postmitotic development, and whether non-synaptically localized receptors may have unsuspected effects on developing neurons.

1.2 A plausible role of kainate receptors in the development of abDGCs

Both direct and indirect evidence has suggested roles for non-NMDA ionotropic glutamate receptors in modulating various aspects of adult hippocampal neurogenesis. Low concentrations of domoic acid (Dom), an AMPA/kainate receptor agonist, induced upregulation of proliferation and differentiation of neural progenitors in organotypic hippocampal slice cultures (Pérez-Gómez and Tasker, 2012). Notably, there is direct evidence demonstrating the robust presence of KARs in adult hippocampus-derived neurospheres and kainate treatment increases neural progenitor proliferation (Aguado et al., 2007). Moreover, neuroblasts in the subventricular zone (SVZ, the second only neurogenic niche in the adult brain) express both AMPA and kainate receptors, the

tonic activation of which induces intracellular calcium influx (Berg et al., 2013; Brazel et al., 2005; Platel et al., 2010), and application of specific KAR antagonists significantly increases neuroblast migration speed in a whole-mount preparation of the SVZ (Platel et al., 2008). It has also been shown that stimulation of KARs but not AMPARs decreases programmed cell death and increases proliferation of SVZ-derived neural progenitor cells (Brazel et al., 2005).

In addition, as already mentioned, KARs are abundantly expressed by mature DGCs in the hippocampus (Bureau et al., 1999; Paternain et al., 2000); they are normally not detected at postsynaptic sites in mature DGCs but can be translocated to synapses after seizures (Peret et al., 2014). In particular, prior work has demonstrated that GluK2 KO mice, in which the GluK2 subunits of KARs are genetically ablated, display delayed physiological and structural maturation of mossy fiber synapses formed by developmentally born DGCs, establishing the importance of KARs to normal hippocampal circuit development at early postnatal stage (Lanore et al., 2012). Although it is not known whether and when abDGCs express functional KARs, extrasynaptic AMPAR/KAR currents can be reliably recorded from immature abDGCs with high input resistances (Schmidt-Salzmann et al., 2014), indicating that KAR activity could possibly exert influence on abDGC development from an early postmitotic point on.

Furthermore, multiple lines of KAR mutant mice have manifested a disruption in anxiety-related and affective-like behaviors (Iida et al., 2021; Shaltiel et al., 2008), which can be directly correlated with altered adult hippocampal neurogenesis (Anacker et al., 2018; Snyder et al., 2011). For instance, genetic deletion of the high-affinity KAR subunit GluK4 resulted in mice with reduced anxiety in the elevated zero-maze test and an antidepressant-like phenotype in the forced swim test

(Catches et al., 2012), whereas mice overexpressing GluK4 in the forebrain including the hippocampus displayed severe anxiety and aggravated depression-like status (Aller et al., 2015). These behavioral phenotypes could hypothetically be explained by functional abnormalities in abDGCs as a result of aberrant KAR signaling.

Taken together, existing evidence has pinpointed a plausible yet undefined role of KARs in modulating adult hippocampal neurogenesis which could lead to subsequent behavioral alterations, and the question whether KARs regulate the functional properties of developing abDGCs going through the critical period of activity-dependent maturation remains to be answered. This research project has been prompted by the above question and we hope that the findings will expand our current knowledge scope on KAR function in the CNS and as well as the regulatory factors of abDGC development in the mammalian hippocampus.

1.3 Specific aims

The primary objective of this thesis project is to investigate the potential regulatory roles of kainate receptors in the functional development of abDGCs in the hippocampus. There are three main specific aims in my study:

1) Determine the role of GluK2-containing KARs in regulating functional properties of abDGCs in both global and conditional GluK2 KO mouse models. Since GluK2 is the principle KAR subunit expressed in the hippocampus (Bureau et al., 1999; Paternain et al., 2000), global GluK2 KO mice will be first used to assess the cellular phenotype of ablating GluK2 KARs in retrovirally birth-dated abDGCs at varying postmitotic time points. The purpose of using

conditional GluK2 KO (GluK2 cKO) mice is to determine whether GluK2 mediates a cell-autonomous effect on regulating functional properties of abDGCs. Both electrophysiological and morphological properties will be measured and compared between GluK2-ablated and control abDGCs. Measures of electrophysiological properties will include input resistances, resting membrane potentials, rheobase, action potential threshold, intrinsic excitability, and as well as GABA and glutamate-mediated synaptic activities. Morphological measures will include quantification of total dendritic length and number of branch points.

2) Test the hypothesis that loss of GluK2-containing KARs disrupts the normal development of GABA reversal potential, which may in turn alter abDGC functional properties (Ge et al., 2006; Jagasia et al., 2009).

3) Investigate the behavioral consequences associated with disrupted functional properties of young abDGCs in cell-specific GluK2 KO mice. I will compare control and conditional GluK2 KO mice in four hippocampal-dependent behavioral tasks that according to previous studies are sensitive to alterations in AHN: a) the object location memory (Castillon et al., 2018; Goodman et al., 2010), b) trace fear conditioning memory (Shors et al., 2001), c) contextual fear memory (Gu et al., 2012; Saxe et al., 2006), and d) two-choice spatial discrimination pattern separation task (Clelland et al., 2009; Creer et al., 2010), respectively.

Chapter 2 – Materials and Methods

2.1 Animals

All animal care and procedures were approved by and conducted in accordance with the Northwestern University Institutional Animal Care and Use Committee (IACUC). Mice of the same sex were group-housed as two to five littermates per cage with free access to food and water with a 14 h/10 h light/dark cycle in standard conditions. GluK2 knockout (GluK2 KO, previously known as GluR6$^{-/-}$) mice were bred in house from animals supplied originally from Dr. Stephen Heinemann (Salk Institute, La Jolla, CA) (Mulle et al., 1998). GluK4 KO (*Grik4*$^{-/-}$) mice have been previously generated and maintained in house (Catches et al., 2012; Fernandes et al., 2009). Generation of mutant floxed *Grik2* (*Grik2*f/f) mice for conditional knockout of the kainate receptor subunit GluK2 (GluK2 cKO) upon Cre recombinase expression has been previously described (Marshall et al., 2018). Ascl1$^{\text{CreERT2}}$ (*Ascl1*$^{tm1.1(Cre/ERT2)Jejo}$/J) mice were purchased from the Jackson Laboratory, and crossed with our *Grik2*f/f;Ai9 mice (Marshall et al., 2018) to generate Ascl1$^{\text{CreERT2}}$;*Grik2*f/f;Ai9 mice to achieve conditional knockout of GluK2 (Ascl1 cKO) in abDGCs that can be identified by tdTomato reporter fluorescence following tamoxifen-induced activation of Cre recombinase. Adult mice (8-10 weeks of age) of both sexes were used in all experiments.

2.2 Retroviral birth-dating of abDGCs

In order to study the effects of loss of GluK2 in the development of abDGCs I employed a well-established retroviral-mediated birth-dating and single-cell gene knockout technique to target dividing cells (which would develop into abDGCs later) in the SGZ of adult mice (van Praag et al., 2002; Tashiro et al., 2006b). Concentrated Moloney murine leukemia virus-based replication-

deficient retroviral vectors were prepared in accordance to an earlier published protocol (Tashiro et al., 2006b) with slight modifications. Specifically, GP2-293 cells, which already had been engineered to express the essential retroviral packaging proteins Gag and Pol, were co-transfected with plasmids encoding VSV-G (the viral envelope) and one of the three transgenes: CAG-RFP, CAG-GFP, or CAG-GFP-IRES-CRE (Addgene plasmid # 48201) using Lipofectamine 2000 (Invitrogen, catalog No. 11668019) in Opti-MEM (Invitrogen, catalog No. 31985070). The GP2-293 packaging cell line and VSV-G plasmid were both gifts from Dr. John Kessler (Northwestern University, Chicago, IL). The CAG-RFP and CAG-GFP plasmids were kindly provided by Dr. Fred Gage (Salk Institute, La Jolla, CA). After 4-5 hours, transfection media were aspirated and replaced with GP2-293 media consisting of DMEM with high glucose, L-glutamine, sodium pyruvate, penicillin/streptomycin, and 10% FBS. Transfected cells were incubated at 37°C/5% CO_2 for virus production. On the 3rd and 6th day after transfection, growth media containing packaged retroviruses were collected, filtered through a 0.22 μm filter top, and centrifuged at 25,000 rpm for 2-2.5 hours at 4°C using a SW28 rotor (Beckman Coulter). The supernatant media were then decanted, and the remaining precipitated viral pellet was allowed to dry by placing the centrifuge tube (Seton Scientific, #7052) upside down on 4-6 stacked Kimwipes for 10 min, followed by resuspension in PBS (1 μl for each 2 ml viral media) overnight at 4°C. The next day, the concentrated viral solution was mixed gently, aliquoted and stored at -80°C until use.

To label and birth-date abDGCs, 0.5-1.5 μl of the above retroviral solution was delivered bilaterally to the subgranular zone (SGZ) of 8-10 weeks old mice at a rate of 0.1-0.3 μl/min via stereotaxic injection under ketamine/xylazine (150 μg ketamine/15 μg xylazine in 10 μl PBS/g) anesthesia as previously described (Remmers and Contractor, 2018; Remmers et al., 2020; Tashiro

et al., 2006b). The following injection coordinates from bregma (in millimeters) were used: -2.0 anteroposterior, ±1.6 mediolateral, and -2.4 dorsoventral.

2.3 Hippocampal slice electrophysiology

Mice were anesthetized with isoflurane followed by ketamine/xylazine, then rapidly perfused with ice-cold sucrose artificial cerebrospinal fluid (ACSF) containing the following (in mM): 85 NaCl, 2.5 KCl, 1.25 NaH_2PO_4, 25 $NaHCO_3$, 25 glucose, 75 sucrose, 0.5 $CaCl_2$, and 4 $MgCl_2$, equilibrated with 95% O_2/5% CO_2 before mice were decapitated. Brains were quickly removed and placed in the same ice-cold sucrose ACSF as described above. Coronal hippocampal slices (250 μm thick) were prepared using a Leica VT1000 S or VT1200 S vibratome and transferred to a heated (28-32°C) holding chamber containing the same sucrose ACSF, which was gradually exchanged for regular ACSF containing the following (in mM): 125 NaCl, 2.5 KCl, 1.25 NaH_2PO_4, 25 $NaHCO_3$, 25 glucose, 2 $CaCl_2$, and 1 $MgCl_2$, equilibrated with 95% O_2/5% CO_2 at room temperature. After incubation in regular ACSF for at least one hour, slices were transferred to a recording chamber and perfused continuously with oxygenated regular ACSF at a flow rate of 2 ml/min. The dentate gyrus was visualized under DIC optics and retroviral-labeled abDGCs were identified based on RFP or GFP reporters.

Recording electrodes were made from borosilicate glass pipettes and had a resistance of 3.5-6.5 MΩ when filled with an internal solution containing the following (in mM): 130 K-gluconate, 10 KCl, 10 HEPES, 4 Mg-ATP, 0.3 Na-GTP, and 10 Na_2Phosphocreatine, pH adjusted to 7.3 with KOH. Input resistances were determined in whole-cell voltage-clamp mode by holding cells at -70 mV and presenting a -5 mV hyperpolarizing voltage step with a duration of 100 ms. Action

potential thresholds were calculated as the voltage value at the onset of inward sodium currents by applying a voltage ramp from -100 mV to +100 mV to cells at a rate of +2 mV/ms. Resting membrane potentials were measured in current-clamp mode at least 5 minutes after formation of the whole-cell recording configuration. Rheobase was defined as the minimum amplitude of a 300 ms current injection step required to elicit the first action potential in abDGCs. Input-output (I/O) relationship was generated by injecting various amount of current to hold each cell's membrane potential close to -70 mV while further injecting current steps from 0-100 pA in 10 pA increments and counting spike number in response to each current step.

For all other voltage clamp recordings, the internal solution contained the following (in mM): 95 CsF, 25 CsCl, 10 HEPES, 10 EGTA, 2 NaCl, 2 Mg-ATP, 10 QX-314, 5 TEA-Cl, and 5 4AP, pH adjusted to 7.3 with CsOH, 280-290 mOsm. KAR-mediated currents were induced by bath application of 1 μM Dom in the presence of 10 μM bicuculline ($GABA_AR$ antagonist), 50 μM picrotoxin ($GABA_AR$ antagonist), 1 μM TTX (Na^+ channel blocker), 50 μM GYKI 52466 (AMPAR antagonist), and 50 μM D-APV (NMDAR antagonist). Spontaneous IPSCs were pharmacologically isolated by bath application of 10 μM CNQX and 50 μM D-APV, while spontaneous EPSCs were pharmacologically isolated by 10 μM bicuculline, 50 μM picrotoxin, and 50 μM D-APV. Miniature IPSCs and EPSCs were recorded as above in the presence of 1 μM TTX. All synaptic events were recorded between 26-30°C and analyzed using Mini Analysis Program (Synaptosoft).

For gramicidin perforated patch recordings, pipettes were filled with (in mM) 150 KCl and 10 HEPES, pH adjusted to 7.2 with Tris-OH, and gramicidin was added at a concentration of 80 μg/ml.

GABAergic currents were evoked in voltage-clamp mode at different holding potentials (-100 to +30 mV, 10 mV step) by focal puff application of 100 μM GABA via a Picospritzer III (50 ms duration, 2-8 psi) in the presence of 1 μM TTX, 10 μM CNQX, and 50 μM D-APV. Current-voltage relationship (I-V curve) for each cell was plotted and E_{GABA} was measured as the voltage value at the intersection between the x-axis and the linear fit of the I-V curve. Unless otherwise stated all electrophysiological data were acquired at 10 kHz and analyzed using pClamp 10 software (Molecular Devices).

2.4 Immunohistochemistry

Preparation of hippocampal sections

Animals were anesthetized with isoflurane (in chamber; 2% delivered at a rate of 0.5-1 L/minute) followed by IP injection of ketamine (90 mg/kg)/xylazine (5 mg/kg) mixture, and perfused transcardially with the following solutions using a peristaltic pump at a rate of 3.5 ml/minute: firstly PBS containing 0.02% sodium nitrite for 3 minutes, then 2% paraformaldehyde (PFA) in 0.1 M sodium acetate buffer (pH 6.5) for 6 minutes, and lastly 2% PFA in 0.1 M sodium borate buffer (pH 8.5) for 18 minutes. The brains were left "*in situ*" overnight at 4°C, carefully removed from the skull, and post-fixed for 12-16 hours in 2% PFA in 0.1 M sodium borate buffer (pH 8.5) at 4°C, then sliced using a Leica VT1000 S vibratome. Free-floating coronal hippocampal sections (50 μm) were collected and stored in PBS + 0.02% sodium azide in sterilized, non-treated 24-well plates (CELLTREAT Scientific Products, part No. 229524) at 4°C.

Immunohistochemistry

Upon immunostaining, free-floating sections were transferred to sterilized, non-treated 6-well or 12-well plates (CELLTREAT Scientific Products, part No. 229506, 229512) with each well containing 5 ml or 3 ml of 25 mM Tris buffered saline (TBS), respectively. Sections were first treated with 50 mM glycine containing 0.01% Triton X-100 and 0.01% NP-40 for 30 minutes to reduce background staining and permeabilize the tissue**,** washed 3 x 15 minutes in TBS containing 0.05% bovine serum albumin (TBS-BSA), then blocked for 1 hour at room temperature (RT) in TBS-BSA containing 1% normal donkey serum (NDS; Jackson ImmunoResearch Laboratories Inc., catalog No. 017-000-121) plus unconjugated donkey anti-rabbit IgG polyclonal (1:1000; Southern Biotech., catalog No. 6411-01), unconjugated donkey anti-chicken IgY polyclonal (1:1000; Fisher Scientific, catalog No. SA172002) and unconjugated donkey anti-goat IgG polyclonal (1:1000; Southern Biotech., catalog No. 6460-01) to prevent non-specific binding of the secondary antibodies. Sections were then washed 3 x 15 minutes in TBS-BSA and incubated overnight on an orbital shaker with the primary antibodies in TBS-BSA + 0.25% NDS at RT as listed below: rabbit polyclonal anti-RFP (1:5000; Abcam, catalog No. ab62341), goat polyclonal anti-DCX IgG (1:3000; Santa Cruz Biotechnology, Inc., catalog No. sc8066), and chicken polyclonal anti-NeuN IgY (1:5000; EMD Millipore, catalog No. ABN91).

On the next day, the sections were washed 3 x 15 minutes in TBS-BSA and blocked for 15 minutes in TBS-BSA + 0.25% NDS before incubation with the following secondary antibodies at RT for 1 hour: donkey anti-rabbit IgG (H & L) Alexa Fluor Plus 594 (1:1000; Thermo Fisher Scientific, catalog No. A32754), donkey anti-goat IgG (H & L) Alexa Fluor Plus 680 (1:1000; Thermo Fisher Scientific, catalog No. A32860) and donkey anti-chicken IgG (H & L) Biotin-SP (1:1000; EMD

Millipore, catalog No. AP194B). Sections were then washed 3 x 15 minutes in TBS and reacted with Alexa Fluor 405, 488, or 680 streptavidin conjugates (1:1000; Thermo Fisher Scientific, catalog No. S32351, S32354, and S32358 respectively) for another hour. Afterwards, sections were rinsed again 3 x 15 minutes in TBS, mounted onto Fisherbrand Superfrost Excell microscope slides (Fisher Scientific, catalog No. 22-037-247), air-dried overnight and cover-slipped (Thermo Scientific Signature Series Cover Glasses; Thermo Fisher Scientific, catalog No. 22-050-232) with either FluorSave Reagent (EMD Millipore, catalog No. 345789) or ProLong Diamond Antifade (Thermo Fisher Scientific, catalog No. P36970). Finally, the samples were allowed to cure overnight before the edges of each cover slip were sealed with clear nail polish, and imaged using a Nikon A1 confocal microscope. All acquired images were adjusted for optimal brightness/contrast in ImageJ. Cell counting was performed using the ImageJ Cell Counter plugin.

Post-hoc biocytin staining and imaging of abDGCs

For abDGC dendritic morphology reconstruction, biocytin was included in the internal solution (5 mg/ml) in the patch pipette in some recordings. After 15-30 min of dialysis, pipette was carefully withdrawn leaving the cell body intact. Slice containing the biocytin-filled abDGC was then treated with 4% PFA/PBS overnight at 4°C, washed 3 x 20 min in PBS, and blocked with 0.4% Triton X-100 plus 1% BSA and 5% NDS in PBS for one hour at RT. Slice was then incubated with streptavidin-conjugated Alexa 488 or 555 (1:500) in blocking buffer (PBS containing 1% BSA, 5% NDS and 0.2% Triton X-100) for 45 min (rocking at RT), rinsed in PBS for 3 x 5 min, and mounted in ProLong Diamond Antifade Mountant for confocal imaging. Z-stacks of all biocytin-filled abDGCs were acquired using a Nikon A1 confocal microscope, and cells with z-axis range < 25 µm were discarded. Analysis of total dendritic length and number of branch points

were performed in the Imaris software (Bitplane) using a combination of auto-path and auto-depth filament tracing modes.

2.5 Behavioral studies

The retroviral approach of restricting Cre recombinase expression in abDGCs is a powerful tool for birth-dating and manipulating individual abDGCs within the hippocampal network, however it is not suitable for behavioral studies since only a limited number of dividing cells can be infected/labeled by retroviruses at a time. To target a larger cohort of abDGCs in a temporally defined manner, a previously validated Ascl1^{CreERT2} mouse line can be used to tag and induce genetic Cre expression in all adult neural stem cells and their lineage upon tamoxifen exposure (Yang et al., 2015). In this project, 8-9 weeks old Ascl1^{CreERT2};*Grik2*f/f;Ai9 and Ascl1^{CreERT2};*Grik2*$^{+/+}$;Ai9 mice received tamoxifen treatment were used for all behavioral assays to test whether there is any behavioral consequence(s) in concurrence with altered functional properties of young abDGCs in conditional GluK2 KO mice. To activate Cre recombinase activity, all mice received daily tamoxifen (Sigma-Aldrich, #T5648) IP injections (180 mg/kg/d, dissolved in 10% EtOH/90% sunflower seed oil) for 5 consecutive days or an equivalent 10-day TAM diet (Envigo, TD. 130858).

Object location memory

The novel object location memory (OLM) test was performed similarly to a previously published protocol (Vogel-Ciernia and Wood, 2014) 21-23 days after TAM induction. Prior to OLM training, animals were habituated to handling by the experimenter 2-5 min daily for 5 days and the testing chamber (33 cm x 33 cm x 35 cm) 5 min daily for 3 days. On OLM training day (21-22 dpi), two

identical objects (randomized from red cuboids, 5.5 x 5.5 x 7.5 cm; blue cuboids, 3 x 3 x 19 cm; and blue cylinders, 7.5 x 7.5 x 7.5 cm) were placed symmetrically relative to a black marking strip inside the testing chamber, and animals were allowed to freely explore both objects for 10 minutes. Mice were gently put back to their home cages and transferred to the animal holding room, and returned for testing 24 hours later, when one of the objects had been moved to a novel location inside the chamber. Animals were allowed to explore both objects for 5 mins. Preference for the novel object location was assessed by the discrimination index (DI) which is calculated as follows: (time exploring object at the novel location - time exploring object at the familiar location) / (time exploring novel + familiar locations) *100. Animals that had DI more than ± 20 during training were considered to have a significant location bias thus were excluded from later analysis. All activities of animals were video recorded, tracked and analyzed using EthoVision XT (Noldus).

Trace fear conditioning and contextual fear memory

Trace fear conditioning test was performed in sound attenuated chambers at the Northwestern University Behavioral Phenotyping Core according to a previous study (Farley et al., 2011). On the training day (21-23 dpi), animals were presented with three pairings of the CS (30 s of pulsed white noise at 5 Hz, 5 ms rise/fall, 75 dB), and a US (a 1 s, 0.7 mA scrambled shock to the cage floor) in fear conditioning cages (30 x 25 x 30 cm, with stainless steel rods on the cage floor for foot shock delivery and scented with 70% EtOH under dim lighting of ≈10 lux). The CS and US were separated by a 20 s trace interval, and the inter-trial interval was 410 s. 24 hours later, animals were reintroduced to the original training context for 5 minutes in the absence of CS/US, and contextual fear memory was accessed by scoring freezing during the first 180 s period. Three hours later, trace fear memory was tested. Animals were placed in a novel context (40 x 50 x 20 cm cage

with a smooth polypropylene floor and scented with Windex® Original under a different lighting of ≈30 lux) for 180 s, then they were presented with the CS for a duration of 60 s. Freezing percentage was calculated for a 180-s baseline (no CS) period, a 60-s CS period, and as well as a 20-s trace period immediately following the CS. All behavior was video recorded, and freezing time was scored automatically using FreezeFrame 4 (Actimetrics), then reviewed by the experimenter blind to the animal genotype. Freezing behavior was defined as pause of movement except for breathing for a minimum period of 1 s. All fear conditioning and novel context cages were cleaned with 70% EtOH and Windex® Original respectively between usage of each mouse to remove olfactory cues from previous animal.

Two-choice spatial discrimination pattern separation task

Pattern separation was evaluated in a two-choice spatial discrimination task using a homemade apparatus similar to the one described in a previously published study (Clelland et al., 2009). All total 16 adult mice (8-9 weeks old) used for this experiment were treated with 5-day TAM IP injections and housed in a reverse light cycle holding room two days after the last day of TAM injection (two weeks prior to the first day of shaping). Animals had ad libitum access to food but could only obtain water as rewards during the behavioral test; other times animals were water-deprived throughout the study. The body weight of each individual mouse was monitored daily to ensure that weight loss did not exceed 20% of pre-testing weight. All tests were conducted during the dark phase of the light-dark cycle for the mice in a room with minimized light between 1 p.m. and 5 p.m.

The testing apparatus consisted of a solid dark grey PVC chamber (22 x 15 x 20 cm) fitted with an infrared touchscreen, an automated self-positioning water supply device, a green LED light as reward cue located 1 cm below a slit through which water was delivered, an infrared LED light and camera for head entry (mouse consuming water) detection, and four white LED lights (for punishment) on the chamber roof. A solid dark grey PVC "mask" containing 1 window (10 x 6.5 cm, for shaping) or 2 identical windows (3 x 6.5 cm each, aligned, spaced by a varying distance for two-choice spatial discrimination) was positioned approximately 1.5 cm above the mouse wood-chip bedding in front of the touchscreen to create an illuminated panel(s) as the touch stimulus(i) on the screen. The infrared sensor (AirBar, Neonode) attached to the IPS screen (10.1 inch) enabled nose poke detection without the need for force, and the water reward (2 s) was cued by the blinking green LED light. Mouse bedding was mixed and distributed evenly on the chamber floor before each testing session, and separate bedding was used for male and female mice.

All mice were handled for 4 min prior to experimenting, then pre-trained to use the touchscreen system over a 5-day shaping period (16-20 dpi) in the operant chamber where they learned to obtain a 2-s water reward by touching any part of a single illuminated panel on the screen and associate water delivery with the blinking green light. The inter-trial interval during the shaping session was 1 s. The following rules applied to all testing sessions: the 1st reward was provided to each mouse at the beginning of each session, which ended when animals had made 80 correct touches (a total water supply of 160 s) or 150 min had passed, whichever occurred first. When animals did not achieve 80 correct touches within 150 min, they were allowed to drink water through the slit with the green light blinking at the end of the testing session for an extra appropriate amount of time to ensure that each mouse received a total of 160 s daily water supply. Failure to

complete 80 correct trials within 150 min occurred in a total of 22 of 176 sessions (12 times from the control group and 10 times from the Ascl1cKO group).

On 21 dpi, mice were placed in the operant chamber to distinguish two illuminated panels with a high degree of separation (distance between the centers of two panels = 15 cm), and mice were only rewarded for touching the correct panel, which was randomly assigned between left and right at the beginning of the session. When the mouse made a correct touch, the green LED light would start to blink, and the water bottle would simultaneously turn to a position close to the operant chamber so that the mouse could enter its head into a slit to reach the sipper and start drinking. After the mouse head entry had been detected for 2 s, the green light went off, and the water bottle automatically turned back to its original position, making the sipper unreachable for the mouse. If the mouse touched the wrong panel, the water bottle would turn to a position away from the operant chamber, and meanwhile the mouse would receive a bright white light-on punishment for 15 s. The inter-trial interval during the two-choice spatial discrimination session was 5 s. The correct panel position remained unchanged until the mouse touched the correct panel 7 times in the latest 8 consecutive trials. Once the mouse achieved the criterion, the correct and incorrect positions were switched, i.e., a reversal between the correct and incorrect panel occurred such that the previous incorrect panel was designated as correct. On the next day (22 dpi), mice were required to distinguish between two illuminated panels with a low degree of separation (distance between the center of two panels = 7.5 cm) with everything else remained the same. All animals were tested alternately between high and low separation mode by day for a total of six days for the evaluation of pattern separation performance.

Three analyses were used for evaluating pattern separation performance: reversal number, correct rate, and trials to criterion. Only reversals in which the mouse reached criterion were counted towards the reversal number, and the last incomplete reversal that the mouse was on at the end of a session was excluded from the correct rate analysis. For trials to criterion analysis, the greater value of the following two calculations was used: the first calculation which excluded the last incomplete reversal, and a second conservative estimate, which was calculated as if the mouse completed the last incomplete reversal with a minimum possible number of additional trials.

2.6 Statistical analysis of data

All statistical analyses were performed in Microsoft Excel and OriginPro software. For all independent comparisons, statistical significance was assessed by the nonparametric Mann-Whitney U test. For comparing multiple-trial data sets including the input-output curve (number of APs in response to increasing current injections), % freezing during the trace fear conditioning test, and pattern separation performance, two-way repeated measures ANOVA was applied. Nonparametric comparisons of the cumulative distributions of spontaneous and miniature postsynaptic current inter-event intervals and amplitudes were made by the Kolmogorov-Smirnov test. Differences were considered significant when $p \leq 0.05$. All data are reported as mean ± SEM.

Chapter 3 – Results: Cellular Phenotypes Due to Loss of KARs

3.1 Young abDGCs display KAR-mediated currents

To follow the development and maturation of abDGCs we used a retroviral labeling strategy which allows dividing cells in the SGZ to be selectively labeled and accurately birth-dated (Tashiro et al., 2006b). Injection into the SGZ of a retrovirus packaged with GFP (RV-GFP) or RFP (RV-RFP) or GFP-IRES-Cre (RV-GFPCre) under a CAG promoter resulted in fluorescently labeled birth-dated abDGCs that could be visualized and targeted for patch clamp recordings at various days-post-injection (dpi) in acute slices (Figures 3.1A-B and 3.2A-B) (Tashiro et al., 2006a, 2006b). We first determined that KAR-mediated currents are present on developing abDGCs in wild-type mice by recording from virally labeled neurons in the dentate gyrus and applying the KAR agonist domoate (10 μM) in the presence of antagonists of AMPARs (GYKI 52466, 50 μM), NMDARs (D-APV, 50 μM) and $GABA_A$Rs (Bicuculline, 10 μM). We found that domoate elicited a small KAR-mediated current in most of the recordings from 14 dpi labeled abDGCs, and increasingly larger currents in almost all recordings from 21 and 28 dpi labeled abDGCs (Figure 3.1C). In a separate set of recordings, we induced KAR-mediated currents by applying domoate (1 μM) in the presence of GYKI 52466 (50-100 μM), D-APV (50 μM), Bicuculline (10 μM) and Tetrodotoxin (Na^+ channel blocker, 1 μM). In comparison, domoate-induced currents were completely eliminated in all recorded neurons (21-28 dpi) in constitutive $GluK2^{-/-}$ (KO) mice indicating that the GluK2 subunit is the primary obligatory KAR subunit expressed in abDGCs (Figures 3.1D-E).

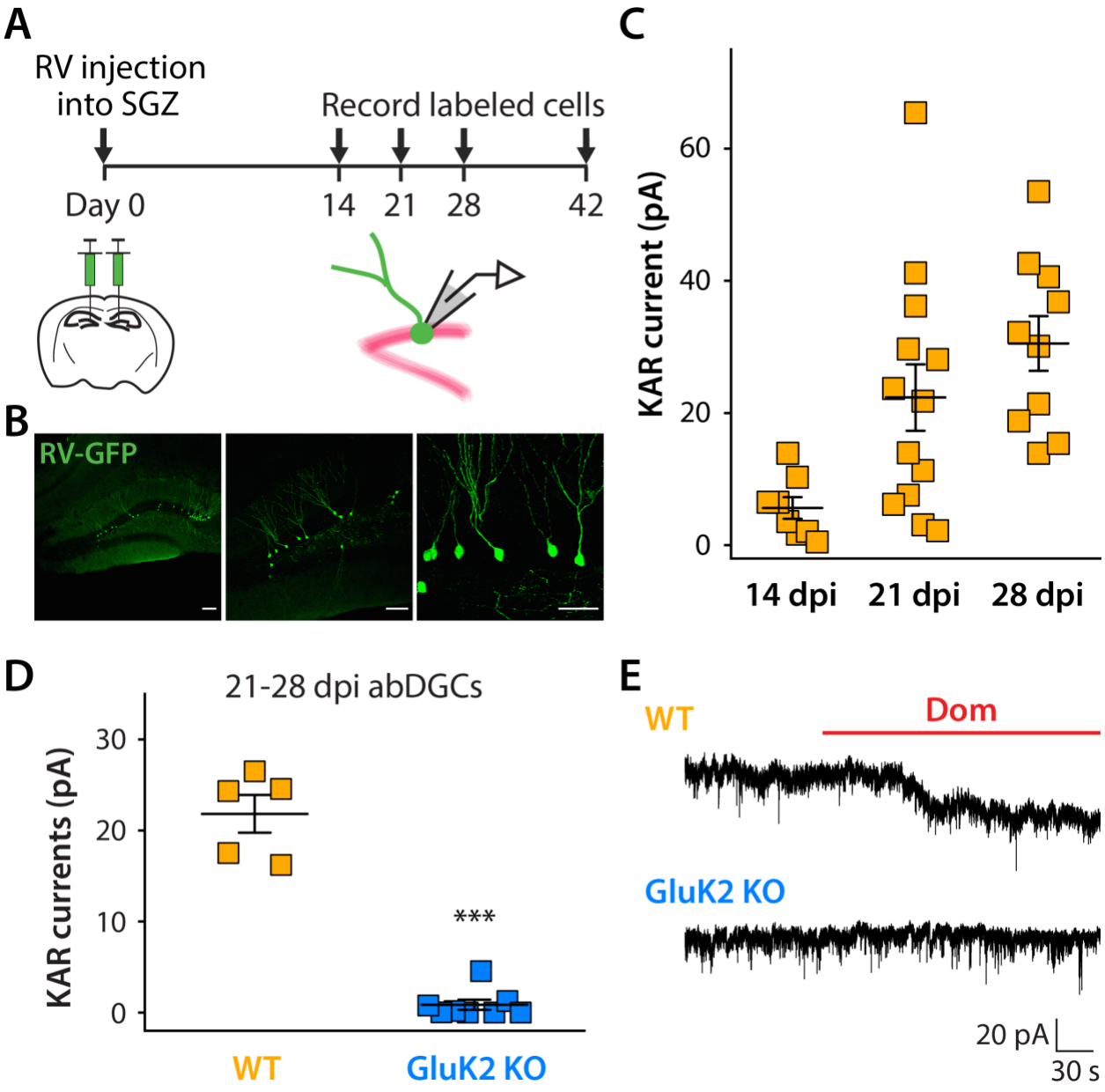

Figure 3.1 Young abDGCs display kainate receptor-mediated currents that are eliminated in the GluK2 KO mice

(A) Schematic illustration of the experimental paradigm: retrovirus carrying a GFP or RFP vector was delivered to the subgranular zone of the dentate gyrus in 8-10 week old mice. Labeled cells were recorded at various days post injection (dpi). **(B)** Representative confocal images showing GFP-expressing (green) abDGCs from a 28 dpi WT mouse. Scale bars: 50 μm. **(C)** KAR-mediated currents in abDGCs (orange) in the WT mice increase progressively with age. **(D)** KAR-mediated currents are eliminated in young abDGCs in the GluK2 KO mice. **(E)** Example recording traces representing 1 μM domoate-induced KAR currents in a 28 dpi WT and GluK2 KO abDGC, respectively. Data are presented as mean ± SEM. Statistical analysis: Mann-Whitney U test; *** indicates $p < 0.001$.

To determine whether a conditional KO strategy for GluK2 would likewise eliminate KAR-mediated currents selectively in birth-dated abDGCs we injected RV-RFP and RV-GFPCre retroviruses into the SGZ of each hemisphere in floxed *Grik2* (*Grik2*f/f) mice (Marshall et al., 2018) to compare both GluK2 knockout (RV-GFPCre) and control (RV-RFP) abDGCs (Figures 3.2A-B). We recorded domoate-induced currents and validated that RV-mediated transduction caused the specific ablation of functional KARs in Cre-expressing GFP-positive abDGCs at all the analyzed time points: 14, 21, 28 and 42 dpi (Figures 3.2C-D). In addition, we also recorded KAR-mediated currents from surrounding unlabeled mature DGCs located in the middle zone (Z2) of the granule cell layer (GCL) and the values were similar to those of 42 dpi control abDGCs (Figure 3.2C). Taken together this demonstrates that KARs containing the GluK2 subunit are expressed during early postmitotic development of abDGCs in the adult hippocampus.

Kainate receptors of the low (GluK1-3)- and high (GluK4-5)-affinity subunits form heteromeric complexes in vivo (Contractor et al., 2011). It is likely that KARs in the DG contain multiple subunits including GluK2, which is essential for functional expression, and also GluK4/5. In additional recordings from birth-dated abDGCs in mice in which the high-affinity GluK4 subunit was ablated (constitutive GluK4$^{-/-}$), we observed a domoate-induced current that was of similar magnitude to recordings in WT mice (Figure 3.3). Together, these results demonstrate that KARs are functionally expressed in young abDGCs and that the GluK2 subunit is the obligatory subunit for functional KARs in newborn neurons in the adult hippocampus.

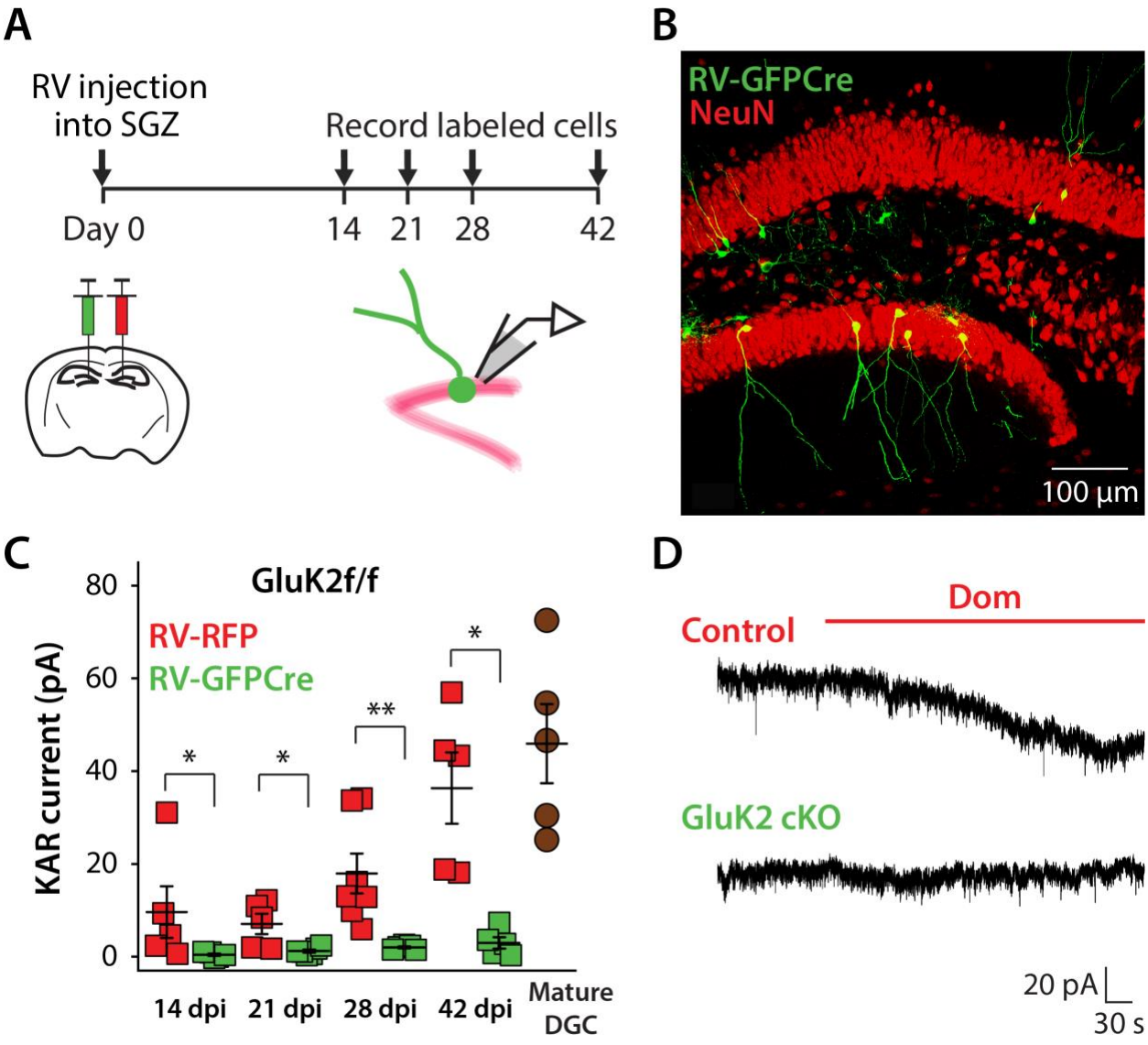

Figure 3.2 GluK2-containing KARs are present in young abDGCs
(A) Schematic illustration of the experimental paradigm: retrovirus carrying an RFP or GFP-IRES-Cre vector was delivered to the subgranular zone of the dentate gyrus in 8-10 week old mice. Labeled cells were recorded at various days post injection (dpi). **(B)** Representative confocal image showing GFP-IRES-Cre-expressing (green) abDGCs from a 28 dpi *Grik2*f/f mouse. NeuN immunofluorescence is shown in red. **(C)** Cre-mediated deletion of GluK2 in Grik2f/f mice results in loss of KAR-mediated current in abDGCs at all time points post injection. **(D)** Example recordings of 1 μM domoate-induced currents in a 28 dpi control and GluK2 cKO abDGC, respectively. Data are presented as mean ± SEM. Statistical analysis: Mann-Whitney U test; * indicates $p < 0.05$; ** indicates $p < 0.01$.

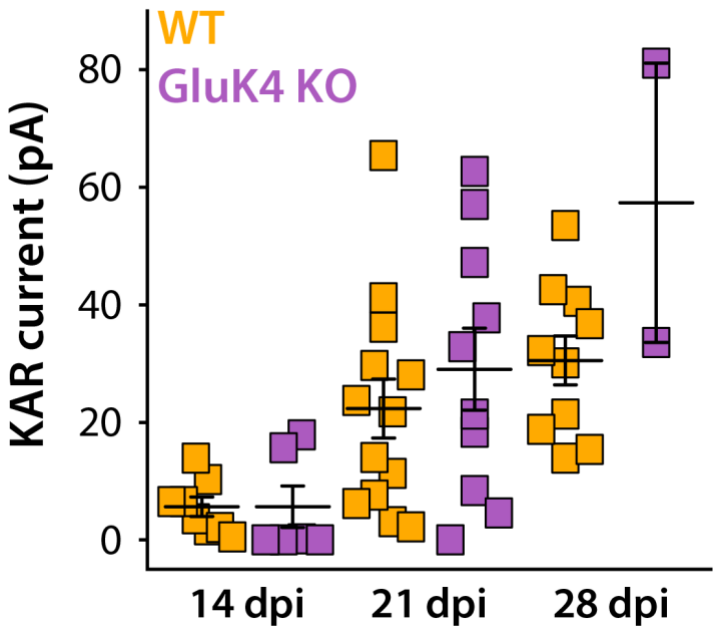

Figure 3.3 GluK4 is not required for the expression of functional KARs in young abDGCs
KAR currents in abDGCs increase progressively with age in the GluK4 KO (purple) and GluK4 WT (orange) mice with similar magnitudes. Retrovirus carrying an RFP or GFP vector was delivered to the SGZ of the dentate gyrus in 8-10 week old GluK4 KO and littermate control mice to birth-date and fluorescently label abDGCs, which were recorded at 14, 21, and 28 dpi respectively. KAR-mediated currents were induced by bath application of 10 μM domoate in the presence of 50 μM GYKI (AMPAR antagonist), 50 μM D-APV (NMDAR antagonist), and 10 μM BIC ($GABA_AR$ antagonist). Data are presented as mean ± SEM. Statistical analysis: Mann-Whitney U test.

3.2 Passive and active membrane properties of young abDGCs during an early critical period are disrupted by ablation of GluK2

To determine whether loss of KARs affects abDGC properties we measured several morpho-functional parameters of maturation in GluK2 cKO neurons during a critical time period of 14-42 dpi for their development and as well as in 21-42 dpi abDGCs in global GluK2 KO mice (Ge et al., 2007; Tashiro et al., 2007).

Lower input resistances in 21 dpi GluK2-ablated abDGCs

As has been demonstrated previously (Mongiat et al., 2009), young neurons possessed high input resistances (R_{in}) that decreased as they matured over time (Figures 3.4A and 3.5). However, we found that the R_{in} was significantly lower in 21 dpi GluK2 cKO abDGCs in comparison to the control young neurons (Figure 3.4A). This lower input resistance also correlated with a higher measured rheobase in cKO neurons specifically at 21 dpi (Figure 3.4B).

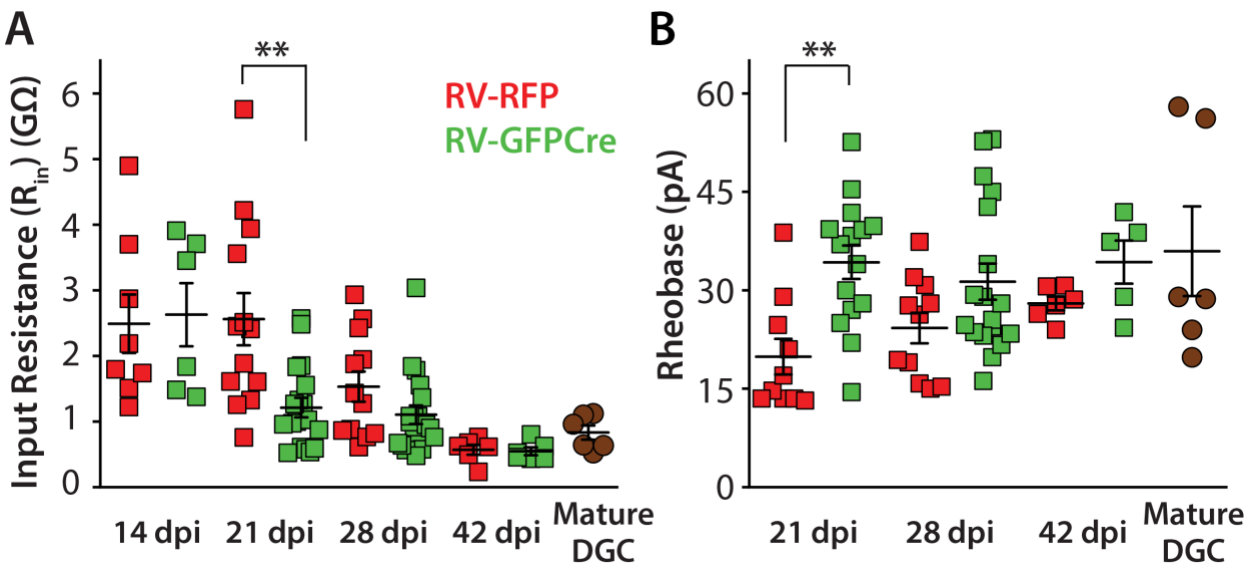

Figure 3.4 Development of intrinsic properties is altered in 21 dpi GluK2 cKO abDGCs
(A) Input resistances (R_{in}) of developing GluK2 cKO abDGCs (RV-GFPCre) compared with control abDGCs (RV-RFP) at 14, 21, 28, and 42 dpi and from unlabeled mature GluK2$^{+/+}$ DGCs in *Grik2*f/f mice. **(B)** Rheobase of developing GluK2 cKO abDGCs compared with controls at 21, 28, 42 dpi and mature DGCs. Significant differences were observed in recordings from 21 dpi abDGCs. Data are presented as mean ± SEM. Statistical analysis: Mann-Whitney U test; ** indicates $p < 0.01$.

In recordings from birth-dated abDGCs in constitutive GluK2 KO mice we saw an even more pronounced effect with significantly lower R_{in} of GluK2 KO neurons at both 21 and 28 dpi (Figure 3.5), demonstrating that this cell-autonomous effect of loss of GluK2 is reproducible across different KO models. The R_{in} of developing abDGCs is a prime indicator of the maturity of the neurons (Schmidt-Hieber et al., 2004;

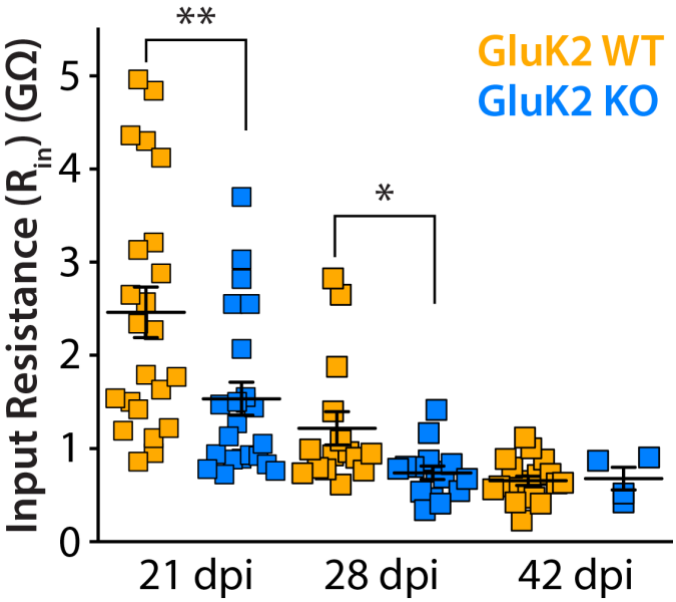

Figure 3.5 Development of input resistance in abDGCs in GluK2 KO mice compared with controls
Input resistances of abDGCs in GluK2 KO and control GluK2 WT mice at 21, 28, and 42 dpi. Data are presented as mean ± SEM. Statistical analysis: Mann-Whitney U test; * indicates $p < 0.05$; ** indicates $p < 0.01$.

Trinchero et al., 2019), thus the lower R_{in} measured in 21 dpi GluK2 cKO abDGCs demonstrates that, surprisingly, loss of GluK2 results in abDGCs with the intrinsic property of more mature newborn neurons.

Increased excitability in 21 dpi GluK2-ablated abDGCs

Newborn neurons also mature in their ability to fire repetitive action potentials as their intrinsic conductances change during development (Mongiat et al., 2009; Schmidt-Hieber et al., 2004). We therefore measured the AP firing capacity of birth-dated abDGCs in response to supra-threshold current step injections. In particular, at 21 dpi GluK2 cKO neurons supported the firing of more APs in response to increasing current, whereas control neurons of this postmitotic age fired only approximately five APs on average at the highest current injection (Figures 3.6A-B). This effect on AP firing properties was pronounced at 21 dpi and no difference was observed in either younger neurons at 14 dpi or more mature neurons at 28 and 42 dpi (Figures 3.6C-F). Elevated firing is surprising given the lower input resistance of 21 dpi GluK2 cKO abDGCs compared with controls, but may reflect the elevated expression of potassium conductances that could reduce the depolarization block of AP firing and also contribute to lower input resistances in relatively more mature cells (Espósito et al., 2005; Mongiat et al., 2009).

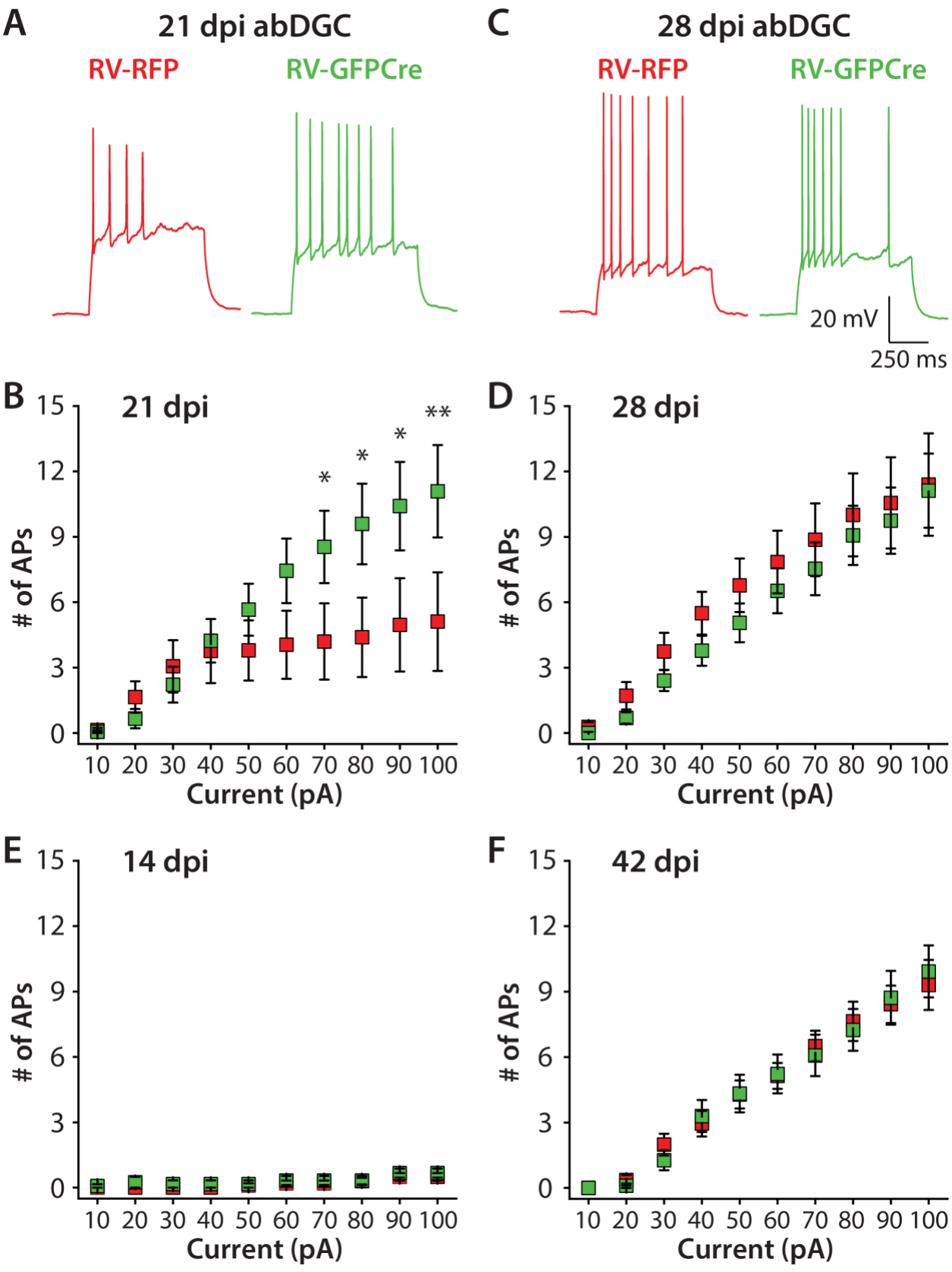
A
21 dpi abDGC
RV-RFP
RV-GFPCre
C
28 dpi abDGC
RV-RFP
RV-GFPCre
20 mV
250 ms
B
21 dpi
# of APs
Current (pA)
D
28 dpi
# of APs
Current (pA)
E
14 dpi
# of APs
Current (pA)
F
42 dpi
# of APs
Current (pA)

Figure 3.6 Development of AP firing properties is altered in 21 dpi GluK2 cKO abDGCs
(A) Example AP firing profiles of 21 dpi control (RV-RFP) and cKO (RV-GFPCre) abDGCs in response to a 70 pA current injection step of a duration of 800 ms. **(B)** AP response properties across a range of current injections in 21 dpi control and cKO abDGCs. Significant increases in number of APs were observed at current injection steps between 70-100 pA in 21 dpi GluK2 cKO abDGCs (RV-RFP, n = 14; RV-GFPCre, n = 16). **(C-D)** Example AP firing traces and input-output AP response of 28 dpi control and GluK2 cKO abDGCs (RV-RFP, n = 12; RV-GFPCre, n = 18). **(E-F)** Input-output AP responses of 14 and 42 dpi abDGCs, respectively. Data are presented as mean ± SEM. Statistical analysis: two-way repeated measures ANOVA; * indicates $p < 0.05$; ** indicates $p < 0.01$.

Consistent with these findings in cKO neurons, birth-dated abDGCs recorded in constitutive GluK2 KO mice also had the same increased AP firing capacity in response to current injections specifically at 21 dpi (Figure 3.7A). Moreover, at 28 dpi when control abDGCs normally displayed elevated excitability compared with 21 and 42 dpi neurons (Figure 3.7), 28 dpi abDGCs in GluK2 KO mice showed a marked reduction in AP firing that resembled more mature, 42 dpi control abDGCs (Figures 3.7B-C). Taken together, our recordings from both GluK2 cKO abDGCs and GluK2 KO mice suggest that the excitability of abDGCs is increased at an early point during their critical period in the absence of GluK2.

Additionally, in both conditional (cKO) and constitutive GluK2 KO mice we also measured the resting membrane potential (RMP) of abDGCs, which became more hyperpolarized at increasing postmitotic times (Figures 3.8A-B). Interestingly, we found a significantly more depolarized RMP in 21 dpi GluK2 cKO abDGCs compared with the controls (Figure 3.8A), but did not observe a genotype-dependent effect on this parameter in the constitutive GluK2 KO mice (Figure 3.8B). Here the change in RMP in 21 dpi GluK2 cKO abDGCs is not in accordance with a more mature neuronal profile. Given that the development of action potential threshold is not altered in abDGCs in either GluK2 cKO or constitutive GluK2 KO mice (Figures 3.8C-D), this cell-autonomous only effect on RMP at 21 dpi might further contribute to the increased excitability of GluK2 cKO

abDGCs at this particular postmitotic age. Nevertheless, a caveat of the RMP measurement is that the accuracy is particularly sensitive to the seal resistance (R_{seal}) for neurons that have a relatively high R_{in} (Heigele et al., 2016). Since we did not routinely measure R_{seal} when making recordings and could not absolutely guarantee that R_{seal} was at least 5 times larger than R_{in}, the real value of resting membrane potential could be more negative in both knockout and WT abDGCs, especially when their input resistances were over 1 GΩ.

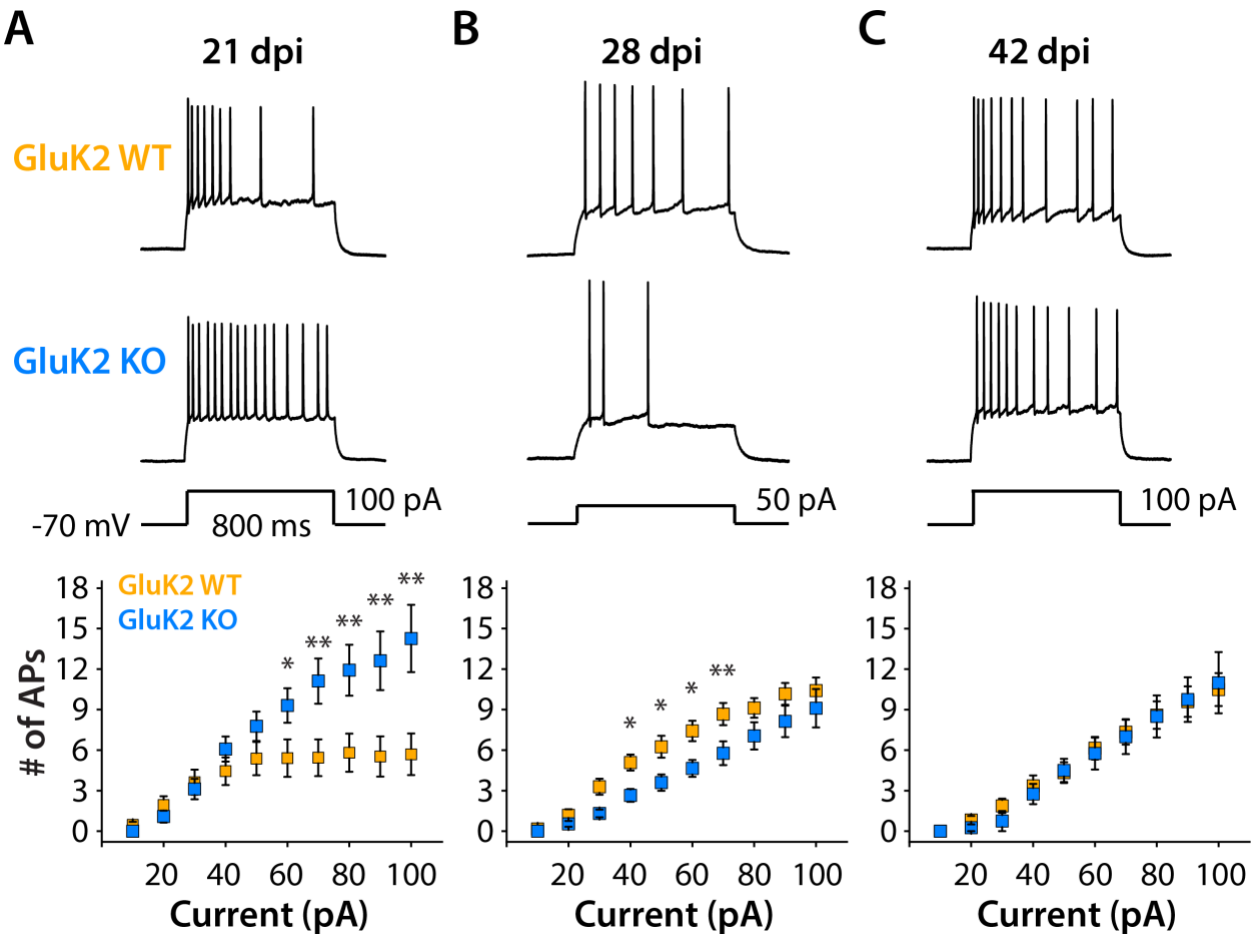

Figure 3.7 AP firing properties of young abDGCs in GluK2 KO mice
Representative traces of APs in GluK2 WT (top) and GluK2 KO (middle) abDGCs in response to current steps and input-output curves (bottom) at 21 dpi **(A)** (WT, n = 16; KO, n = 13), 28 dpi **(B)** (WT, n = 12; KO, n = 13) and 42 dpi **(C)** (WT, n = 14; KO, n = 5), respectively. Significant differences in AP numbers were detected at current steps between 60-100 pA in 21 dpi abDGCs and between 40-70 pA in 28 dpi abDGCs. Statistical analysis: two-way repeated measures ANOVA; * indicates $p < 0.05$; ** indicates $p < 0.01$.

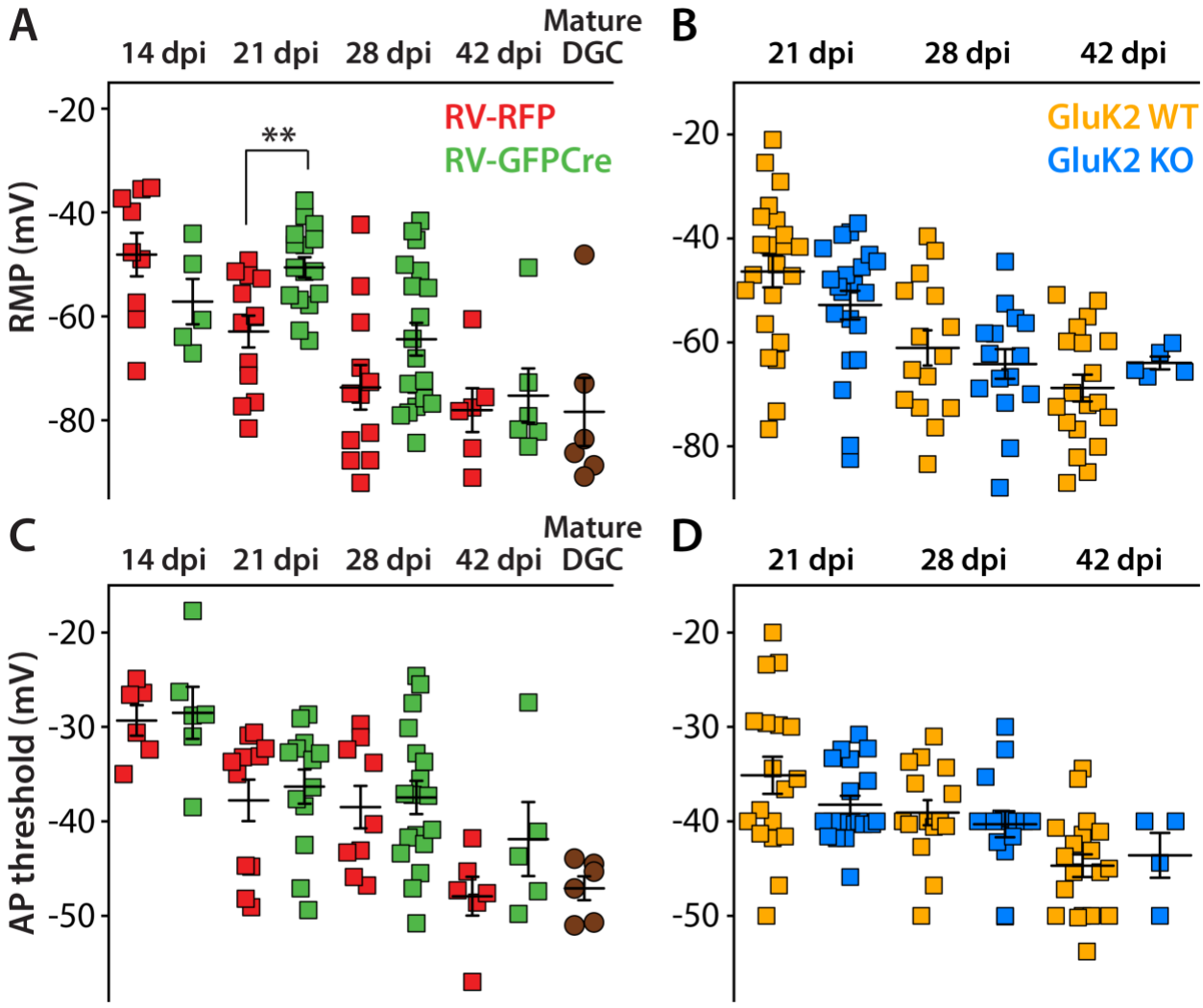

Figure 3.8 Development of resting membrane potentials and action potential thresholds in young GluK2-ablated abDGCs
(A) Resting membrane potential (RMP) of developing GluK2 cKO abDGCs (RV-GFPCre) compared with control neurons (RV-RFP) at 14, 21, 28, 42 dpi and unlabeled mature GluK2$^{+/+}$ DGCs in *Grik2*f/f mice. **(B)** RMP of abDGCs in GluK2 KO and GluK2 WT mice at 21, 28, and 42 dpi. **(C)** Action potential (AP) threshold of developing GluK2 cKO abDGCs compared with control abDGCs at 14, 21, 28, 42 dpi and mature DGCs. **(D)** AP threshold of abDGCs in GluK2 KO and GluK2 WT mice at 21, 28, and 42 dpi. Data are presented as mean ± SEM. Statistical analysis: Mann-Whitney U test; ** indicates $p < 0.01$.

Morphological development is unaffected in GluK2-ablated abDGCs

As measures of the morphological development of abDGCs, the total dendritic length and number of branch points were measured at several postmitotic time points in both conditional knockout (cKO) neurons and global KO mice (GluK2 KO). Consistent with previous measurements made

in vivo (Gonçalves et al., 2016), the total dendritic length we found in 21-42 dpi and mature DGCs ranged between 500-2000 µm (Figure 3.9B), which validates the morphological integrity of the dendritic trees of DGCs in our slices. In addition, there was a clear increase in the total dendritic length in abDGCs between 14 dpi and later postmitotic times, with a marked increase between 14 dpi and 21 dpi, then followed by a plateau after 28 dpi (Figures 3.9A-B). Importantly, same as the previous in vivo study (Gonçalves et al., 2016), we also observed that the number of dendritic branch points peaked in 21 dpi control abDGCs compared with neurons of either younger or older postmitotic ages (Figure 3.9C), indicating a process of overgrowth followed by dendritic pruning during the early development of naive abDGCs. However, there was no difference in total dendritic length or in the number of branch points when GluK2 was conditionally ablated in abDGCs (Figures 3.9B-C).

As an alternate measure of morphological transformation of maturing abDGCs, we also classified the localization of neurons in the SGZ and GCL (Espósito et al., 2005). To label neurons and time ablation of GluK2 in a larger population of abDGCs we used a genetic strategy involving use of the tamoxifen (TAM) inducible Ascl1Cre^{ERT2} mouse (Yang et al., 2015) crossed to Ai9 allele (Ascl1tdTom) and GluK2f/f alleles (Ascl1cKO). Quantifying the localization of tdTom labeled neurons in the SGZ and three radially spaced zones of the GCL (Z1 to Z3) (Figure 3.9E) (Espósito et al., 2005) in Ascl1tdTom and Ascl1cKO mice indicated that there was no difference in the localization of abDGCs 21 days after TAM administration in the cohort with GluK2 ablated (Figures 3.9D-E). Furthermore, the percentage of tdTom+ abDGCs that were positive for DCX was not different in Ascl1tdTom and Ascl1cKO mice at 21 dpi (Figures 3.9D and 3.9F).

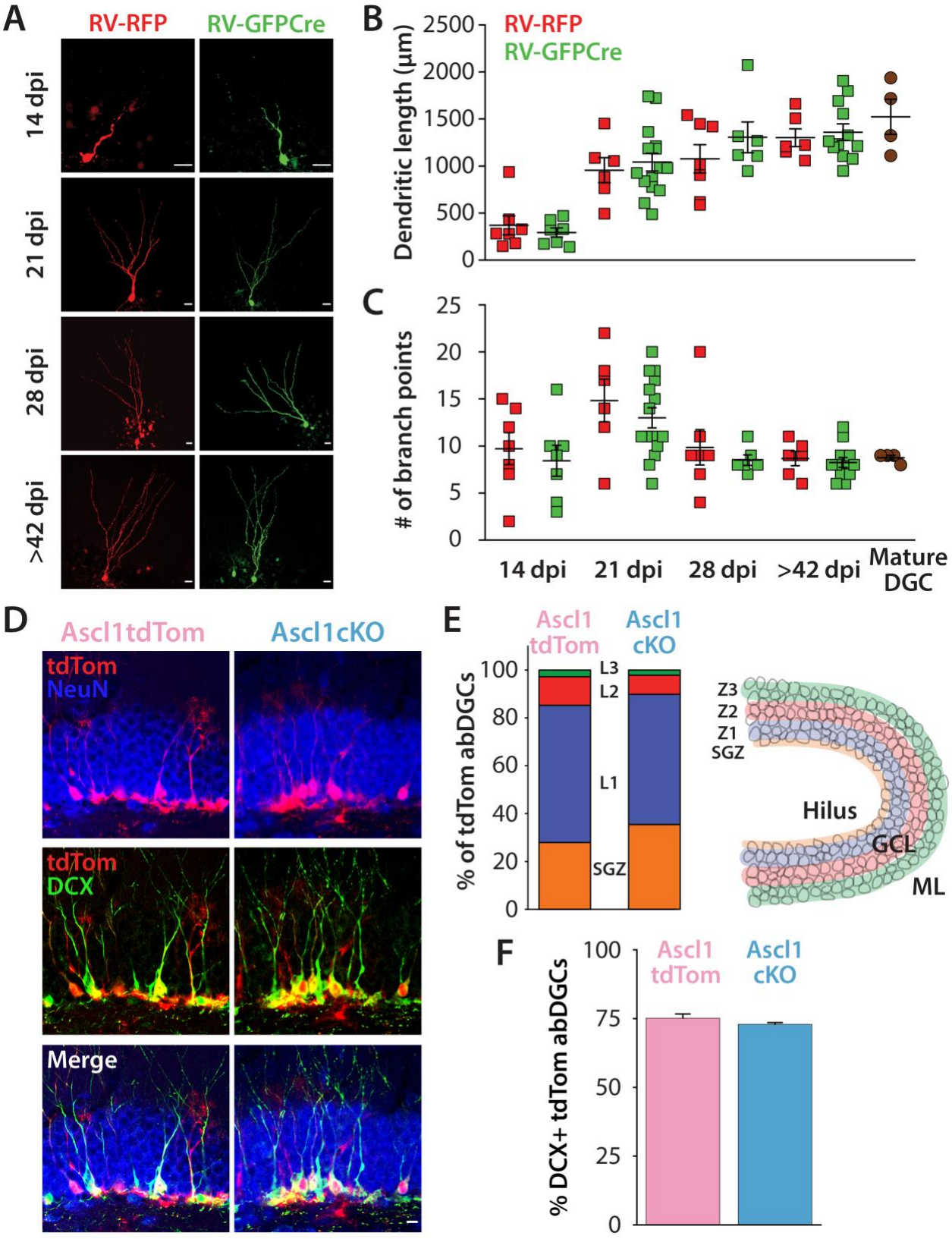
A
RV-RFP
RV-GFPCre
14 dpi
21 dpi
28 dpi
>42 dpi
B
RV-RFP
RV-GFPCre
Dendritic length (µm)
2500
2000
1500
1000
500
0
C
# of branch points
25
20
15
10
5
0
14 dpi
21 dpi
28 dpi
>42 dpi
Mature DGC
D
Ascl1tdTom
Ascl1cKO
tdTom
NeuN
tdTom
DCX
Merge
E
Ascl1 tdTom
Ascl1 cKO
% of tdTom abDGCs
100
80
60
40
20
0
L3
L2
L1
SGZ
Z3
Z2
Z1
SGZ
Hilus
GCL
ML
F
Ascl1 tdTom
Ascl1 cKO
% DCX+ tdTom abDGCs
100
75
50
25
0

Figure 3.9 Morphological development of GluK2 cKO abDGCs
(A) Representative images of biocytin-filled control (RV-RFP) and cKO (RV-GFPCre) abDGCs at several postmitotic dpi stages. **(B)** Total dendritic length of RV-RFP and RV-GFPCre abDGCs at 14, 21, 28, >42 dpi and of unlabeled mature GluK2$^{+/+}$ control DGCs. **(C)** Number of dendritic branch points of abDGCs at each dpi and of mature GluK2$^{+/+}$ DGCs. **(D)** Representative images of abDGCs labeled with tdTom (red), DAPI (blue) and DCX (green) from a cohort of Ascl1tdTom (control) and Ascl1cKO (*GriK2* timed ablation) neurons. In each case the labeled cohort is 21 days old and younger. **(E)** Analysis of radial migration of control and Ascl1cKO abDGCs into the granule cell layers. **(F)** Quantification of co-expression of DCX and tdTom in 21 dpi and younger abDGCs in Ascl1tdTom (control) and Ascl1cKO mice. Scale bars: 15 µm. Error bars indicate SEM. Statistical analysis: Mann-Whitney U test.

We also measured the total dendritic length and number of branch points in 21 and 28 dpi abDGCs in global GluK2 KO mice. Similar to what was observed in GluK2 cKO abDGCs, no significant difference was found in either of these two morphological parameters in GluK2 KO abDGCs compared with GluK2 WT controls (Figure 3.10), suggesting that loss of GluK2 does not have an effect on the morphological maturation of developing abDGCs.

Taken together, ablation of GluK2 has a cell-autonomous effect on the development of the functional intrinsic properties of young newborn abDGCs, and results in their increased abilities to fire APs during a short postmitotic time window 3 weeks after birth. Conversely, there is no observed effect at 21 dpi on the morphological properties that are developing in tandem with the electrophysiological properties of abDGCs. This apparent selective effect on the input resistance and excitability would suggest that GluK2-containing KARs normally regulate abDGC functional properties during an early developmental period.

3.3 Effect of GluK2 ablation on afferent synaptic integration of abDGCs

Because the intrinsic and AP firing properties of abDGCs are altered after GluK2 knockout during the period when synaptic connections are being formed (Ge et al., 2006), we determined the

consequences of GluK2 ablation on abDGC integration into the circuit by recording GABAergic and glutamatergic postsynaptic current events in both GluK2 cKO abDGCs and GluK2 KO mice.

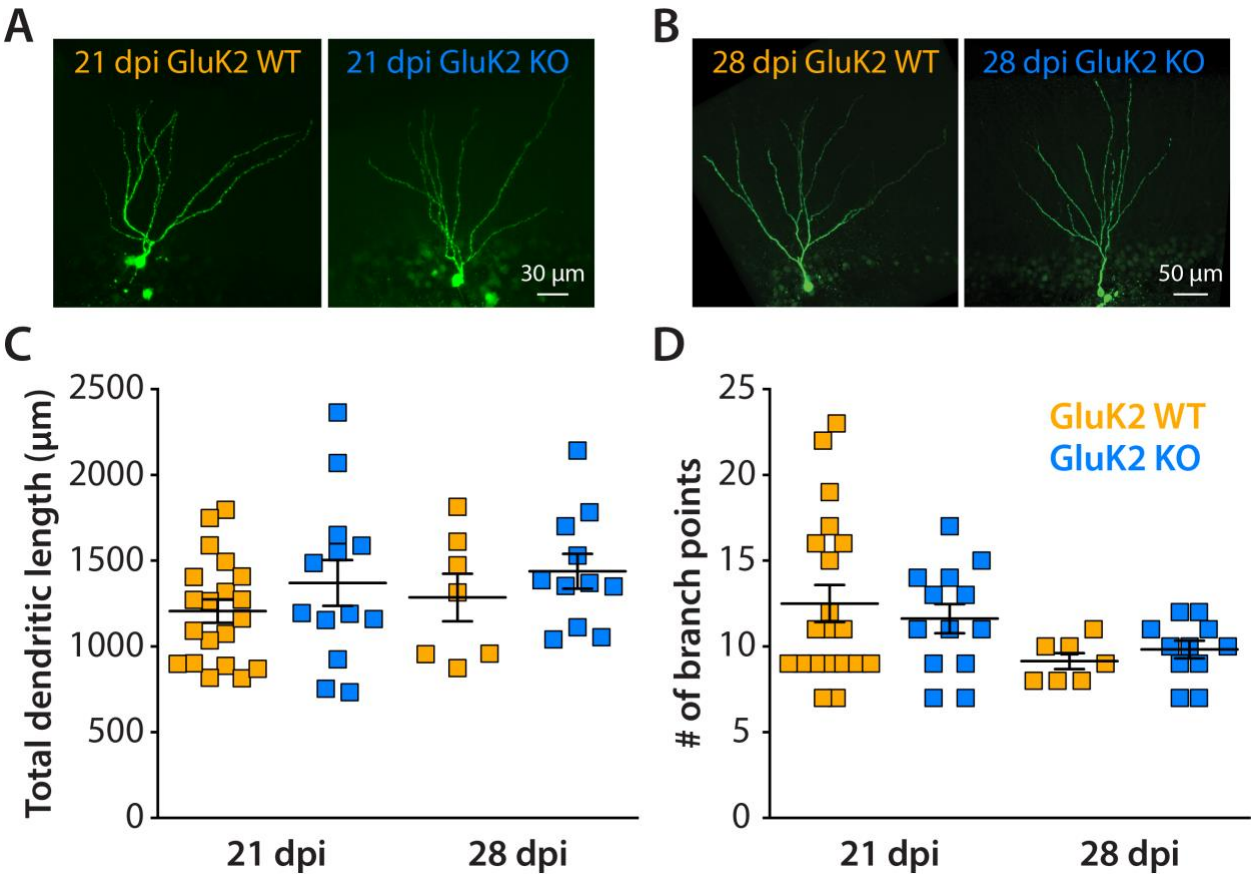

Figure 3.10 Dendritic morphology of abDGCs in GluK2 KO mice
(A-B) Representative images of biocytin-filled GluK2 WT and GluK2 KO abDGC at 21 dpi (A) and 28 dpi (B). **(C)** Grouped data of total dendritic length of GluK2 KO and GluK2 WT abDGCs at 21 and 28 dpi. **(D)** Grouped data of number of dendritic branch points of GluK2 KO and GluK2 WT abDGC at 21 and 28 dpi. Data are presented as mean ± SEM. Statistical analysis: Mann-Whitney U test.

GABAergic synaptic events are elevated in 21 dpi GluK2-ablated abDGCs

Since new abDGCs initially receive GABAergic synaptic inputs (Espósito et al., 2005; Overstreet Wadiche et al., 2005), we first examined spontaneous inhibitory postsynaptic currents (sIPSCs) in abDGCs at several postmitotic time points. In recordings from 14 dpi birth-dated neurons we

observed that the frequency and amplitude of spontaneous events were so low that we could not measure enough events during our recordings to be confident in quantifying the mean amplitude and frequency of sIPSCs to make a comparison between WT and GluK2 cKO abDGCs. A previous paper had also reported very infrequent sIPSC events (0.02 Hz) in abDGCs at 14 dpi (Remmers and Contractor, 2018), therefore we had decided in this study to avoid this early time point. However, we found that the average frequency of sIPSCs was significantly elevated in 21 dpi GluK2 cKO abDGCs (Figures 3.11A and 3.11C); no difference was observed in sIPSC frequency in 28 dpi or older cKO abDGCs (Figure 3.11A). Analysis of the amplitudes of sIPSCs demonstrated that there was also an increase in the mean sIPSC amplitude in GluK2 cKO neurons specifically at 21 dpi but not at other times post injection (Figures 3.11B-C). Cumulative probability plots of sIPSC inter-event interval and amplitude also confirmed that 21 dpi GluK2 cKO abDGCs had more frequent sIPSC events as well as larger sIPSC amplitudes than control abDGCs (Figures 3.11D-E). Moreover, there was no clear increase in release probability of inhibitory synapses and the efficacy of individual synapses was not affected as measured by mIPSC frequency and amplitude at 21 dpi (Figures 3.11F-G).

A similar increase in sIPSC frequency was also found in birth-dated 21 dpi abDGCs in recordings from GluK2 KO mice (Figure 3.12). Together these data demonstrate that there is a specific increase in spontaneous GABAergic synaptic events in 21 dpi GluK2-deficient abDGCs that is likely reflecting an increase in the number of inhibitory synaptic contacts made onto these cells at a critical period of their development.

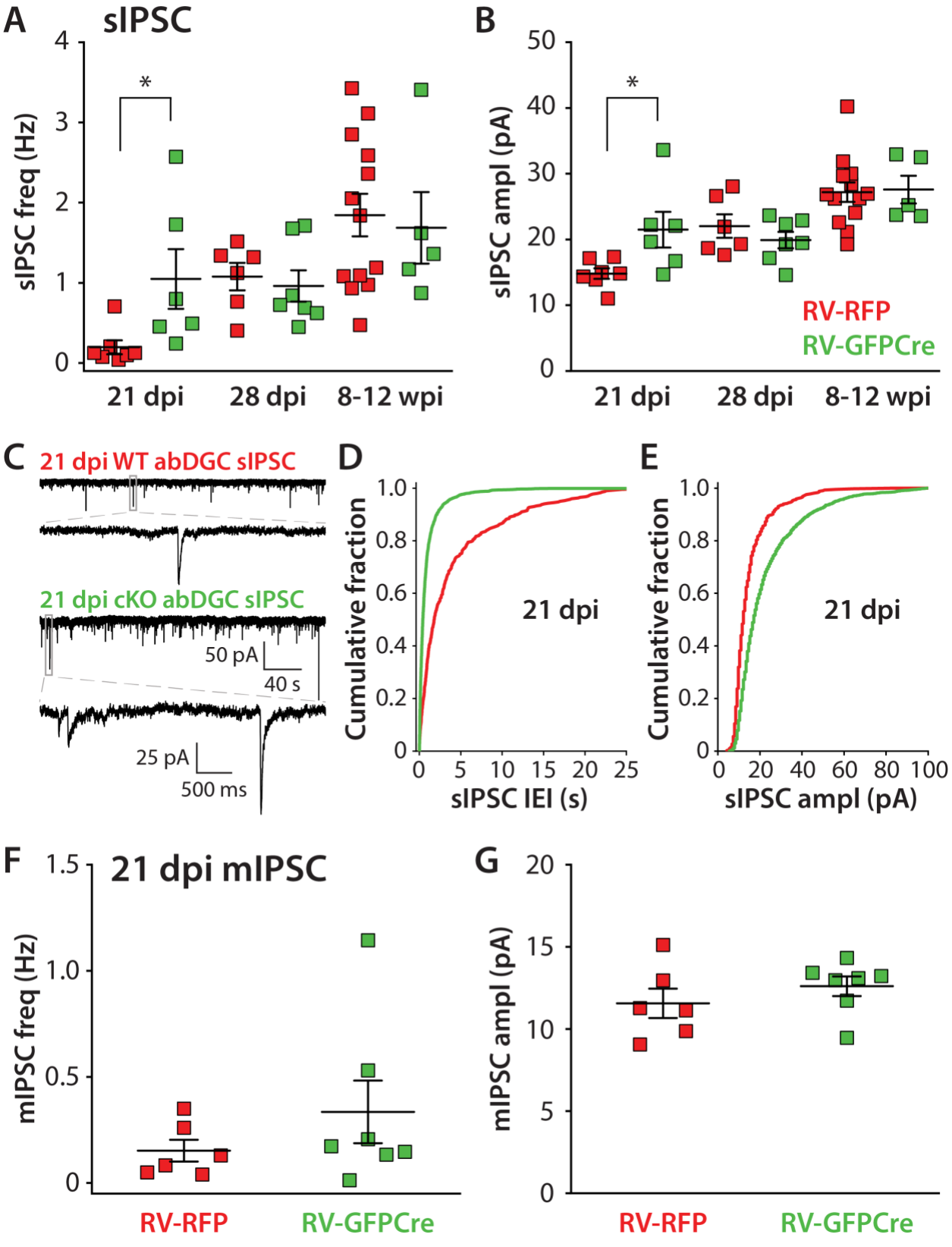
A
sIPSC
sIPSC freq (Hz)
21 dpi
28 dpi
8-12 wpi
B
sIPSC ampl (pA)
RV-RFP
RV-GFPCre
C
21 dpi WT abDGC sIPSC
21 dpi cKO abDGC sIPSC
50 pA
40 s
25 pA
500 ms
D
Cumulative fraction
21 dpi
sIPSC IEI (s)
E
sIPSC ampl (pA)
F
21 dpi mIPSC
mIPSC freq (Hz)
G
mIPSC ampl (pA)

Figure 3.11 GABAergic synapses are elevated in 21 dpi GluK2 cKO abDGCs
(A-B) Average sIPSC frequency and amplitudes in GluK2 cKO abDGCs (RV-GFPCre) and control abDGCs (RV-RFP) at 21 dpi, 28 dpi, and 8-12 wpi. **(C)** Representative traces of sIPSC recorded from a 21 dpi control and GluK2 cKO abDGC, respectively. **(D)** Cumulative fraction of all sIPSC inter-event intervals for 21 dpi GluK2 cKO and control abDGCs. **(E)** Cumulative fraction of all sIPSC amplitudes for 21 dpi GluK2 cKO and control abDGCs. **(F-G)** Average mIPSC frequency and amplitudes in GluK2 cKO abDGCs (RV-GFPCre) and control abDGCs (RV-RFP) at 21 dpi. Data are presented as mean ± SEM. Statistical analysis: Mann-Whitney U test (A, B, F and G) and Kolmogorov–Smirnov test (D and E); * indicates p <0.05.

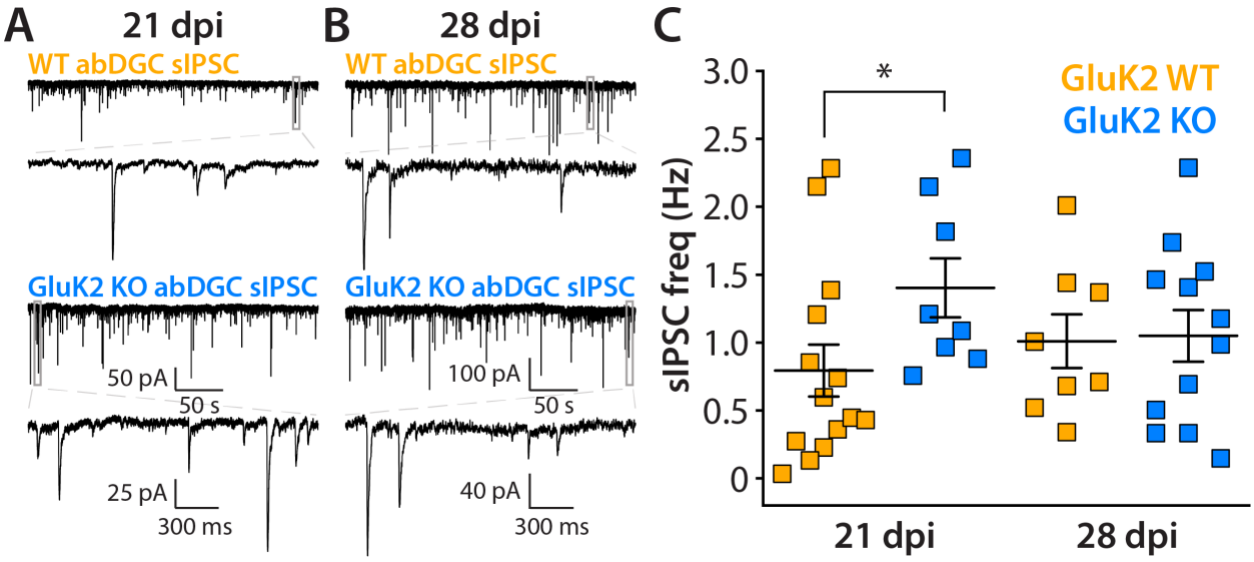

Figure 3.12 Spontaneous IPSCs in young abDGCs in GluK2 KO mice
(A-B) Representative traces of pharmacologically isolated sIPSCs in 21 dpi (A) and 28 dpi (B) abDGCs in GluK2 WT (top) and GluK2 KO (bottom) mice. **(C)** Average sIPSC frequency in 21 and 28 dpi abDGCs from GluK2 WT and Gluk2 KO mice. Statistical analysis: Mann-Whitney U test, * indicates p < 0.05.

Glutamatergic synaptic events are unaffected in 21 dpi GluK2-ablated abDGCs

The afferent excitatory synaptic inputs were also examined in birth-dated 21 dpi GluK2-ablated abDGCs since we observed the most pronounced effects at this postmitotic age. However, separate recordings from 21 dpi neurons demonstrated no difference in either the frequency or amplitude of spontaneous excitatory postsynaptic currents (sEPSCs) in both GluK2 KO mice and GluK2 cKO abDGCs (Figure 3.13).

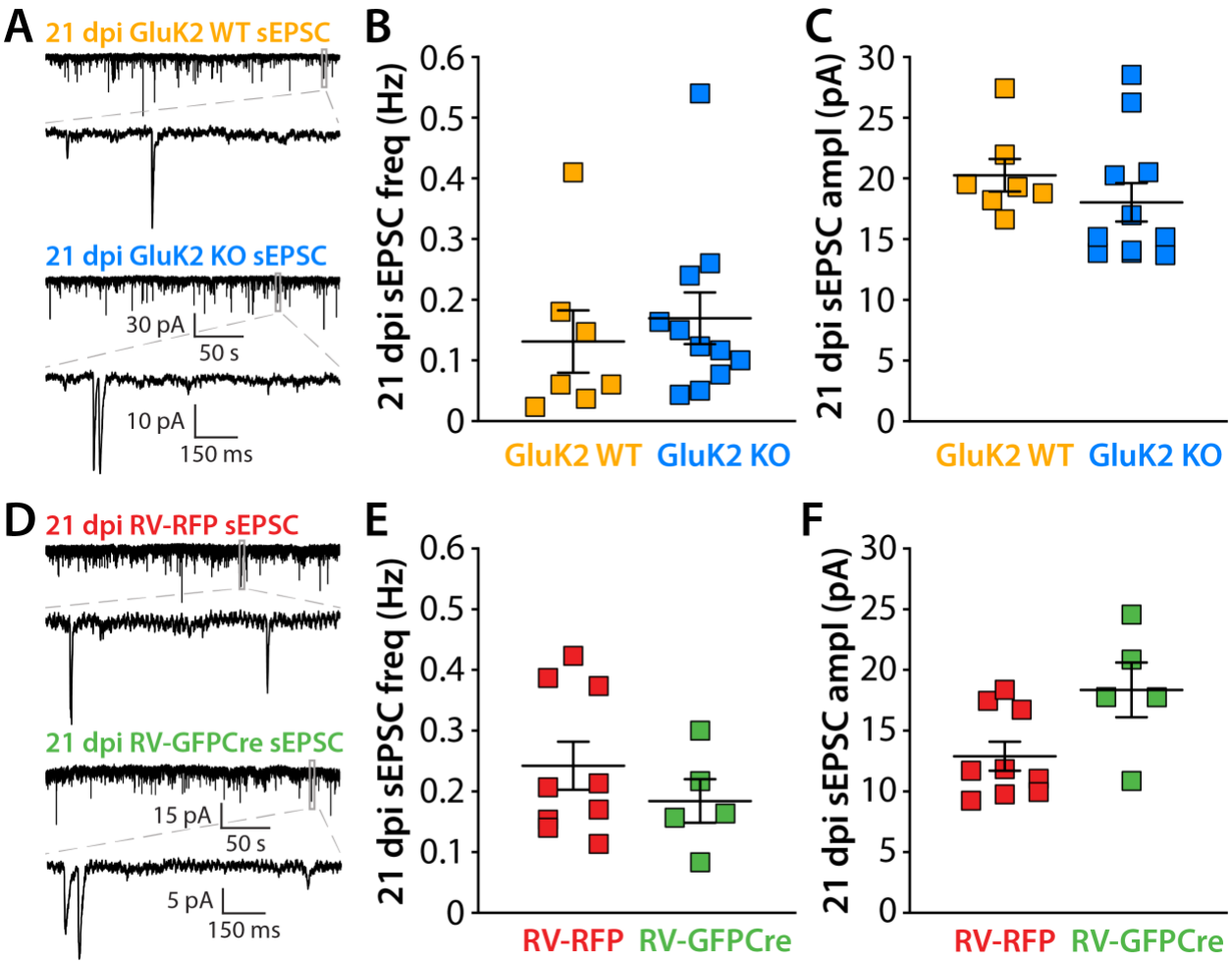

Figure 3.13 Spontaneous EPSCs in 21 dpi abDGCs from GluK2 global KO mice and after GluK2 cKO **(A)** Representative traces of pharmacologically isolated sEPSCs in 21 dpi abDGCs in GluK2 KO and GluK2 WT mice. **(B-C)** Average sEPSC frequency (B) and amplitude (C) measured in abDGCs from GluK2 KO and GluK2 WT mice. **(D)** Representative traces of sEPSCs in 21 dpi control (RV-RFP) and cKO (RV-GFPCre) abDGCs. **(E-F)** Average sEPSC frequency (E) and amplitude (F) in cKO and control abDGCs at 21 dpi. Data are presented as mean ± SEM. Statistical analysis: Mann-Whitney U test.

3.4 GluK2-ablated abDGCs demonstrate a more depolarized E_{GABA} at 21 dpi

Our findings to this point are consistent with altered functional properties of 21 dpi GluK2-ablated abDGCs during a critical time of their neuronal maturation, suggesting that GluK2-containing KARs have a powerful role in the development of newborn neurons. One way that GluK2 KARs may affect abDGC functional properties is through their known effects on GABA which in turn can have a trophic effect on abDGCs (Catavero et al., 2018; Ge et al., 2006). During early development of abDGCs, GABA is depolarizing due to the relatively high intracellular chloride concentration $[Cl^-]_{int}$ that results in a depolarized reversal potential for GABA (E_{GABA}) (Ge et al., 2006). $[Cl^-]_{int}$ is developmentally regulated by the Cl^- cotransporters and disrupting Cl^- homeostasis in abDGCs alters formation of their synaptic connections (Ge et al., 2006). KARs can exist in a complex with the K^+-Cl^- cotransporter KCC2 and loss of KARs from this complex in hippocampal neurons leads to a reduction in KCC2 surface expression and a depolarization of E_{GABA} (Mahadevan et al., 2014). Therefore, we asked whether loss of GluK2 could potentially disrupt Cl^- homeostasis and result in a more depolarized E_{GABA} in developing abDGCs. Gramicidin perforated patch recordings were performed to measure GABA-evoked currents in abDGCs at 14, 21, and 28 dpi, when E_{GABA} is progressively maturing to more hyperpolarized values (Ge et al., 2006). In control recordings (RV-RFP), there was a significant shift in E_{GABA} to more hyperpolarized values between 14 dpi and 21 dpi (Figure 3.14C). However, in GluK2 cKO neurons, this shift was delayed and occurred between 21 dpi and 28 dpi (Figure 3.14C). Specifically, E_{GABA} remained depolarized in 21 dpi GluK2 cKO abDGCs and was significantly more depolarized compared with recordings from control abDGCs (Figure 3.14).

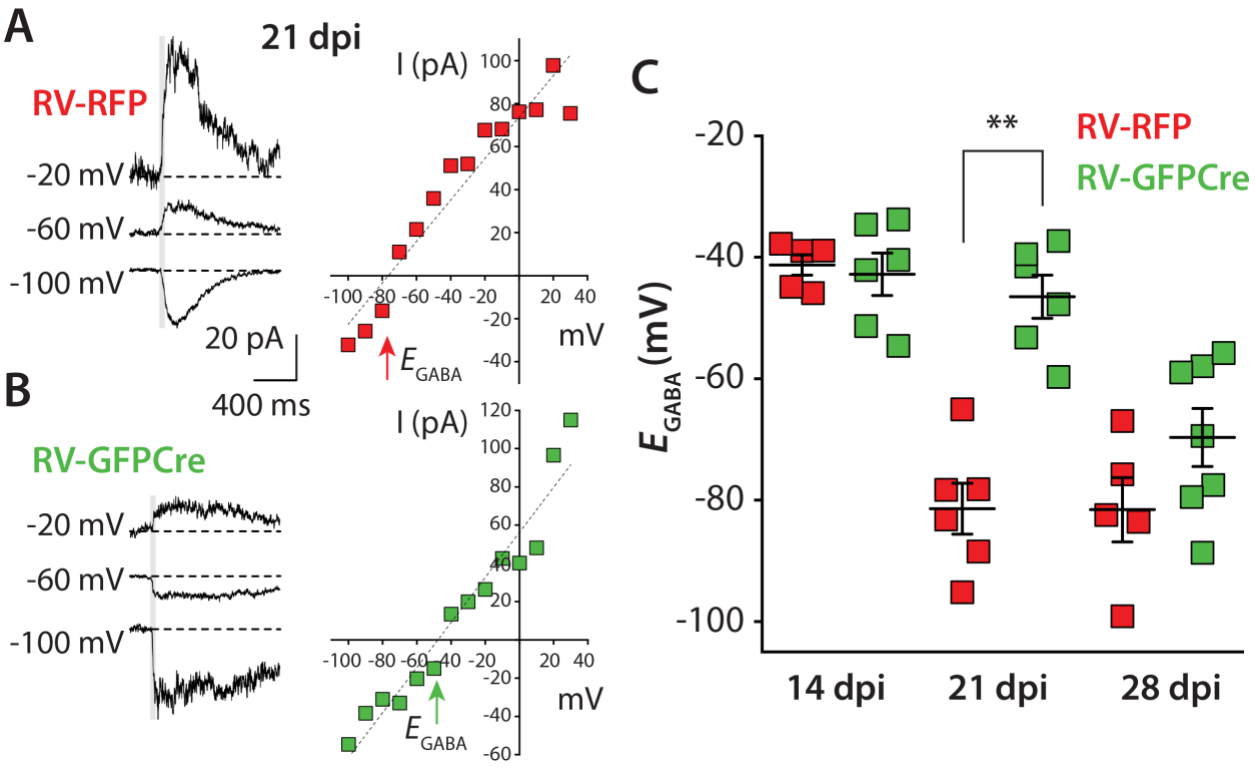

Figure 3.14 E_{GABA} polarity switch is disrupted in 21 dpi GluK2 cKO abDGCs
(A-B) Representative GABA-evoked currents from gramicidin-perforated patch recording and associated current-voltage relationship curves with the GABA reversal potential denoted from a 21 dpi control (RV-RFP) and GluK2 cKO (RV-GFPCre) abDGC, respectively. **(C)** Grouped data from all recordings of E_{GABA} measured in control and GluK2 cKO abDGCs at 14, 21, and 28 dpi. Data are presented as mean ± SEM. Statistical analysis: Mann-Whitney U test; ** indicates $p < 0.01$.

Importantly, similar perforated patch recordings of GABA currents from the constitutive GluK2 KO mice demonstrated that E_{GABA} was consistently more depolarized in 21 dpi birth-dated abDGCs than in recordings from WT mice (Figure 3.15), while E_{GABA} recorded from 28 dpi abDGCs was normal (Figure 3.15B). Altogether, these data demonstrate that during an early critical period of abDGC development, GluK2 receptors are required for the normal hyperpolarizing switch in E_{GABA} that occurs between 14 dpi and 21 dpi, at a time when NKCC1 and KCC2 expressions are changing reciprocally (Ge et al., 2006) and when synaptic inputs to abDGCs switch from being primarily GABAergic to supporting both excitatory and inhibitory synapses (Espósito et al., 2005).

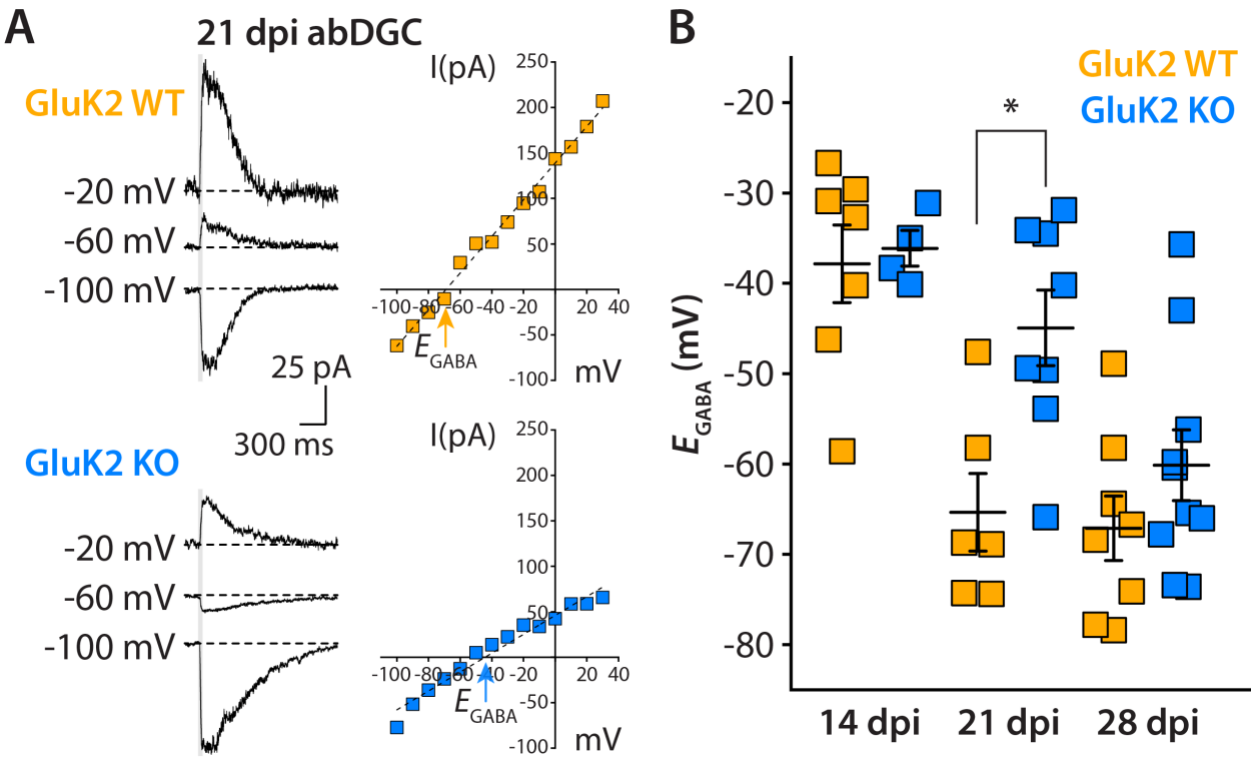

Figure 3.15 E_{GABA} polarity switch in abDGCs in GluK2 KO mice
(A) Representative GABA-evoked currents recorded in gramicidin-perforated patch mode from 21 dpi abDGCs in GluK2 WT (top) and GluK2 KO (bottom) mice. Typical current-voltage relationships from these recordings are illustrated in the panels on the right. **(B)** Grouped data of all E_{GABA} measurements from abDGCs at 14, 21 and 28 dpi in GluK2 WT and GluK2 KO mice. Data are presented as mean ± SEM. Statistical analysis: Mann Whitney U test; * indicates $p < 0.05$.

Chapter 4 – Results: Behavioral Phenotypes Due to Loss of KARs

4.1 Behavioral consequences of cell-specific ablation of GluK2 in young abDGCs

Young abDGCs are thought to have privileged roles in the hippocampus, stemming from the unique and evolving functional properties that make them particularly important for certain cognitive tasks (Gonçalves et al., 2016). In particular, tasks that require discrimination of similar objects or situations are proposed to involve activity of abDGCs (Johnston et al., 2016; Nakashiba et al., 2012), and ablation of abDGCs can impair mice in tasks that require discrimination of similar patterns (Clelland et al., 2009). In contrast, ablation of GluK2 in abDGCs produces a relatively specific change in the functional properties of abDGCs during a brief window of their development. To determine whether GluK2 knockout in abDGCs affects relevant hippocampal-dependent behaviors, we investigated the consequences of specifically ablating GluK2 receptors in a cohort of young abDGCs. We crossed the tamoxifen (TAM) inducible Ascl1^{CreERT2} mice with the *Grik2*f/f mice in order to time the ablation of GluK2 restricted to a cohort of abDGCs (Yang et al., 2015). Because Cre recombinase is activated by TAM in both Type 1 and Type 2 cells in the neurogenic niche, it has been predicted that recombination occurs in a large population of neurons generated at the time of TAM administration (derived from Type 2 fast amplifying progenitors), followed by recombination in younger cohorts (derived from Type 1 slowly dividing stem cells) (Yang et al., 2015). Therefore, for TAM administration started 21 days before behavioral assays, GluK2 cKO occurred in 21-day-old and younger postmitotic abDGCs (Figure 4.1A). Ascl1^{CreERT2} mice crossed to reporter mice had clear labeling of abDGCs, which were largely distributed in L1 of the GC layer, with some neurons showing easily visible morphology of young abDGCs (Figure 4.1B). Additionally, cell counts did not demonstrate any difference in the number of labeled neurons

between Ascl1tdTom and Ascl1cKO mice 21 days after TAM induction (Figure 4.1C), indicating that ablation of GluK2 has no discernable effect on the proliferation and/or survival of abDGCs.

Spatial discrimination is impaired in 21-22 dpi Ascl1cKO mice

Discrimination behavior of mice was analyzed in an object location memory (OLM) task in which they explored between novel and familiar spatial locations to determine whether cKO of GluK2 in a cohort of young abDGCs affects their performance. Prior work has established that spatial discrimination in mice is dependent upon the DG and manipulations of AHN disrupt spatial discrimination (Castillon et al., 2018; Clelland et al., 2009; Goodman et al., 2010; Laszczyk et al., 2017; Marschallinger et al., 2015). Mice were habituated for 3 consecutive days prior to training on the first day of the task, which occurred 21 days after TAM induction (Figure 4.1A). During OLM training, mice explored for a 10-min period, at will, in a chamber where two identical objects were placed at two arranged locations (Figure 4.1D). Mice were returned to the chamber 24 h after OLM training for OLM testing. During OLM testing, the location of one of the objects was rearranged to a new position, and mice were allowed to freely explore in the same chamber during a 5-min session (Figure 4.1E). The discrimination index was calculated to reflect the exploratory preference of the mice for the novel object location. While control (Ascl1tdTom) mice had a clear preference (DI = 23.5 ± 6.1) which was comparable to previous reports in WT mice (Goodman et al., 2010; Laszczyk et al., 2017) for the object moved to a new location, mice in which GluK2 had been ablated in the 21-day-old and younger cohort of abDGCs (Ascl1cKO) demonstrated no preference (DI = 5.8 ± 4.4) (Figure 4.1F). The total exploration time for both object locations during training and testing sessions (Figures 4.1G-H), as well as the total distance traveled during OLM testing (Figure 4.1I) were the same between Ascl1tdTom and Ascl1cKO animals.

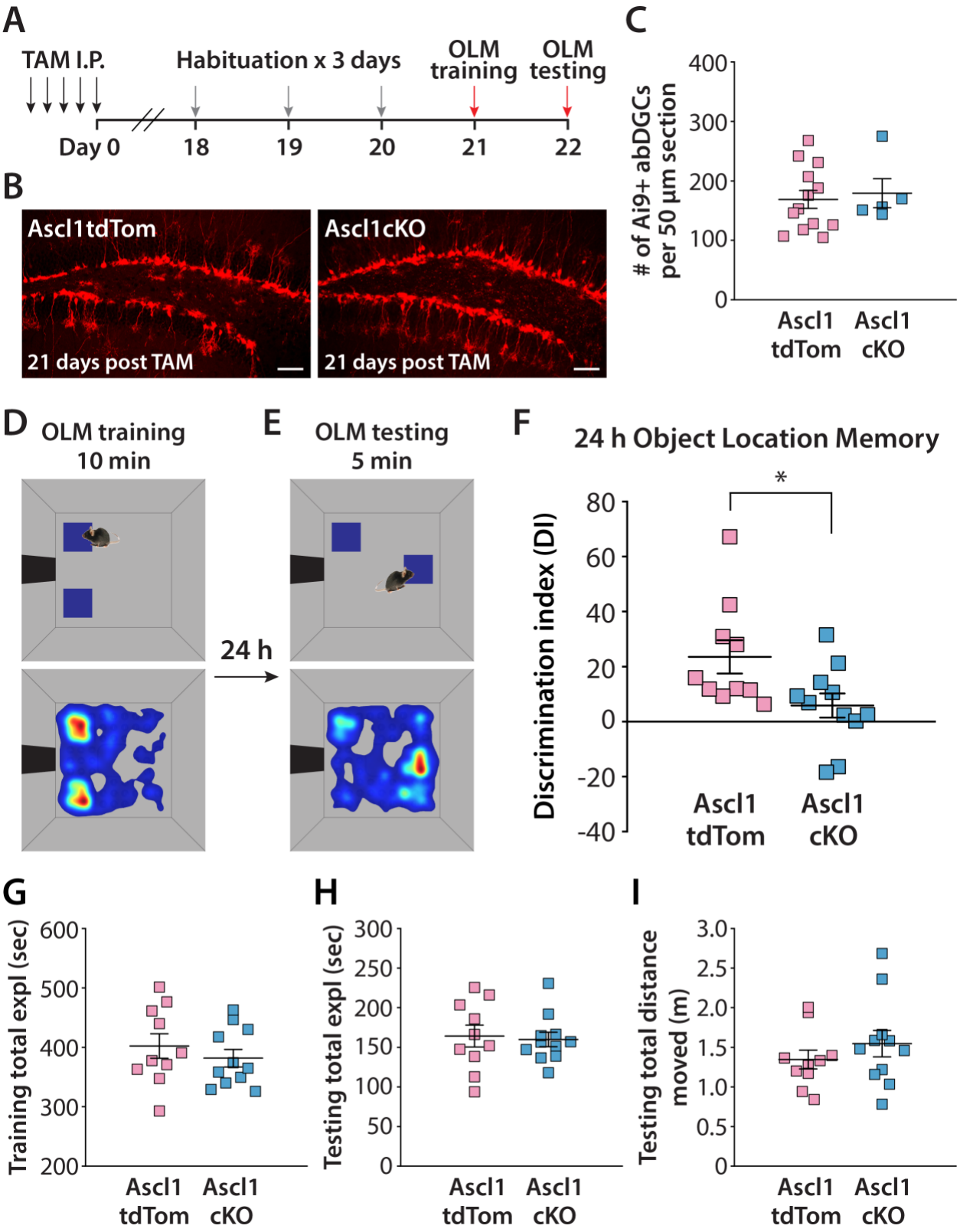
A
TAM I.P.
Habituation x 3 days
OLM training
OLM testing
Day 0
18
19
20
21
22
B
Ascl1tdTom
Ascl1cKO
21 days post TAM
21 days post TAM
C
# of Ai9+ abDGCs per 50 µm section
400
300
200
100
0
Ascl1 tdTom
Ascl1 cKO
D
OLM training
10 min
E
OLM testing
5 min
24 h
F
24 h Object Location Memory
*
Discrimination index (DI)
80
60
40
20
0
-20
-40
Ascl1 tdTom
Ascl1 cKO
G
Training total expl (sec)
600
500
400
300
200
Ascl1 tdTom
Ascl1 cKO
H
Testing total expl (sec)
300
250
200
150
100
50
0
Ascl1 tdTom
Ascl1 cKO
I
Testing total distance moved (m)
3.0
2.5
2.0
1.5
1.0
0.5
0
Ascl1 tdTom
Ascl1 cKO

Figure 4.1 Spatial discrimination is impaired by cKO of GluK2 in a young cohort of abDGCs
(A) Timeline of cKO of GluK2 using TAM administration and object location memory task. 180 mg/kg tamoxifen was administered to 8-9 week old *Grik2*f/f;Ai9;Ascl1^{CreERT2} or *Grik2*$^{+/+}$;Ai9;Ascl1^{CreERT2} mice via IP injection**. (B)** Example images of hippocampal dentate region from Ascl1tdTom and Ascl1cKO mice with tdTom labeled abDGCs 21 days after TAM induction. **(C)** Quantification of number of tdTom labeled abDGCs in 50 μm coronal hippocampal sections from Ascl1tdTom and Ascl1cKO mice 21 days after TAM induction. **(D)** Schematic of OLM training (top) and **(E)** OLM testing (top) and representative heat maps of mouse position during each session (bottom). **(F)** Calculated discrimination index from all experiments reflecting preference for novel object location in Ascl1tdTom (n = 10) and Ascl1cKO (n = 11) mice 22 days after TAM induction. **(G-H)** Total exploration time of mice for both object locations during OLM training phase and OLM testing phase. **(I)** Total distance Ascl1tdTom and Ascl1cKO mice moved during OLM testing. Data are presented as mean ± SEM. Statistical analysis: Mann-Whitney U test; * indicates p <0.05.

Trace fear conditioning and contextual fear memory is normal in Ascl1cKO mice

In a further test of whether there were more general disruptions in behaviors that require hippocampal activity but not specifically the DG or abDGCs, we tested mice in trace fear conditioning (Chowdhury et al., 2005). On day 21-23 after TAM induction, mice were conditioned with three pairings of a conditioned stimulus (CS; tone) and an unconditioned stimulus (US; foot shock) (Figures 4.2A-B). On the subsequent day, mice were tested for contextual fear in the same chamber and separately for CS freezing in a novel context (Figure 4.2C). In each case, there was no difference in freezing behaviors either during acquisition or testing, suggesting that cKO of GluK2 in a cohort of young abDGCs does not have a general effect on hippocampal-dependent memory tasks.

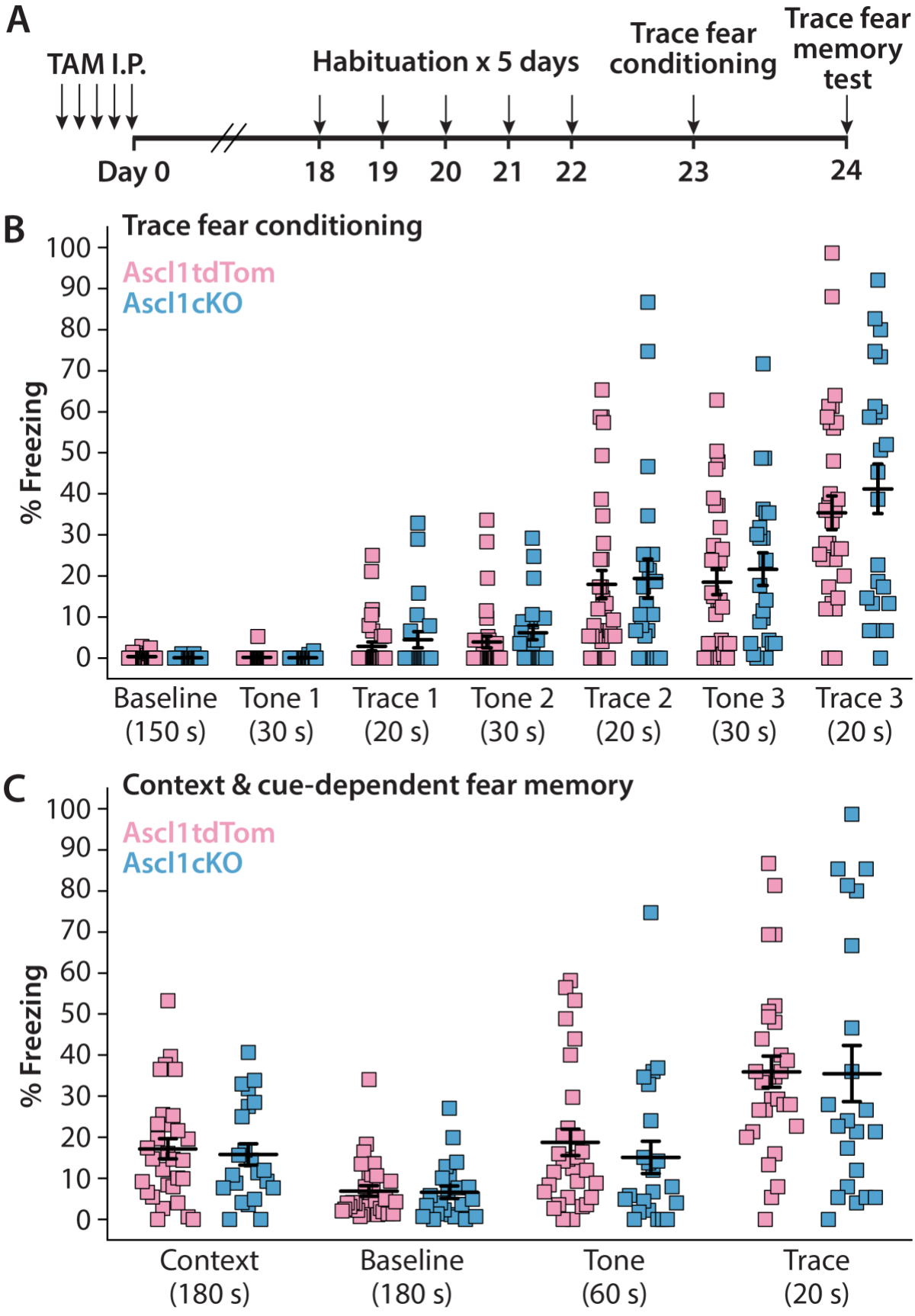
A
TAM I.P.
Habituation x 5 days
Trace fear conditioning
Trace fear memory test
Day 0
18
19
20
21
22
23
24
B
Trace fear conditioning
Ascl1tdTom
Ascl1cKO
% Freezing
Baseline (150 s)
Tone 1 (30 s)
Trace 1 (20 s)
Tone 2 (30 s)
Trace 2 (20 s)
Tone 3 (30 s)
Trace 3 (20 s)
C
Context & cue-dependent fear memory
Ascl1tdTom
Ascl1cKO
% Freezing
Context (180 s)
Baseline (180 s)
Tone (60 s)
Trace (20 s)

Figure 4.2 Trace fear conditioning and contextual fear memory three weeks after TAM-induced cKO of GluK2

(A) Timeline of TAM induction and trace fear conditioning and testing paradigm. 180 mg/kg tamoxifen was administered to 8-9 week old *Grik2*f/f;Ai9;Ascl1^{CreERT2} or *Grik2*$^{+/+}$;Ai9;Ascl1^{CreERT2} mice via IP injection. **(B)** Percentage freezing of Ascl1tdTom and Ascl1cKO mice during trace fear conditioning phase. **(C)** Percentage freezing of Ascl1tdTom and Ascl1cKO mice during contextual and cue-dependent fear memory tests. Data are presented as mean ± SEM. Statistical analysis: Mann-Whitney U test.

Two-choice spatial discrimination performance is normal in 21-26 dpi Ascl1cKO mice

As an additional behavioral assay to evaluate whether loss of GluK2 in a cohort of young abDGCs impacts pattern separation function (Clelland et al., 2009; Creer et al., 2010), we trained a separate group of TAM-treated mice to perform a two-choice spatial discrimination task using a touch screen system. Mice were maintained on 24 h water restriction and pre-trained to obtain a 2-s water reward from touching an illuminated panel on the touch screen during a 5-day shaping period before being tested alternately between large and small spatial separation modes from 21 to 26 dpi (Figures 4.3A-B). All mice displayed improved discrimination in both separation modes over the 6-day testing period; however, no difference was found in Ascl1cKO mice as measured by trials to criterion, correct touch rate and as well as number of reversals completed within each testing session (Figures 4.3C-H).

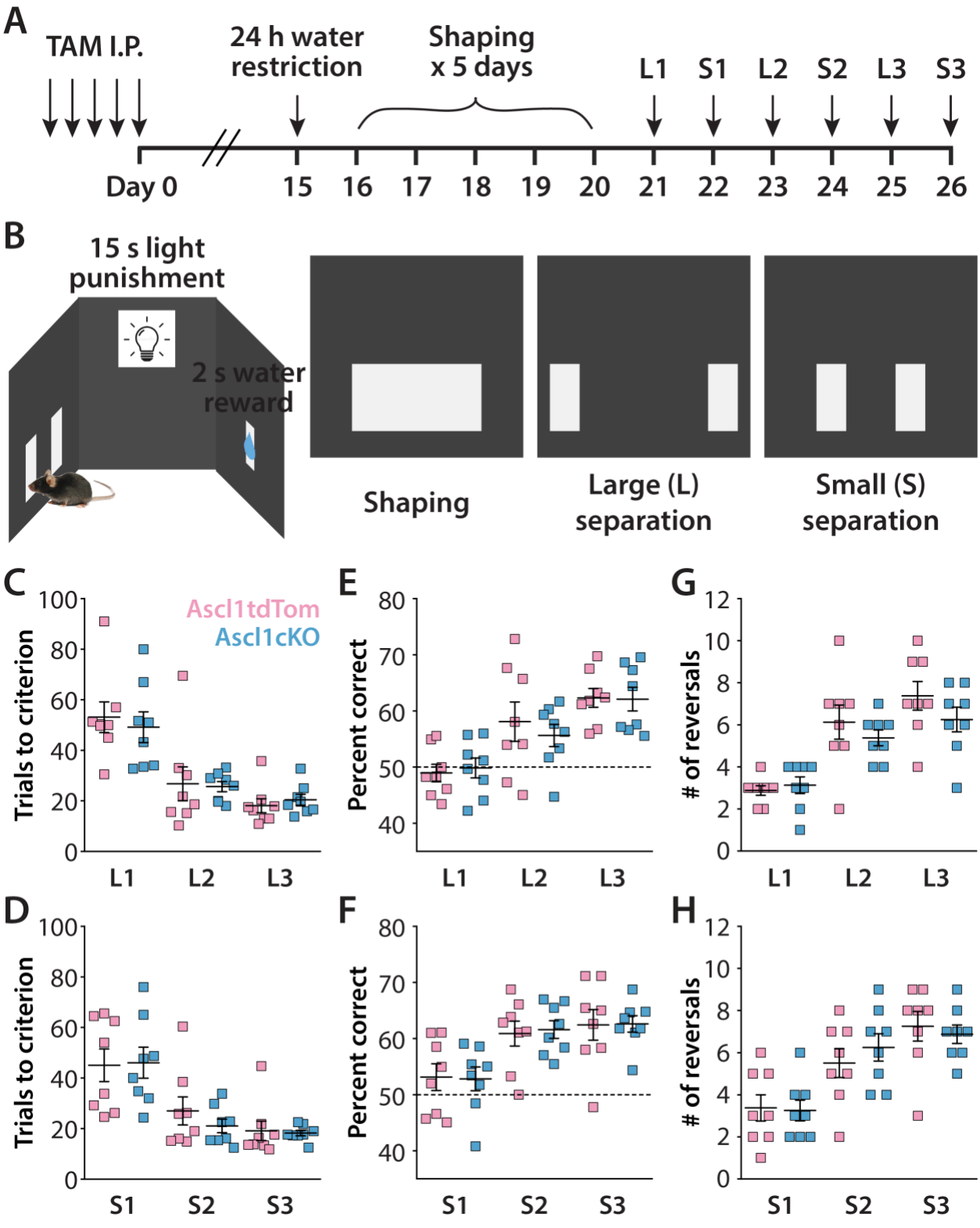
A
TAM I.P.
24 h water restriction
Shaping x 5 days
L1
S1
L2
S2
L3
S3
Day 0
15
16
17
18
19
20
21
22
23
24
25
26
B
15 s light punishment
2 s water reward
Shaping
Large (L) separation
Small (S) separation
C
Ascl1tdTom
Ascl1cKO
Trials to criterion
L1
L2
L3
D
Trials to criterion
S1
S2
S3
E
Percent correct
L1
L2
L3
F
Percent correct
S1
S2
S3
G
# of reversals
L1
L2
L3
H
# of reversals
S1
S2
S3

Figure 4.3 Two-choice spatial discrimination pattern separation performance is normal in 21-26 dpi Ascl1cKO mice

(A) Timeline of TAM induction and the two-choice spatial discrimination task paradigm. 180 mg/kg tamoxifen was administered to 8-9 week old *Grik2*f/f;Ai9;Ascl1^{CreERT2} or *Grik2*$^{+/+}$;Ai9;Ascl1^{CreERT2} mice via IP injection. **(B)** Schematic illustration of a mouse making a choice between two identical illuminated panels on a touch screen and three PVC "masks" used for shaping, large spatial separation, and small spatial separation sessions respectively. Animals received a 2 s water reward for making a correct touch or a 15 s light-on punishment for making a wrong touch during the testing sessions. **(C-D)** Trials to criterion for Ascl1tdTom and Ascl1cKO mice during the three large separation testing sessions (C) and three small separation testing sessions (D). **(E-F)** Percentage of Ascl1tdTom and Ascl1cKO mice touching the correct panel during large separation (E) and small separation (F) testing sessions respectively. **(G-H)** Number of reversals Ascl1tdTom and Ascl1cKO mice completed during large (G) and small (H) separation sessions respectively. Data are presented as mean ± SEM. Statistical analysis: two-way repeated measures ANOVA.

Chapter 5 – Discussion

5.1 Interplay between GABA and glutamatergic signaling in the development of abDGCs

How abDGCs develop and integrate into the hippocampal network is of considerable interest because there are numerous studies that have demonstrated that young adult-born neurons have unique functional properties that imbue them with distinct roles in hippocampal function (Gonçalves et al., 2016). Neuronal activities driven through the action of the neurotransmitters GABA and glutamate are of primary relevance to the maturation of postmitotic neurons in the DG (Chancey et al., 2013; Duveau et al., 2011; Ge et al., 2006; Piatti et al., 2011; Toni and Schinder, 2015). Adult-born DGCs are initially innervated by GABAergic inputs during the first and second postmitotic week (Espósito et al., 2005; Groisman et al., 2020; Remmers et al., 2020), with glutamatergic synapses developing later at around the fourth postmitotic week (Espósito et al., 2005). GABA also has a non-synaptic role with a prominent tonic $GABA_AR$ current found in newly differentiated neurons (Ge et al., 2006) as well as in neural stem cells (Song et al., 2012). Importantly, as with developmentally born neurons, abDGCs undergo a period during an early postmitotic stage when the reversal potential for GABA is relatively depolarized and activation of $GABA_ARs$ can potentially depolarize abDGCs (Chancey et al., 2013; Ge et al., 2006). Selective knockdown of the Cl^- transporter NKCC1 in abDGCs resulted in a disruption of $[Cl^-]_{int}$ homeostasis and disrupted synapse formation and dendritic growth (Ge et al., 2006). Depolarizing GABA is also critical to experience-dependent NMDAR-mediated synaptic plasticity mechanisms in abDGCs by providing the membrane depolarization required for easing Mg^{2+} block at NMDAR-only synapses (Chancey et al., 2013). Therefore, as in other developing neurons, there is an important interplay between GABA and glutamatergic signaling in developing abDGCs.

Cellular phenotypes in developing abDGCs due to loss of GluK2

Here we focused on the potential role that KARs may play in abDGCs. KARs are a distinct family of glutamate receptors whose functions are both diverse and not fully realized (Carta et al., 2014; Lerma and Marques, 2013). They are primarily ionotropic receptors but can also signal through metabotropic signaling pathways at both pre- and postsynaptic sites (Contractor et al., 2011). Kainate receptors are present in most cell types in the hippocampus; in the DG, the GluK2 KAR subunit is expressed at high levels, likely existing in a heteromeric complex with the high-affinity subunits (Bureau et al., 1999), and presynaptic KARs have been well characterized on the DGC axons and presynaptic terminals (Contractor et al., 2000, 2001; Lauri et al., 2001; Schmitz et al., 2001). Although there are KARs on the somatodendritic membrane of mature DGCs, KARs are not present at postsynaptic sites under normal conditions (Epsztein et al., 2005). While functional KARs were previously described in DCX-positive neuroblasts in the lateral ventricle (Platel et al., 2008), there has been no established work on KARs in abDGCs, and it was unknown whether and when they are present on early postmitotic developing abDGCs. Using birth-dating and labeling of newborn neurons, we found that KARs containing the GluK2 subunit are functionally expressed by abDGCs at early postmitotic times. This raised an important question about their roles, given that they are present at times when there are no or very sparse glutamatergic synapses on abDGCs, and moreover, KARs are not localized to synaptic sites. We adopted a conditional single-cell KO approach to birth-date and record from cKO neurons. We also recorded from birth-dated abDGCs in a constitutive KO mouse model. Surprisingly, we found multiple functional consequences of loss of GluK2 at the earliest postmitotic time points during what has been defined as a critical period for development of abDGCs (Chancey et al., 2013; Kitamura et al., 2010; Tashiro et al., 2007). Specifically, at 21 dpi, the input resistance of GluK2 cKO abDGCs was significantly lower

and was more consistent with neurons of later postmitotic times. In addition, 21 dpi cKO abDGCs responded to current injection with increased AP firing compared with control neurons. Measures of inhibitory synapses also suggested that the 21 dpi abDGCs with GluK2 ablated had a more mature functional profile with increased frequency and elevated amplitude of sIPSCs. While the above functional measures of intrinsic and synaptic properties suggested a more mature profile for GluK2-deficient abDGCs, measurements of RMP and excitatory synaptic activities did not support a faster maturation of these neurons. Thus, the decrease in input resistance and increase in firing capacity might reflect only an upregulation of potassium channel density, rather than a general acceleration of neuronal maturation. Furthermore, there was no correlated change in morphological parameters that are also measures of maturation. Given these specific alterations in the functional properties of abDGCs, it is interesting to note that they seem to be separable from dendritic development, in that the disruption of one does not correlate with changes in the other.

A potential interaction between KCC2 and GluK2 in the development of abDGCs

Our study led us to examine the progression of E_{GABA} in GluK2 cKO abDGCs. Both developmentally born and adult-born neurons are subject to trophic effects of shifts in the GABA reversal potential as neurons mature. In abDGCs, the transition from a relatively depolarized E_{GABA} to a more hyperpolarized mature value of E_{GABA} occurs between 14 dpi and 21 dpi (Figures 3.14C and 3.15B) (Ge et al., 2006). Importantly, the GluK2 receptor subunit exists in a complex with the Cl^- extruder KCC2, which maintains lower $[Cl^-]_{int}$ as neurons develop (Mahadevan et al., 2014). GluK2 increases the abundance of surface KCC2 (Pressey et al., 2017) and affects the maturation of spines in developmentally born hippocampal neurons (Kesaf et al., 2020). We found that, in GluK2 cKO abDGCs, the normal developmental switch from depolarizing to hyperpolarizing

E_{GABA} was delayed, such that, at 21 dpi, E_{GABA} was still depolarized. A similar result was observed in birth-dated abDGCs in GluK2 KO mice. These data demonstrate that loss of GluK2 KARs in abDGCs affects the GABA polarity switch during a critical time window when abDGCs are maturing. This action of KARs in regulating the functionality of KCC2 may be the prominent role they play in developing neurons, which have few or sparse glutamatergic inputs and also which, in many cases, never localize KARs to synapses where they can be activated by synaptically released glutamate. As such, it is possible that a primary role that KARs have in abDGCs is as a non-canonical partner of the Cl^- transporter (Mahadevan et al., 2014).

How GluK2-containing KARs may normally regulate abDGC functional properties

Here, we propose a potential model wherein GluK2 may regulate the functional properties of young abDGCs through an interaction with KCC2 that controls a low intracellular chloride concentration of neurons (Kesaf et al., 2020; Mahadevan et al., 2014; Pressey et al., 2017). In normal conditions, proper interaction with GluK2 is required for upregulation of KCC2 surface expression (Mahadevan et al., 2014), which is genetically programmed to occur in abDGCs between 2-3 weeks post mitosis. In the absence of GluK2, functional membrane KCC2 is reduced, resulting in a delayed shift of E_{GABA} from being depolarized to hyperpolarized. While E_{GABA} remains temporarily depolarized and abDGCs factually receive more excitatory drive, expression of potassium channels likely boosts in the short-term, resulting in a lower input resistance and increased ability to fire repetitive action potentials in 21 dpi GluK2 cKO abDGCs, in line with previous observations that increased depolarization promotes the overall functional development of abDGCs (Ge et al., 2006; Piatti et al., 2011; Sim et al., 2013). Since mature DGCs receive more inhibitory inputs than young abDGCs under control conditions, the higher frequency and larger

amplitude of sIPSCs can be viewed as a speeded development of inhibitory synapses that is also a probable result of globally elevated depolarization, such as the case in the Sim et al. study (2013). Importantly, according to our results most measurements of the functional properties appeared normalized by 28 dpi, indicating that certain compensatory mechanisms exist and take effect within a week, potentially even within several days. In conclusion, while a premature decrease of intracellular Cl^- clearly impedes dendritic and synaptic development of abDGCs (Ge et al., 2006), a delayed decrease of intracellular Cl^- due to loss of GluK2 briefly alters their intrinsic electrical properties and specifically increases inhibitory synapse formation onto them. The accurate timing for the GABA polarity switch should be tightly controlled to ensure a proper neuronal profile and establishment of synaptic connections of abDGCs for them to play privileged roles in the hippocampal circuitry.

Why depolarizing E_{GABA} induces no change in dendritic growth and glutamatergic synapses

Our findings that a depolarized shift in E_{GABA} in 21 dpi GluK2 cKO abDGCs did not affect their dendritic growth and glutamatergic synapses were initially surprising, as depolarizing E_{GABA} has a known effect on promoting dendritic growth and glutamatergic synapse formation in young abDGCs (Ge at al., 2006). Specifically, the authors rendered E_{GABA} values hyperpolarized by knocking down NKCC1, and found impaired dendritic growth in 14 dpi abDGCs and reduced sEPSC frequency in 28 dpi abDGCs (Ge et al., 2006). Therefore, one might expect more complex dendritic morphology and increased excitatory synaptic transmission in 21 dpi GluK2 cKO abDGCs in which E_{GABA} remains depolarized. However, our results demonstrate no change in the average frequency or amplitude of sEPSCs or the gross dendritic morphology, possibly due to four reasons in my perspective: 1) our measurements are not sensitive enough to detect subtle changes

such as the dendritic spine density; 2) the effects might have been compensated; 3) in our data the change in E_{GABA} is more nuanced as there is just a temporary delay in the normal development of the hyperpolarized Cl^- reversal potential that could account for the differences; and 4) depolarizing GABA may not necessarily impact these parameters as hyperpolarizing GABA does in developing neurons.

Potential compensatory mechanisms for a corrected E_{GABA} at 28 dpi may include downregulation of NKCC1 and/or upregulation of surface KCC2 expression through other pathways. Our results are consistent with the possibility that such compensatory mechanism(s) take place between 3-4 weeks post mitosis, around the same time when glutamatergic synapses are increasingly being formed (Espósito et al., 2005). Therefore, how a short period of depolarizing E_{GABA} would affect formation of excitatory inputs is less clear, as it might not actually have an effect, or, the E_{GABA} could already be rectified before glutamatergic synapses can be significantly impacted. Intriguingly, previous studies also do not always generate consistent results with regards to how excitatory synaptic connections are affected by altered functional properties of abDGCs. For example, decreasing the intrinsic excitability of abDGCs resulted in reduced mEPSC frequency but larger mEPSC amplitude in 21 dpi neurons that exhibited a generally delayed maturation (Piatti et al., 2011). Conversely, increasing the intrinsic excitability resulted in more mature abDGCs, but also reduced sEPSC frequency as well as larger sEPSC amplitude, with the overall spontaneous excitatory postsynaptic currents received by 28 dpi neurons the same (Sim et al., 2013). There seems to be a reduction in the number of excitatory synapses in young abDGCs no matter their functional maturation is overall more accelerated or delayed. Indeed, in this study, upon examination of mEPSCs, 21 dpi GluK2 cKO abDGCs do display a reduced mEPSC frequency. It

is also worth noting that, in global GluK2 KO mice, there is a reduction in sEPSC frequency in 28 dpi abDGCs that is not seen in GluK2 cKO neurons, hinting at a non-cell autonomous role of GluK2 in regulating formation of excitatory synapses in developing abDGCs.

Another possibility is that the change in E_{GABA} does not produce enough depolarization capable of impacting dendritic growth and glutamatergic synapse formation in 21 dpi GluK2 cKO abDGCs. Notably, in parallel with the shift in E_{GABA}, there is an additional increase in GABAergic synaptic inputs. Stronger GABAergic conductances have been shown to induce shunting inhibition (Heigele et al., 2016), which could compensate for the effects of a more depolarized E_{GABA} and ultimately provide comparable inhibitory control to developing abDGCs. In fact, the measured action potential threshold of 21 dpi GluK2 cKO abDGCs in current clamp recordings was -36.3 ± 1.8 mV (Figure 3.8C), and given an E_{GABA} value of -46.5 ± 3.6 mV and relatively weak glutamatergic synaptic inputs at 21 dpi, it is likely that the upregulated formation of inhibitory synapses could also be a compensatory mechanism that provides shunting inhibition to abDGCs. Nevertheless, whether the action of elevated GABAergic inputs on abDGCs is more excitatory, more inhibitory, or not different at all would not change the significance of our findings or effectively clarify the effects of the delayed switch in E_{GABA} on dendritic growth. In the case of increased network activities or an enriched environment, we suspect that depolarizing GABA may increase the frequency of mEPSCs in 21 dpi GluK2 cKO neurons, because the E_{GABA} is still in the range of NMDAR activation, which would critically promote experience-dependent synapse unsilencing (Chancey et al., 2013). Last but not least, the effects of maintaining a depolarized E_{GABA} in developing abDGCs have never been directly tested, and it is not impossible that between

2-4 weeks of age, a still depolarizing E_{GABA} exerts no substantial influence on dendritic growth or glutamatergic synapse formation.

5.2 Behavioral significance of GluK2 KARs in hippocampal function

GluK2 ablation has a selective effect on a spatial discrimination behavior

Young abDGCs are of special importance to hippocampal circuits and have been proposed to have a large impact on behaviors involving the hippocampus. Newborn neurons have a particularly important role in behaviors during the critical period soon after they make contacts with other components of the DG-CA3 microcircuit. Adult-born DGCs form functional output synapses with CA3 as early as 2 weeks postmitotic, and these excitatory connections reach maximum amplitude between 21 and 28 dpi (Gu et al., 2012). It is also during the third to fourth postmitotic week that abDGCs are active during hippocampal-dependent learning tasks, and reversible optical silencing of 4-week-old neurons disrupts memory retrieval (Gu et al., 2012). Because loss of KARs had a selective effect on the functional properties of abDGCs during this critical time window, we tested whether conditional disruption of GluK2 affected behavior of mice. It is possible that the functional changes in abDGCs during this time cause cumulative effects because neurons with altered properties are continuously added to the network, producing a more dramatic change to the circuit. To ablate GluK2 in a large cohort of abDGCs, we used the Ascl1^{CreERT2};*Grik2*f/f;Ai9 mice, which allowed us to temporally and spatially restrict KO of GluK2 to the adult SGZ. Although this provided the advantage of a broader KO of GluK2, the temporal precision was less than that achieved with a retroviral approach, giving a wider range of postmitotic ages of abDGCs in which GluK2 was ablated (Yang et al., 2015). We tested mice in which cKO of GluK2 had been initiated 21 days preceding a spontaneous spatial discrimination task (Dix and Aggleton, 1999). In the

testing phase, the level of discrimination was significantly reduced in Ascl1cKO (GluK2 cKO) mice. We also tested mice in a trace fear conditioning task, which requires involvement of the hippocampal circuitry, and found no difference in the cKO mice during either acquisition or recall of fear memory. Together, these results suggest that disruption of the normal functional properties of developing abDGCs leads to selective effects on a spatial discrimination behavior but leaves other behaviors that require uncompromised functioning of the hippocampal circuits unaffected.

Understanding the deficit in the object location memory

In our study, the object location memory in mice with selective GluK2-knockout in a cohort of ~3 wpi abDGCs is significantly disrupted. On the cellular level, 21 dpi GluK2 cKO abDGCs display lower input resistances, increased ability to generate repetitive AP firing in response to current injections and as well as elevated GABAergic synaptic inputs, while glutamatergic synapses appear unchanged. Interestingly, these properties of 21 dpi GluK2 cKO abDGCs resemble those of 28 dpi WT abDGCs, suggesting that ~3 wpi GluK2 cKO abDGCs could potentially be activated at least at a similar probability compared with ~4 wpi control abDGCs, which have been born one week earlier, expanding the pool of "hyperexcitable" abDGCs available for use during behavioral tasks in which ~4 wpi abDGCs are normally preferentially engaged. Paradoxically, in a previous study, mice depleted of abDGCs exhibited a corrupted spatial memory performance in a similar object location memory test (Goodman et al., 2010). Although it will take future studies to fully understand how the altered cellular properties of cKO abDGCs affect behavior, here I discuss some potential mechanisms that might account for the selective deficit in spatial discrimination in ~3 wpi Ascl1cKO mice. First, since there is no difference in the number of Ai9-postive new neurons between the Ascl1cKO and control animals (Figure 4.1C), this rules out one possibility of how

behaviors are altered in the mice. Second, the depolarized GABA reversal potential at ~3 wpi may lead to increased, nonspecific activities of abDGCs, which might disrupt relevant behaviors. Third, the efferent synaptic connectivity and plasticity should ultimately determine how these ~3 wpi GluK2 cKO neurons differentially impact behavior outputs. Therefore, the behavioral alteration could be caused by a disruption of normal hippocampal network by a cohort of ~3 wpi GluK2 cKO abDGCs having a relatively lower input specificity but aberrant synaptic connections with their downstream targets, such as CA3 pyramidal neurons and/or local interneurons.

3 wpi GluK2 cKO abDGCs may prematurely engage in behavior due to lower input specificity

Increased excitability, less robust inhibition, and enhanced synaptic plasticity lead to the prediction that young abDGCs during their critical window would be more broadly responsive to afferent activities than mature DGCs and thus more likely to be recruited during behaviors that engage the hippocampus (Johnston et al., 2016), despite the fact that under physiological conditions the elevated intrinsic excitability of immature abDGCs can be counterbalanced by inadequate excitatory synaptic drive from EC to restrict their spiking to a certain degree (Dieni et al., 2016). In particular, 4 wpi abDGCs in normal adult mice have been reliably found to fire at a higher probability than mature DGCs in response to perforant path fiber stimulation (Dieni et al., 2013; Li et al., 2012; Marín-Burgin et al., 2012), indicating that young abDGCs tend to be selected over mature DGCs during behaviors featuring spatially concerted EC synaptic outputs (Lodge and Bischofberger, 2019). Our data suggest that, 21 dpi GluK2 cKO abDGCs would have at least a similar, or even relatively lower input specificity (due to depolarizing E_{GABA}) towards environmental stimuli compared with 28 dpi control abDGCs, given their indistinguishable electrophysiological properties including input resistance and intrinsic excitability, and

comparable levels of GABAergic and glutamatergic inputs. Therefore, in behaviors where 4-week postmitotic abDGCs are preferentially activated in control animals, 3 wpi GluK2 cKO abDGCs might compete with 4-week postmitotic naive abDGCs for neuronal activation in Ascl1cKO mice.

A potential undermined coupling between 3 wpi GluK2 cKO abDGC and downstream targets

The efferent synaptic connectivity and plasticity of GluK2 cKO abDGCs were not examined in this project. Importantly, it has been shown that abDGCs establish functional projections to CA3 starting at 2 wpi, and MF-EPSCs evoked by optogenetic stimulation of abDGCs increase to stable amplitudes at 4 wpi (Gu et al., 2012), indicating that full synaptic output strength is normally reached at 4 weeks post mitosis. It is worth noting that there is a huge increase in control abDGC-evoked EPSC amplitude between 3 wpi and 4 wpi, as the average amplitude of MF-EPSC at 3 wpi is only about 30% of the value at 4 wpi (Gu et al., 2012). In addition, stimulation of abDGCs at 4 weeks (but not 3 or 8 weeks) of age induced the maximal plasticity in field EPSPs in CA3 (Gu et al., 2012), which would synergize with their higher likelihood of firing at this particular postmitotic point. Hence, the "hyperplasticity" phase of abDGCs and their output synapses to CA3 should be coordinated in time for them to function efficiently as individual coding units during relevant behaviors. Interestingly, a delay in the morphofunctional maturation of mossy fiber synapses has been previously reported in the absence of GluK2 KARs during early postnatal development (Lanore et al., 2012). It also has been shown that MF LTP is impaired in young (P16-26) GluK2 KO mice, presumably via a presynaptic mechanism (Contractor et al., 2001). Moreover, GluK2 KO mice exhibit enhanced propensity towards pattern completion but not pattern separation (Micheau et al., 2014), in line with our finding that 3 wpi Ascl1cKO mice display an impaired performance in the object location memory test, indicative of a compromised spatial location

discrimination (i.e., a form of pattern separation). Although it is unclear what exact role GluK2 KARs play in the development of mossy fiber synapses established by abDGCs, it is possible that loss of GluK2 has a similar delayed effect on the development of abDGC efferent MF-EPSCs at 21 dpi. Interestingly, NaChBac (a bacterial form of sodium channel)-overexpressed abDGCs resemble GluK2 cKO abDGCs by their increased intrinsic excitability, and these neurons display decreased number of large mossy fiber terminals at 28 and 42 dpi (Sim et al., 2013). As a consequence, when ~3 wpi GluK2 cKO abDGCs replace some 4-week-old naive abDGCs to be activated during the hippocampal-dependent spatial discrimination task due to a similar or lower threshold of activation, behavioral performance could be disrupted because of an undermined coupling between 3 wpi GluK2 cKO abDGCs and their downstream CA3 partners.

Another synaptic output target for abDGCs is hilar interneurons that impinge back onto mature DGCs (Drew et al., 2016; Toni et al., 2008). It has been proposed that such connections provide feedback inhibition to promote sparse activity of mature DGCs, which is essential for generating non-overlapping memory representations of similar experiences (Johnston et al., 2016). Optogenetic activation of 7 wpi abDGCs has been shown to recruit strong inhibitory inputs to mature DGCs, and this inhibitory modulation of mature DGCs might be an important function of abDGCs in addition to their direct participation in information encoding (Drew et al., 2016). In contrast, 4 wpi abDGCs have been shown to poorly innervate proximal interneurons but sufficiently drive distal CA3 targets (Temprana et al., 2015). Therefore, it looks less likely that abDGCs younger than 4 weeks old would play a major role in modulating local circuitry responsible for feedback inhibition onto mature DGCs, and that an altered coupling between a

cohort of 3 wpi GluK2 cKO abDGCs and local interneurons, if there is any, would significantly affect the inhibition levels of mature DGCs and subsequently impact behavioral outcome.

A cohort of 21-26 dpi GluK2 cKO abDGCs do not impact two-choice spatial pattern separation

Many studies have suggested an essential role of abDGCs in pattern separation. In a similar version of this task, adult mice depleted of newborn neurons via focal x-irradiation showed an impairment when discriminating two identical stimuli that were presented with little separation in space (Clelland et al., 2009), and mice with increased AHN through running displayed enhanced discrimination of such two adjacent stimuli (Creer et al., 2010), indicating that an increased number of abDGCs available at the time of testing would improve pattern separation performance. However, how pattern separation is achieved by abDGCs on the cellular and circuit basis remains to be solved. In our experiment, Ascl1cKO mice showed a deficit in the object location spatial discrimination task but not in the two-choice spatial discrimination task, potentially attributable to several reasons. First is the difference in the time course of those behavioral tests. The former was designed to test whether the altered functional properties in a cohort of GluK2 cKO abDGCs within a tight postmitotic window of 21-22 dpi are correlated with any impact on object location pattern separation, whereas the testing phase of the two-choice spatial discrimination task spanned six days, from 21-26 dpi, at the end of which GluK2 cKO abDGCs appeared no longer functionally different from WT neurons and during which the relevant effects could have been compensated.

Second, the temporal separations of the spatial stimuli that need to be discriminated in these two forms of pattern separation task are on different scales. The OLM task tests the ability of the mice to form a long-term (24 h) memory of familiar spatial locations so as to recognize a novel spatial

location within the same context the following day, while the two-choice spatial discrimination task tests the working memory of the mice for performing pattern separation when animals are challenged with repetitive stimuli within a maximum of 2.5 hours on the same day. Variations in temporal separation of stimuli would probably influence how young abDGCs encode spatial and contextual information, as it has been shown that less temporal separation increases the probability of reactivating a DGC that has been previously recruited in the same environment (Drew et al., 2013). Therefore, an impaired phenotype in one pattern separation paradigm may not necessarily predict a similar disruption in another, and sometimes it is even possible that opposite effects can be observed, depending on other variable factors.

Third, the two-choice spatial discrimination pattern separation may normally be mediated by abDGCs of a different postmitotic age, or by a larger population of abDGCs spanning a wider range of ages, rather than primarily by ~4 wpi abDGCs. It is of interest to note that prior studies in which increased AHN was shown to improve pattern separation were carried out 1.5-2 months after manipulation (Creer et al., 2010; Sahay et al., 2011b), and that 1.5-2 months old abDGCs were unlikely affected in our Ascl1cKO mice 21-26 days after tamoxifen induction.

One more possibility is that in our current two-choice spatial discrimination task the two illuminated panels were still too widely located from each other in the small separation mode so that both groups of animals were able to discern the correct panel with alike performance. When the difficulty of the discrimination task is increased as the spatial distance between the two panels is further reduced, a subtle phenotype might then be revealed in the Ascl1cKO mice.

21-24 dpi GluK2 cKO abDGCs do not disrupt trace fear conditioning and contextual fear memory

It has been previously shown that reducing the number of ~2 weeks postmitotic abDGCs results in impaired trace conditioning (Shors et al., 2001). Besides, either genetic elimination of 0-6 weeks old abDGCs or optogenetic silencing of abDGCs between 4-6 weeks of age impairs contextual fear memory (Gu et al., 2012; Huckleberry et al., 2018; Saxe et al., 2006). Using a prior trace fear conditioning test paradigm (Farley et al., 2011), we were able to examine both trace and contextual fear memory conveniently following the same training session.

We first performed the test at 23-24 dpi using the same group of animals that were subjected to the OLM test from 21-22 dpi, as we assumed that a non-aversive exploratory task relying on animals' innate preference for spatial novelty would have a minimal impact on a subsequent, perhaps more stressful behavioral test (Vogel-Ciernia et al., 2014). Later on, we carried out the same trace fear conditioning experiment on a separate group of animals at 21-22 dpi, and combined data from all 21-24 dpi mice since we did not discover any difference in freezing behaviors among these time points. Neither did we find a difference in either the trace fear or contextual fear memory performance between WT and Ascl1cKO mice, suggesting that a cohort of abDGCs with altered functional properties at around 3 weeks post mitosis in the DG network do not interfere with normal formation of these two types of hippocampal-dependent memories.

Our results do not conflict with previous research showing that 4-6 weeks old WT abDGCs are critical for acquisition and recall of contextual fear memory (Gu et al., 2012; Huckleberry et al., 2018). Furthermore, in another study, mice with increased AHN at 8 weeks post treatment displayed normal hippocampal-dependent learning including contextual fear conditioning, except

for enhanced pattern separation (Sahay et al., 2011b), indicating that the kind of behavior altered by manipulating abDGCs depends on the postmitotic age of affected abDGCs, and probably the nature of manipulations (e.g. populational vs neuronal) as well. Interestingly, recent evidence suggests that 4-6 wpi abDGCs oppositely modulate spatial information transferred through the MEC pathway and non-spatial information transferred through the LEC pathway via direct monosynaptic inhibition and excitation of mature DGCs respectively (Luna et al., 2019). Thus, it is not surprising that Ascl1cKO mice showed a selective deficit in a spatial discrimination task but intact contextual and trace fear memory. It is conceivable that behaviors involving fine spatial/contextual discrimination that requires more detailed computation will depend more heavily on the engagement of young abDGCs (~4 wpi), and tend to be modified by a cohort of ~3 wpi GluK2 cKO abDGCs having increased excitability and sensitivity to minor changes in inputs from the external world.

To summarize our behavioral studies, we found that aberrant functional properties in a cohort of ~3 wpi abDGCs as a result of GluK2 knockout were correlated with a specific impairment in animals' performance in a spatial discrimination task but not in other hippocampal-dependent behaviors. To our knowledge, this is the first study demonstrating that alterations in the intrinsic and synaptic properties during a small postmitotic window within the critical period of newly differentiated abDGCs, correlate with a deficit in spatial discrimination indicative of compromised pattern separation. Our results implicate that behaviors related to pattern separation are more sensitive to intrinsic excitability changes in a population of relatively young abDGCs, in alignment with existing evidence suggesting that young (3-4 weeks old) WT abDGCs are sufficient and necessary to mediate pattern separation, whereas mature DGCs promote pattern completion

(Nakashiba et al., 2012). After all, information processing within the DG is likely sophisticated as the DG needs to maintain a dynamic balance between pattern separation and completion that are both important to life, and the selection of active DGCs during episodic events should be highly regulated in healthy conditions (Drew et al., 2013). Intriguingly, an impaired spatial pattern separation was found in Rsk2-KO mice, in which abDGCs displayed delayed maturation at two weeks of age (Castillon et al., 2018). Therefore, a tightly controlled development of abDGCs may be essential for their optimized function in the hippocampus, as any disturbance in their properties along the maturation course could lead to suboptimal behavioral outcomes.

5.3 Limitations

Inadequate staining data for GluK2 and KCC2 in abDGCs

There are some limitations in my study. First, although our Dom-induced KAR-mediated current recordings demonstrating complete elimination of functional KARs in GluK2-deficient abDGCs strongly imply that GluK2 is the obligatory subunit in KAR complexes in abDGCs, it might still be relatively weak to conclude the sole mediating role of GluK2 in immature abDGCs. It would be desirable to strengthen this conclusion with additional staining data showing the expression of GluK2 in abDGCs, which we were unfortunately not able to generate within the time limit of this study. However, there is strong data from in situ studies that GluK2 is expressed at high levels in the DG (Bureau et al., 1999). As an additional support for our findings that GluK2 is the primary subunit that contributes to functional KARs in abDGCs, we also recorded from abDGCs in mice in which the high-affinity GluK4 subunit was ablated and found that Dom-induced currents were still present.

Furthermore, our observation of a depolarized Cl^- reversal potential E_{GABA} in 21 dpi GluK2-deficient abDGCs supports an important interaction between GluK2-containing KARs and the neuron-specific K^+-Cl^- cotransporter KCC2 in the development of abDGCs. Such interaction significantly increases KCC2 surface expression (in order for KCC2 to be functional as a membrane protein), and has been previously reported in multiple preparations including whole-brain native membrane lysates (Mahadevan et al., 2014), cultured hippocampal neurons (Pressey et al., 2017), and CA3 pyramidal neurons in vivo (Kesaf et al., 2020). Likewise, it would be more convincing to demonstrate a reduced KCC2 surface expression in 21 dpi GluK2 cKO abDGCs via KCC2 immunolabeling. Unfortunately, although we observed a robust perisomatic staining pattern of KCC2 in mature DGCs (Figure 5.1), we found it challenging to reliably quantify the KCC2 surface expression in young abDGCs, due to the fact that the best focal plane for KCC2 and tdTom signals for the same cell might not always be the same, and not all tdTom+ abDGCs were located within the same focal plane. Furthermore, since all mature DGCs express high levels of KCC2 and there are multiple layers of DGCs along the z-axis within a DG section, the surface KCC2 signals of an abDGC of interest could be confused with those belonging to surrounding unlabeled DGCs. Qualitatively, there seems no difference in KCC2 membrane expression between 21 dpi tdTom labeled WT and GluK2 cKO abDGCs (Figure 5.1).

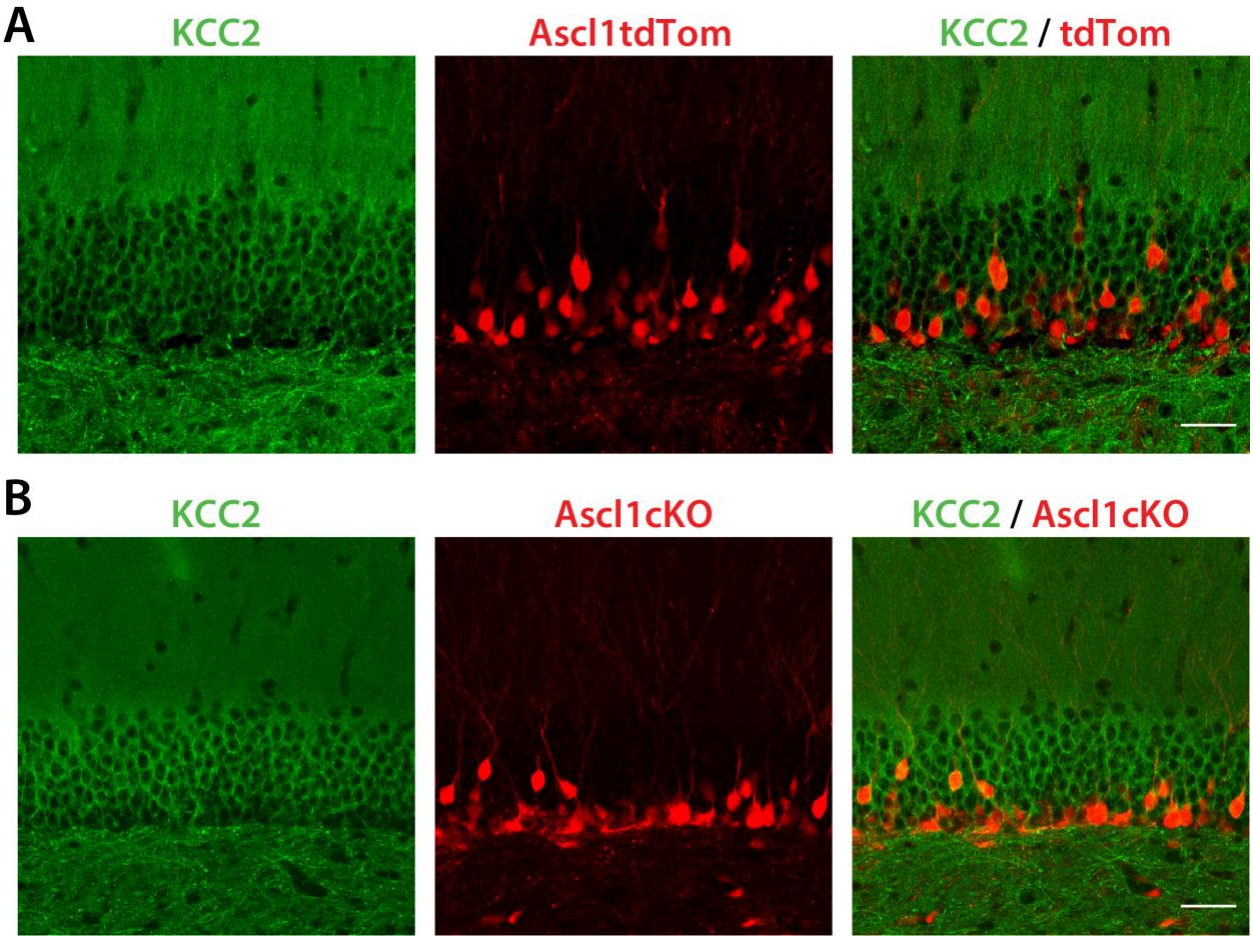

Figure 5.1 KCC2 staining in 21 dpi Ascl1tdTom and Ascl1cKO abDGCs

5.4 Future directions

The efferent synaptic connectivity and plasticity of GluK2 cKO abDGCs

As already mentioned, the output synaptic connectivity and the plasticity at the MF-CA3 synapse of GluK2 knockout abDGCs have not been investigated in this thesis project due to time constraints. However, it would be expected that these are changed in 21 dpi abDGCs in which GluK2 is ablated, as implied by our behavioral analysis and previous relevant studies demonstrating delayed physiological maturation of AMPA-EPSC amplitude and reduced LTP at MF-CA3 synapses in global GluK2 KO mice during early postnatal development (Contractor et

al., 2001; Lanore et al., 2012). Moreover, these are important questions for understanding integration of abDGCs into the hippocampal circuit and how KARs may affect this process. First of all, whether the development of physiological properties as well as plasticity is changed at MF-CA3 synapses formed by GluK2 cKO abDGCs remains to be determined. In addition, the feedforward inhibition (FFI) mediated by abDGCs' outputs to distal interneurons in the CA3 should also be examined by recording the postsynaptic potential in CA3 pyramidal neurons and comparing the disynaptic inhibitory component. The excitation/inhibition ratio of the abDGC-evoked response can be determined to provide additional insights into how a depolarizing GABA reversal potential resulting from loss of GluK2 may contribute to alterations in abDGCs' efferent synaptogenesis with interneurons and pyramidal neurons in the CA3 hence influence the hippocampal microcircuit. Furthermore, abDGCs have been proposed to inhibit firing of mature DGCs via connections to a rich network of local interneurons and mossy cells in the hilus (Johnston et al., 2016). It would also be important to compare the FBI recruited by abDGCs at different postmitotic ages as they develop to gain a greater understanding of how unusual functional properties of abDGCs might alter information processing in the DG. To perform a full analysis of the development of abDGC-mediated MF-CA3 synapses, FFI onto CA3 neurons and FBI onto mature DGCs would require use of optogenetic approaches in birth-dated GluK2 cKO abDGCs, and comparing light-evoked responses in CA3 pyramidal neurons or mature DGCs respectively.

Test the causative role of GluK2 in altering the functional properties of abDGCs

We propose but have not tested yet that GluK2-KCC2 interaction is the causative mechanism that accounts for the abnormal functional properties of abDGCs that we observed after ablation of GluK2. Several future experiments could be performed to confirm such a causal role of GluK2-

KCC2 interaction in regulating the functional development of abDGCs: 1) since it has been shown that Neto2, the KAR auxiliary subunit (Zhang et al., 2009), is also a KCC2 interacting protein and that loss of Neto2 results in depolarized E_{GABA} (Ivakine et al., 2013; Mahadevan et al., 2015), recordings from abDGCs in Neto2-null mice should phenocopy and verify what we have found in GluK2 knockout cells; 2) manipulation of chloride transporters to rectify E_{GABA} should be able to restore normal intrinsic properties and inhibitory synapse formation in GluK2 knockout abDGCs. For example, since NKCC1 is normally expressed at low levels in mature neurons, systematic administration of the NKCC1 antagonist bumetanide (Ben-Ari, 2017) would putatively lead to re-equilibration of Cl^- homeostasis in immature abDGCs and reverse their functional anomalies with little influence on mature neurons. Alternatively, a KCC2 enhancer CLP257 (Gagnon et al., 2013) can also be possibly used to complement and confirm the causal role of depolarized E_{GABA} due to disrupted GluK2-KCC2 interaction. These experiments will help establish a novel role for KARs in regulating abDGC functional properties and hippocampal function through an interaction with the GABA signaling system.

In vivo calcium imaging to study the neural substrates of altered behavior

Furthermore, how altered intrinsic and synaptic properties of abDGCs due to loss of GluK2 influence their circuit function and ultimately lead to the deficit in spatial discrimination remains a mystery. In vivo calcium imaging that can monitor the real-time activation of a cohort of birth-dated abDGCs using head-mounted micro-endoscopes as animals are performing the behavioral tasks is promising, as this may help to clarify the neural substrates and any circuit-level alteration underlying the impaired discrimination behavior in Ascl1cKO mice by providing the necessary spatial and temporal resolution.

5.5 Concluding remarks

The development of abDGCs is highly regulated and sensitive to many genetic and environmental factors. Our data have uncovered a role for GluK2 KARs in the development of proper functional properties of abDGCs at an early critical postmitotic time. We propose that an interaction between KARs and the GABA signaling system may underlie this role, and disruption of this interaction results in misrepresented abDGC functional properties that impact behavior. Adult hippocampal neurogenesis is a daily, ongoing dynamic process so that the hippocampus always contains mixed populations of immature and mature DGCs born at different times throughout life. As newly generated abDGCs mature and integrate into the circuit over time, they may assume different roles in different types of hippocampal-dependent behaviors, depending on their distinct cellular properties and synaptic connectivity at different postmitotic ages. The roles that KARs have in circuit development and function are still not fully appreciated. This new description of their roles in abDGCs during a short critical time window of their development provides another important facet of KARs' contribution to the hippocampal function, and further expands our growing understanding of the intricate interplay between excitatory and inhibitory neurotransmitter signaling in the central nervous system.

References

Aguado, T., Romero, E., Monory, K., Palazuelos, J., Sendtner, M., Marsicano, G., Lutz, B., Guzmán, M., and Galve-Roperh, I. (2007). The CB1 cannabinoid receptor mediates excitotoxicity-induced neural progenitor proliferation and neurogenesis. J Biol Chem *282*, 23892–23898.

Aller, M.I., Pecoraro, V., Paternain, A.V., Canals, S., and Lerma, J. (2015). Increased Dosage of High-Affinity Kainate Receptor Gene grik4 Alters Synaptic Transmission and Reproduces Autism Spectrum Disorders Features. J Neurosci *35*, 13619–13628.

Alvarez, D.D., Giacomini, D., Yang, S.M., Trinchero, M.F., Temprana, S.G., Büttner, K.A., Beltramone, N., and Schinder, A.F. (2016). A disynaptic feedback network activated by experience promotes the integration of new granule cells. Science *354*, 459–465.

Amaral, D.G., Scharfman, H.E., and Lavenex, P. (2007). The dentate gyrus: fundamental neuroanatomical organization (dentate gyrus for dummies). Prog. Brain Res. *163*, 3–22.

Anacker, C., Luna, V.M., Stevens, G.S., Millette, A., Shores, R., Jimenez, J.C., Chen, B., and Hen, R. (2018). Hippocampal neurogenesis confers stress resilience by inhibiting the ventral dentate gyrus. Nature *559*, 98–102.

Becker, S., and Wojtowicz, J.M. (2007). A model of hippocampal neurogenesis in memory and mood disorders. Trends Cogn Sci (Regul Ed) *11*, 70–76.

Ben-Ari, Y. (2017). NKCC1 chloride importer antagonists attenuate many neurological and psychiatric disorders. Trends Neurosci *40*, 536–554.

Berg, D.A., Belnoue, L., Song, H., and Simon, A. (2013). Neurotransmitter-mediated control of neurogenesis in the adult vertebrate brain. Development *140*, 2548–2561.

Boldrini, M., Fulmore, C.A., Tartt, A.N., Simeon, L.R., Pavlova, I., Poposka, V., Rosoklija, G.B.,

Stankov, A., Arango, V., Dwork, A.J., et al. (2018). Human Hippocampal Neurogenesis Persists throughout Aging. Cell Stem Cell *22*, 589-599.e5.

Brazel, C.Y., Nuñez, J.L., Yang, Z., and Levison, S.W. (2005). Glutamate enhances survival and proliferation of neural progenitors derived from the subventricular zone. Neuroscience *131*, 55–65.

Bureau, I., Bischoff, S., Heinemann, S.F., and Mulle, C. (1999). Kainate receptor-mediated responses in the CA1 field of wild-type and GluR6-deficient mice. J Neurosci *19*, 653–663.

Burghardt, N.S., Park, E.H., Hen, R., and Fenton, A.A. (2012). Adult-born hippocampal neurons promote cognitive flexibility in mice. Hippocampus *22*, 1795–1808.

Carta, M., Fièvre, S., Gorlewicz, A., and Mulle, C. (2014). Kainate receptors in the hippocampus. Eur. J. Neurosci. *39*, 1835–1844.

Castillon, C., Lunion, S., Desvignes, N., Hanauer, A., Laroche, S., and Poirier, R. (2018). Selective alteration of adult hippocampal neurogenesis and impaired spatial pattern separation performance in the RSK2-deficient mouse model of Coffin-Lowry syndrome. Neurobiol Dis *115*, 69–81.

Catavero, C., Bao, H., and Song, J. (2018). Neural mechanisms underlying GABAergic regulation of adult hippocampal neurogenesis. Cell Tissue Res *371*, 33–46.

Catches, J.S., Xu, J., and Contractor, A. (2012). Genetic ablation of the GluK4 kainate receptor subunit causes anxiolytic and antidepressant-like behavior in mice. Behav Brain Res *228*, 406–414.

Chancey, J.H., Adlaf, E.W., Sapp, M.C., Pugh, P.C., Wadiche, J.I., and Overstreet-Wadiche, L.S. (2013). GABA depolarization is required for experience-dependent synapse unsilencing in adult-born neurons. J Neurosci *33*, 6614–6622.

Chancey, J.H., Poulsen, D.J., Wadiche, J.I., and Overstreet-Wadiche, L. (2014). Hilar mossy cells provide the first glutamatergic synapses to adult-born dentate granule cells. J Neurosci *34*, 2349–2354.

Chowdhury, N., Quinn, J.J., and Fanselow, M.S. (2005). Dorsal hippocampus involvement in trace fear conditioning with long, but not short, trace intervals in mice. Behav Neurosci *119*, 1396–1402.

Clelland, C.D., Choi, M., Romberg, C., Clemenson, G.D., Fragniere, A., Tyers, P., Jessberger, S., Saksida, L.M., Barker, R.A., Gage, F.H., et al. (2009). A functional role for adult hippocampal neurogenesis in spatial pattern separation. Science *325*, 210–213.

Cole, J.D., Espinueva, D.F., Seib, D.R., Ash, A.M., Cooke, M.B., Cahill, S.P., O'Leary, T.P., Kwan, S.S., and Snyder, J.S. (2020). Adult-Born Hippocampal Neurons Undergo Extended Development and Are Morphologically Distinct from Neonatally-Born Neurons. J Neurosci *40*, 5740–5756.

Contractor, A., Swanson, G.T., Sailer, A., O'Gorman, S., and Heinemann, S.F. (2000). Identification of the kainate receptor subunits underlying modulation of excitatory synaptic transmission in the CA3 region of the hippocampus. J. Neurosci. *20*, 8269–8278.

Contractor, A., Swanson, G., and Heinemann, S.F. (2001). Kainate receptors are involved in short- and long-term plasticity at mossy fiber synapses in the hippocampus. Neuron *29*, 209–216.

Contractor, A., Mulle, C., and Swanson, G.T. (2011). Kainate receptors coming of age: milestones of two decades of research. Trends Neurosci *34*, 154–163.

Creer, D.J., Romberg, C., Saksida, L.M., van Praag, H., and Bussey, T.J. (2010). Running enhances spatial pattern separation in mice. Proc Natl Acad Sci U S A *107*, 2367–2372.

Danielson, N.B., Kaifosh, P., Zaremba, J.D., Lovett-Barron, M., Tsai, J., Denny, C.A., Balough,

E.M., Goldberg, A.R., Drew, L.J., Hen, R., et al. (2016). Distinct Contribution of Adult-Born Hippocampal Granule Cells to Context Encoding. Neuron *90*, 101–112.

Deisseroth, K., Singla, S., Toda, H., Monje, M., Palmer, T.D., and Malenka, R.C. (2004). Excitation-neurogenesis coupling in adult neural stem/progenitor cells. Neuron *42*, 535–552.

Deng, W., Aimone, J.B., and Gage, F.H. (2010). New neurons and new memories: how does adult hippocampal neurogenesis affect learning and memory? Nat Rev Neurosci *11*, 339–350.

Deshpande, A., Bergami, M., Ghanem, A., Conzelmann, K.-K., Lepier, A., Götz, M., and Berninger, B. (2013). Retrograde monosynaptic tracing reveals the temporal evolution of inputs onto new neurons in the adult dentate gyrus and olfactory bulb. Proc Natl Acad Sci U S A *110*, E1152–E1161.

Dieni, C.V., Nietz, A.K., Panichi, R., Wadiche, J.I., and Overstreet-Wadiche, L. (2013). Distinct determinants of sparse activation during granule cell maturation. J Neurosci *33*, 19131–19142.

Dieni, C.V., Panichi, R., Aimone, J.B., Kuo, C.T., Wadiche, J.I., and Overstreet-Wadiche, L. (2016). Low excitatory innervation balances high intrinsic excitability of immature dentate neurons. Nat Commun *7*, 11313.

Dix, S.L., and Aggleton, J.P. (1999). Extending the spontaneous preference test of recognition: evidence of object-location and object-context recognition. Behav. Brain Res. *99*, 191–200.

Drew, L.J., Fusi, S., and Hen, R. (2013). Adult neurogenesis in the mammalian hippocampus: why the dentate gyrus? Learn Mem *20*, 710–729.

Drew, L.J., Kheirbek, M.A., Luna, V.M., Denny, C.A., Cloidt, M.A., Wu, M.V., Jain, S., Scharfman, H.E., and Hen, R. (2016). Activation of local inhibitory circuits in the dentate

gyrus by adult-born neurons. Hippocampus *26*, 763–778.

Duveau, V., Laustela, S., Barth, L., Gianolini, F., Vogt, K.E., Keist, R., Chandra, D., Homanics, G.E., Rudolph, U., and Fritschy, J.-M. (2011). Spatiotemporal specificity of GABAA receptor-mediated regulation of adult hippocampal neurogenesis. Eur. J. Neurosci. *34*, 362–373.

Epsztein, J., Represa, A., Jorquera, I., Ben-Ari, Y., and Crépel, V. (2005). Recurrent mossy fibers establish aberrant kainate receptor-operated synapses on granule cells from epileptic rats. J Neurosci *25*, 8229–8239.

Eriksson, P.S., Perfilieva, E., Björk-Eriksson, T., Alborn, A.M., Nordborg, C., Peterson, D.A., and Gage, F.H. (1998). Neurogenesis in the adult human hippocampus. Nat Med *4*, 1313–1317.

Espósito, M.S., Piatti, V.C., Laplagne, D.A., Morgenstern, N.A., Ferrari, C.C., Pitossi, F.J., and Schinder, A.F. (2005). Neuronal differentiation in the adult hippocampus recapitulates embryonic development. J Neurosci *25*, 10074–10086.

Farley, S.J., McKay, B.M., Disterhoft, J.F., and Weiss, C. (2011). Reevaluating hippocampus-dependent learning in FVB/N mice. Behav Neurosci *125*, 871–878.

Fernandes, H.B., Catches, J.S., Petralia, R.S., Copits, B.A., Xu, J., Russell, T.A., Swanson, G.T., and Contractor, A. (2009). High-affinity kainate receptor subunits are necessary for ionotropic but not metabotropic signaling. Neuron *63*, 818–829.

Gage, F.H. (2019). Adult neurogenesis in mammals. Science *364*, 827–828.

Gagnon, M., Bergeron, M.J., Lavertu, G., Castonguay, A., Tripathy, S., Bonin, R.P., Perez-Sanchez, J., Boudreau, D., Wang, B., Dumas, L., et al. (2013). Chloride extrusion enhancers as novel therapeutics for neurological diseases. Nat Med *19*, 1524–1528.

Ge, S., Goh, E.L.K., Sailor, K.A., Kitabatake, Y., Ming, G., and Song, H. (2006). GABA regulates

synaptic integration of newly generated neurons in the adult brain. Nature *439*, 589–593.

Ge, S., Yang, C.-H., Hsu, K.-S., Ming, G.-L., and Song, H. (2007). A critical period for enhanced synaptic plasticity in newly generated neurons of the adult brain. Neuron *54*, 559–566.

Gonçalves, J.T., Bloyd, C.W., Shtrahman, M., Johnston, S.T., Schafer, S.T., Parylak, S.L., Tran, T., Chang, T., and Gage, F.H. (2016). In vivo imaging of dendritic pruning in dentate granule cells. Nat Neurosci *19*, 788–791.

Goodman, T., Trouche, S., Massou, I., Verret, L., Zerwas, M., Roullet, P., and Rampon, C. (2010). Young hippocampal neurons are critical for recent and remote spatial memory in adult mice. Neuroscience *171*, 769–778.

Gould, E., McEwen, B.S., Tanapat, P., Galea, L.A., and Fuchs, E. (1997). Neurogenesis in the dentate gyrus of the adult tree shrew is regulated by psychosocial stress and NMDA receptor activation. J Neurosci *17*, 2492–2498.

Gould, E., Beylin, A., Tanapat, P., Reeves, A., and Shors, T.J. (1999). Learning enhances adult neurogenesis in the hippocampal formation. Nat. Neurosci. *2*, 260–265.

Groisman, A.I., Yang, S.M., and Schinder, A.F. (2020). Differential Coupling of Adult-Born Granule Cells to Parvalbumin and Somatostatin Interneurons. Cell Rep. *30*, 202-214.e4.

Gu, Y., Arruda-Carvalho, M., Wang, J., Janoschka, S.R., Josselyn, S.A., Frankland, P.W., and Ge, S. (2012). Optical controlling reveals time-dependent roles for adult-born dentate granule cells. Nat Neurosci *15*, 1700–1706.

Heigele, S., Sultan, S., Toni, N., and Bischofberger, J. (2016). Bidirectional GABAergic control of action potential firing in newborn hippocampal granule cells. Nat. Neurosci. *19*, 263–270.

Huckleberry, K.A., Shue, F., Copeland, T., Chitwood, R.A., Yin, W., and Drew, M.R. (2018).

Dorsal and ventral hippocampal adult-born neurons contribute to context fear memory. Neuropsychopharmacology *43*, 2487–2496.

Iida, I., Konno, K., Natsume, R., Abe, M., Watanabe, M., Sakimura, K., and Terunuma, M. (2021). A comparative analysis of kainate receptor GluK2 and GluK5 knockout mice in a pure genetic background. Behav Brain Res *405*, 113194.

Ivakine, E.A., Acton, B.A., Mahadevan, V., Ormond, J., Tang, M., Pressey, J.C., Huang, M.Y., Ng, D., Delpire, E., Salter, M.W., et al. (2013). Neto2 is a KCC2 interacting protein required for neuronal Cl- regulation in hippocampal neurons. Proc Natl Acad Sci U S A *110*, 3561–3566.

Jack, A., Hamad, M.I.K., Gonda, S., Gralla, S., Pahl, S., Hollmann, M., and Wahle, P. (2019). Development of cortical pyramidal cell and interneuronal dendrites: a role for kainate receptor subunits and NETO1. Mol. Neurobiol. *56*, 4960–4979.

Jagasia, R., Steib, K., Englberger, E., Herold, S., Faus-Kessler, T., Saxe, M., Gage, F.H., Song, H., and Lie, D.C. (2009). GABA-cAMP response element-binding protein signaling regulates maturation and survival of newly generated neurons in the adult hippocampus. J Neurosci *29*, 7966–7977.

Jessberger, S., and Parent, J.M. (2015). Epilepsy and adult neurogenesis. Cold Spring Harb. Perspect. Biol. *7*.

Johnston, S.T., Shtrahman, M., Parylak, S., Gonçalves, J.T., and Gage, F.H. (2016). Paradox of pattern separation and adult neurogenesis: A dual role for new neurons balancing memory resolution and robustness. Neurobiol Learn Mem *129*, 60–68.

Jung, M.W., and McNaughton, B.L. (1993). Spatial selectivity of unit activity in the hippocampal granular layer. Hippocampus *3*, 165–182.

Kempermann, G., Kuhn, H.G., and Gage, F.H. (1997). More hippocampal neurons in adult mice living in an enriched environment. Nature *386*, 493–495.

Kempermann, G., Gage, F.H., Aigner, L., Song, H., Curtis, M.A., Thuret, S., Kuhn, H.G., Jessberger, S., Frankland, P.W., Cameron, H.A., et al. (2018). Human adult neurogenesis: evidence and remaining questions. Cell Stem Cell *23*, 25–30.

Kerloch, T., Clavreul, S., Goron, A., Abrous, D.N., and Pacary, E. (2019). Dentate Granule Neurons Generated During Perinatal Life Display Distinct Morphological Features Compared With Later-Born Neurons in the Mouse Hippocampus. Cereb Cortex *29*, 3527–3539.

Kesaf, S., Khirug, S., Dinh, E., Saez Garcia, M., Soni, S., Orav, E., Delpire, E., Taira, T., Lauri, S.E., and Rivera, C. (2020). The kainate receptor subunit gluk2 interacts with KCC2 to promote maturation of dendritic spines. Front Cell Neurosci *14*, 252.

Kitamura, T., Saitoh, Y., Murayama, A., Sugiyama, H., and Inokuchi, K. (2010). LTP induction within a narrow critical period of immature stages enhances the survival of newly generated neurons in the adult rat dentate gyrus. Mol. Brain *3*, 13.

Klempin, F., and Kempermann, G. (2007). Adult hippocampal neurogenesis and aging. Eur. Arch. Psychiatry Clin. Neurosci. *257*, 271–280.

Kuhn, H.G., Dickinson-Anson, H., and Gage, F.H. (1996). Neurogenesis in the dentate gyrus of the adult rat: age-related decrease of neuronal progenitor proliferation. J Neurosci *16*, 2027–2033.

Kumar, D., Koyanagi, I., Carrier-Ruiz, A., Vergara, P., Srinivasan, S., Sugaya, Y., Kasuya, M., Yu, T.-S., Vogt, K.E., Muratani, M., et al. (2020). Sparse Activity of Hippocampal Adult-Born Neurons during REM Sleep Is Necessary for Memory Consolidation. Neuron *107*,

552–565.e10.

Lanore, F., Labrousse, V.F., Szabo, Z., Normand, E., Blanchet, C., and Mulle, C. (2012). Deficits in morphofunctional maturation of hippocampal mossy fiber synapses in a mouse model of intellectual disability. J Neurosci *32*, 17882–17893.

Laplagne, D.A., Espósito, M.S., Piatti, V.C., Morgenstern, N.A., Zhao, C., van Praag, H., Gage, F.H., and Schinder, A.F. (2006). Functional convergence of neurons generated in the developing and adult hippocampus. PLoS Biol *4*, e409.

Laszczyk, A.M., Fox-Quick, S., Vo, H.T., Nettles, D., Pugh, P.C., Overstreet-Wadiche, L., and King, G.D. (2017). Klotho regulates postnatal neurogenesis and protects against age-related spatial memory loss. Neurobiol Aging *59*, 41–54.

Lauri, S.E., Bortolotto, Z.A., Bleakman, D., Ornstein, P.L., Lodge, D., Isaac, J.T., and Collingridge, G.L. (2001). A critical role of a facilitatory presynaptic kainate receptor in mossy fiber LTP. Neuron *32*, 697–709.

Lauri, S.E., Vesikansa, A., Segerstråle, M., Collingridge, G.L., Isaac, J.T.R., and Taira, T. (2006). Functional maturation of CA1 synapses involves activity-dependent loss of tonic kainate receptor-mediated inhibition of glutamate release. Neuron *50*, 415–429.

Lepousez, G., Nissant, A., and Lledo, P.-M. (2015). Adult neurogenesis and the future of the rejuvenating brain circuits. Neuron *86*, 387–401.

Lerma, J., and Marques, J.M. (2013). Kainate receptors in health and disease. Neuron *80*, 292–311.

Li, Y., Aimone, J.B., Xu, X., Callaway, E.M., and Gage, F.H. (2012). Development of GABAergic inputs controls the contribution of maturing neurons to the adult hippocampal network. Proc Natl Acad Sci U S A *109*, 4290–4295.

Lodge, M., and Bischofberger, J. (2019). Synaptic properties of newly generated granule cells support sparse coding in the adult hippocampus. Behav. Brain Res. *372*, 112036.

Lopez-Rojas, J., and Kreutz, M.R. (2016). Mature granule cells of the dentate gyrus--Passive bystanders or principal performers in hippocampal function? Neurosci. Biobehav. Rev. *64*, 167–174.

Luna, V.M., Anacker, C., Burghardt, N.S., Khandaker, H., Andreu, V., Millette, A., Leary, P., Ravenelle, R., Jimenez, J.C., Mastrodonato, A., et al. (2019). Adult-born hippocampal neurons bidirectionally modulate entorhinal inputs into the dentate gyrus. Science *364*, 578–583.

Mahadevan, V., Pressey, J.C., Acton, B.A., Uvarov, P., Huang, M.Y., Chevrier, J., Puchalski, A., Li, C.M., Ivakine, E.A., Airaksinen, M.S., et al. (2014). Kainate receptors coexist in a functional complex with KCC2 and regulate chloride homeostasis in hippocampal neurons. Cell Rep *7*, 1762–1770.

Mahadevan, V., Dargaei, Z., Ivakine, E.A., Hartmann, A.-M., Ng, D., Chevrier, J., Ormond, J., Nothwang, H.G., McInnes, R.R., and Woodin, M.A. (2015). Neto2-null mice have impaired GABAergic inhibition and are susceptible to seizures. Front Cell Neurosci *9*, 368.

Malberg, J.E., Eisch, A.J., Nestler, E.J., and Duman, R.S. (2000). Chronic antidepressant treatment increases neurogenesis in adult rat hippocampus. J. Neurosci. *20*, 9104–9110.

Marín-Burgin, A., Mongiat, L.A., Pardi, M.B., and Schinder, A.F. (2012). Unique processing during a period of high excitation/inhibition balance in adult-born neurons. Science *335*, 1238–1242.

Marschallinger, J., Schäffner, I., Klein, B., Gelfert, R., Rivera, F.J., Illes, S., Grassner, L., Janssen, M., Rotheneichner, P., Schmuckermair, C., et al. (2015). Structural and functional

rejuvenation of the aged brain by an approved anti-asthmatic drug. Nat Commun *6*, 8466.

Marshall, J.J., Xu, J., and Contractor, A. (2018). Kainate receptors inhibit glutamate release via mobilization of endocannabinoids in striatal direct pathway spiny projection neurons. J Neurosci *38*, 3901–3910.

Micheau, J., Vimeney, A., Normand, E., Mulle, C., and Riedel, G. (2014). Impaired hippocampus-dependent spatial flexibility and sociability represent autism-like phenotypes in GluK2 mice. Hippocampus *24*, 1059–1069.

Ming, G.-L., and Song, H. (2011). Adult neurogenesis in the mammalian brain: significant answers and significant questions. Neuron *70*, 687–702.

Mirescu, C., and Gould, E. (2006). Stress and adult neurogenesis. Hippocampus *16*, 233–238.

Misane, I., Tovote, P., Meyer, M., Spiess, J., Ogren, S.O., and Stiedl, O. (2005). Time-dependent involvement of the dorsal hippocampus in trace fear conditioning in mice. Hippocampus *15*, 418–426.

Mongiat, L.A., Espósito, M.S., Lombardi, G., and Schinder, A.F. (2009). Reliable activation of immature neurons in the adult hippocampus. PLoS ONE *4*, e5320.

Moreno-Jiménez, E.P., Flor-García, M., Terreros-Roncal, J., Rábano, A., Cafini, F., Pallas-Bazarra, N., Ávila, J., and Llorens-Martín, M. (2019). Adult hippocampal neurogenesis is abundant in neurologically healthy subjects and drops sharply in patients with Alzheimer's disease. Nat Med *25*, 554–560.

Mu, Y., Zhao, C., Toni, N., Yao, J., and Gage, F.H. (2015). Distinct roles of NMDA receptors at different stages of granule cell development in the adult brain. Elife *4*, e07871.

Mulle, C., Sailer, A., Pérez-Otaño, I., Dickinson-Anson, H., Castillo, P.E., Bureau, I., Maron, C., Gage, F.H., Mann, J.R., Bettler, B., et al. (1998). Altered synaptic physiology and reduced

susceptibility to kainate-induced seizures in GluR6-deficient mice. Nature *392*, 601–605.

Nakashiba, T., Cushman, J.D., Pelkey, K.A., Renaudineau, S., Buhl, D.L., McHugh, T.J., Rodriguez Barrera, V., Chittajallu, R., Iwamoto, K.S., McBain, C.J., et al. (2012). Young dentate granule cells mediate pattern separation, whereas old granule cells facilitate pattern completion. Cell *149*, 188–201.

Orav, E., Atanasova, T., Shintyapina, A., Kesaf, S., Kokko, M., Partanen, J., Taira, T., and Lauri, S.E. (2017). NETO1 guides development of glutamatergic connectivity in the hippocampus by regulating axonal kainate receptors. ENeuro *4*.

O'Reilly, R.C., and McClelland, J.L. (1994). Hippocampal conjunctive encoding, storage, and recall: avoiding a trade-off. Hippocampus *4*, 661–682.

Overstreet Wadiche, L., Bromberg, D.A., Bensen, A.L., and Westbrook, G.L. (2005). GABAergic signaling to newborn neurons in dentate gyrus. J Neurophysiol *94*, 4528–4532.

Paternain, A.V., Herrera, M.T., Nieto, M.A., and Lerma, J. (2000). GluR5 and GluR6 kainate receptor subunits coexist in hippocampal neurons and coassemble to form functional receptors. J Neurosci *20*, 196–205.

Peret, A., Christie, L.A., Ouedraogo, D.W., Gorlewicz, A., Epsztein, J., Mulle, C., and Crépel, V. (2014). Contribution of aberrant GluK2-containing kainate receptors to chronic seizures in temporal lobe epilepsy. Cell Rep. *8*, 347–354.

Pérez-Gómez, A., and Tasker, R.A. (2012). Enhanced neurogenesis in organotypic cultures of rat hippocampus after transient subfield-selective excitotoxic insult induced by domoic acid. Neuroscience *208*, 97–108.

Piatti, V.C., Davies-Sala, M.G., Espósito, M.S., Mongiat, L.A., Trinchero, M.F., and Schinder, A.F. (2011). The timing for neuronal maturation in the adult hippocampus is modulated by

local network activity. J Neurosci *31*, 7715–7728.

Platel, J.-C., Heintz, T., Young, S., Gordon, V., and Bordey, A. (2008). Tonic activation of GLUK5 kainate receptors decreases neuroblast migration in whole-mounts of the subventricular zone. J Physiol (Lond) *586*, 3783–3793.

Platel, J.-C., Stamboulian, S., Nguyen, I., and Bordey, A. (2010). Neurotransmitter signaling in postnatal neurogenesis: The first leg. Brain Res Rev *63*, 60–71.

van Praag, H., Christie, B.R., Sejnowski, T.J., and Gage, F.H. (1999). Running enhances neurogenesis, learning, and long-term potentiation in mice. Proc Natl Acad Sci U S A *96*, 13427–13431.

van Praag, H., Schinder, A.F., Christie, B.R., Toni, N., Palmer, T.D., and Gage, F.H. (2002). Functional neurogenesis in the adult hippocampus. Nature *415*, 1030–1034.

Pressey, J.C., Mahadevan, V., Khademullah, C.S., Dargaei, Z., Chevrier, J., Ye, W., Huang, M., Chauhan, A.K., Meas, S.J., Uvarov, P., et al. (2017). A kainate receptor subunit promotes the recycling of the neuron-specific K+-Cl- co-transporter KCC2 in hippocampal neurons. J Biol Chem *292*, 6190–6201.

Remmers, C.L., and Contractor, A. (2018). Development of gabaergic inputs is not altered in early maturation of adult born dentate granule neurons in fragile X mice. eNeuro *5*.

Remmers, C.L., Castillon, C.C.M., Armstrong, J.N., and Contractor, A. (2020). Recruitment of parvalbumin and somatostatin interneuron inputs to adult born dentate granule neurons. Sci. Rep. *10*, 17522.

Rivera, C., Voipio, J., Payne, J.A., Ruusuvuori, E., Lahtinen, H., Lamsa, K., Pirvola, U., Saarma, M., and Kaila, K. (1999). The K+/Cl- co-transporter KCC2 renders GABA hyperpolarizing during neuronal maturation. Nature *397*, 251–255.

Sahay, A., and Hen, R. (2007). Adult hippocampal neurogenesis in depression. Nat Neurosci *10*, 1110–1115.

Sahay, A., Wilson, D.A., and Hen, R. (2011a). Pattern separation: a common function for new neurons in hippocampus and olfactory bulb. Neuron *70*, 582–588.

Sahay, A., Scobie, K.N., Hill, A.S., O'Carroll, C.M., Kheirbek, M.A., Burghardt, N.S., Fenton, A.A., Dranovsky, A., and Hen, R. (2011b). Increasing adult hippocampal neurogenesis is sufficient to improve pattern separation. Nature *472*, 466–470.

Sah, N., Peterson, B.D., Lubejko, S.T., Vivar, C., and van Praag, H. (2017). Running reorganizes the circuitry of one-week-old adult-born hippocampal neurons. Sci. Rep. *7*, 10903.

Sakha, P., Vesikansa, A., Orav, E., Heikkinen, J., Kukko-Lukjanov, T.-K., Shintyapina, A., Franssila, S., Jokinen, V., Huttunen, H.J., and Lauri, S.E. (2016). Axonal kainate receptors modulate the strength of efferent connectivity by regulating presynaptic differentiation. Front. Cell. Neurosci. *10*, 3.

Santarelli, L., Saxe, M., Gross, C., Surget, A., Battaglia, F., Dulawa, S., Weisstaub, N., Lee, J., Duman, R., Arancio, O., et al. (2003). Requirement of hippocampal neurogenesis for the behavioral effects of antidepressants. Science *301*, 805–809.

Saxe, M.D., Battaglia, F., Wang, J.-W., Malleret, G., David, D.J., Monckton, J.E., Garcia, A.D.R., Sofroniew, M.V., Kandel, E.R., Santarelli, L., et al. (2006). Ablation of hippocampal neurogenesis impairs contextual fear conditioning and synaptic plasticity in the dentate gyrus. Proc Natl Acad Sci U S A *103*, 17501–17506.

Schmidt-Hieber, C., Jonas, P., and Bischofberger, J. (2004). Enhanced synaptic plasticity in newly generated granule cells of the adult hippocampus. Nature *429*, 184–187.

Schmidt-Salzmann, C., Li, L., and Bischofberger, J. (2014). Functional properties of extrasynaptic

AMPA and NMDA receptors during postnatal hippocampal neurogenesis. J Physiol (Lond) *592*, 125–140.

Schmitz, D., Mellor, J., and Nicoll, R.A. (2001). Presynaptic kainate receptor mediation of frequency facilitation at hippocampal mossy fiber synapses. Science *291*, 1972–1976.

Seib, D.R., Espinueva, D.F., Princz-Lebel, O., Chahley, E., Stevenson, J., O'Leary, T.P., Floresco, S.B., and Snyder, J.S. (2021). Hippocampal neurogenesis promotes preference for future rewards. Mol. Psychiatry.

Shaltiel, G., Maeng, S., Malkesman, O., Pearson, B., Schloesser, R.J., Tragon, T., Rogawski, M., Gasior, M., Luckenbaugh, D., Chen, G., et al. (2008). Evidence for the involvement of the kainate receptor subunit GluR6 (GRIK2) in mediating behavioral displays related to behavioral symptoms of mania. Mol Psychiatry *13*, 858–872.

Shors, T.J., Miesegaes, G., Beylin, A., Zhao, M., Rydel, T., and Gould, E. (2001). Neurogenesis in the adult is involved in the formation of trace memories. Nature *410*, 372–376.

Sim, S., Antolin, S., Lin, C.-W., Lin, Y., and Lois, C. (2013). Increased cell-intrinsic excitability induces synaptic changes in new neurons in the adult dentate gyrus that require Npas4. J Neurosci *33*, 7928–7940.

Snyder, J.S., Soumier, A., Brewer, M., Pickel, J., and Cameron, H.A. (2011). Adult hippocampal neurogenesis buffers stress responses and depressive behaviour. Nature *476*, 458–461.

Song, J., Zhong, C., Bonaguidi, M.A., Sun, G.J., Hsu, D., Gu, Y., Meletis, K., Huang, Z.J., Ge, S., Enikolopov, G., et al. (2012). Neuronal circuitry mechanism regulating adult quiescent neural stem-cell fate decision. Nature *489*, 150–154.

Song, J., Sun, J., Moss, J., Wen, Z., Sun, G.J., Hsu, D., Zhong, C., Davoudi, H., Christian, K.M., Toni, N., et al. (2013). Parvalbumin interneurons mediate neuronal circuitry-neurogenesis

coupling in the adult hippocampus. Nat Neurosci *16*, 1728–1730.

Spalding, K.L., Bergmann, O., Alkass, K., Bernard, S., Salehpour, M., Huttner, H.B., Boström, E., Westerlund, I., Vial, C., Buchholz, B.A., et al. (2013). Dynamics of hippocampal neurogenesis in adult humans. Cell *153*, 1219–1227.

Tashiro, A., Sandler, V.M., Toni, N., Zhao, C., and Gage, F.H. (2006a). NMDA-receptor-mediated, cell-specific integration of new neurons in adult dentate gyrus. Nature *442*, 929–933.

Tashiro, A., Zhao, C., and Gage, F.H. (2006b). Retrovirus-mediated single-cell gene knockout technique in adult newborn neurons in vivo. Nat Protoc *1*, 3049–3055.

Tashiro, A., Makino, H., and Gage, F.H. (2007). Experience-specific functional modification of the dentate gyrus through adult neurogenesis: a critical period during an immature stage. J Neurosci *27*, 3252–3259.

Temprana, S.G., Mongiat, L.A., Yang, S.M., Trinchero, M.F., Alvarez, D.D., Kropff, E., Giacomini, D., Beltramone, N., Lanuza, G.M., and Schinder, A.F. (2015). Delayed coupling to feedback inhibition during a critical period for the integration of adult-born granule cells. Neuron *85*, 116–130.

Toda, T., Parylak, S.L., Linker, S.B., and Gage, F.H. (2019). The role of adult hippocampal neurogenesis in brain health and disease. Mol Psychiatry *24*, 67–87.

Toni, N., Laplagne, D.A., Zhao, C., Lombardi, G., Ribak, C.E., Gage, F.H., and Schinder, A.F. (2008). Neurons born in the adult dentate gyrus form functional synapses with target cells. Nat. Neurosci. *11*, 901–907.

Toni, N., and Schinder, A.F. (2015). Maturation and Functional Integration of New Granule Cells into the Adult Hippocampus. Cold Spring Harb. Perspect. Biol. *8*, a018903.

Tozuka, Y., Fukuda, S., Namba, T., Seki, T., and Hisatsune, T. (2005). GABAergic excitation

promotes neuronal differentiation in adult hippocampal progenitor cells. Neuron *47*, 803–815.

Trinchero, M.F., Buttner, K.A., Sulkes Cuevas, J.N., Temprana, S.G., Fontanet, P.A., Monzón-Salinas, M.C., Ledda, F., Paratcha, G., and Schinder, A.F. (2017). High plasticity of new granule cells in the aging hippocampus. Cell Rep. *21*, 1129–1139.

Trinchero, M.F., Herrero, M., Monzón-Salinas, M.C., and Schinder, A.F. (2019). Experience-Dependent Structural Plasticity of Adult-Born Neurons in the Aging Hippocampus. Front Neurosci *13*, 739.

Tronel, S., Belnoue, L., Grosjean, N., Revest, J.-M., Piazza, P.-V., Koehl, M., and Abrous, D.N. (2012). Adult-born neurons are necessary for extended contextual discrimination. Hippocampus *22*, 292–298.

Tunc-Ozcan, E., Peng, C.-Y., Zhu, Y., Dunlop, S.R., Contractor, A., and Kessler, J.A. (2019). Activating newborn neurons suppresses depression and anxiety-like behaviors. Nat Commun *10*, 3768.

Vogel-Ciernia, A., and Wood, M.A. (2014). Examining object location and object recognition memory in mice. Curr Protoc Neurosci *69*, 8.31.1–17.

Wang, C., Shimizu-Okabe, C., Watanabe, K., Okabe, A., Matsuzaki, H., Ogawa, T., Mori, N., Fukuda, A., and Sato, K. (2002). Developmental changes in KCC1, KCC2, and NKCC1 mRNA expressions in the rat brain. Brain Res Dev Brain Res *139*, 59–66.

Yang, S.M., Alvarez, D.D., and Schinder, A.F. (2015). Reliable Genetic Labeling of Adult-Born Dentate Granule Cells Using Ascl1 CreERT2 and Glast CreERT2 Murine Lines. J Neurosci *35*, 15379–15390.

Zhang, W., St-Gelais, F., Grabner, C.P., Trinidad, J.C., Sumioka, A., Morimoto-Tomita, M., Kim,

K.S., Straub, C., Burlingame, A.L., Howe, J.R., et al. (2009). A transmembrane accessory subunit that modulates kainate-type glutamate receptors. Neuron *61*, 385–396.

Zhao, C., Teng, E.M., Summers, R.G., Ming, G.-L., and Gage, F.H. (2006). Distinct morphological stages of dentate granule neuron maturation in the adult mouse hippocampus. J Neurosci *26*, 3–11.

Zhao, C., Deng, W., and Gage, F.H. (2008). Mechanisms and functional implications of adult neurogenesis. Cell *132*, 645–660.